An Approach to Understand Network Challenges of Wireless Sensor Network in Real-World Environments

Lim Cheng Leong

Submitted in fulfilment of the requirements for the

Degree of Doctor of Philosophy

School of Engineering

College of Science & Engineering

University of Glasgow

Ph.D   April 2019

.

An Approach to Understand Network Challenges of Wireless Sensor Network in Real-World Environments

Lim Cheng Leong

Abstract

The demand for large-scale sensing capabilities and scalable communication networks to monitor and control entities within smart buildings have fuelled the exponential growth in Wireless Sensor Network (WSN). WSN proves to be an attractive enabler because of its accurate sensing, low installation cost and flexibility in sensor placement. While WSN offers numerous benefits, it has yet to realise its full potential due to its susceptibility to network challenges in the environment that it is deployed. Particularly, spatial challenges in the indoor environment are known to degrade WSN communication reliability and have led to poor estimations of link quality. Existing WSN solutions often generalise all link failures and tackle them as a single entity. However, under the persistent influence of spatial challenges, failing to provide precise solutions may cause further link failures and higher energy consumption of battery-powered devices. Therefore, it is crucial to identify the causes of spatial-related link failures in order to improve WSN communication reliability.

This thesis investigates WSN link failures under the influence of spatial challenges in real-world indoor environments. Novel and effective strategies are developed to evaluate the WSN communication reliability. By distinguishing between spatial challenges such as a poorly deployed environment and human movements, solutions are devised to reduce link failures and improve the lifespans of energy constraint WSN nodes.

In this thesis, WSN test beds using proprietary wireless sensor nodes are developed

and deployed in both controlled and uncontrolled office environments. These test beds provide diverse platforms for investigation into WSN link quality. In addition, a new data extraction feature called Network Instrumentation (NI) is developed and implemented onto the communication stacks of wireless sensor nodes to collect ZigBee PRO parameters that are under the influence of environmental dynamics.

To understand the relationships between WSN and Wi-Fi devices communications, an investigation on frequency spectrum sharing is conducted between IEEE 802.15.4 and IEEE 802.11 bgn standards. It is discovered that the transmission failure of WSN nodes under persistent Wi-Fi interference is largely due to channel access failure rather than corrupted packets. The findings conclude that both technologies can co-exist as long as there is sufficient frequency spacing between Wi-Fi and WSN communication and adequate operating distance between the WSN nodes, and between the WSN nodes and the Wi-Fi interference source.

Adaptive Network-based Fuzzy Inference System (ANFIS) models are developed to predict spatial challenges in an indoor environment. These challenges are namely, "no failure", "failure due to poorly deployed environment" and "failure due to human movement". A comparison of models has found that the best-produced model represents the properties of signal strength, channel fluctuations, and communication success rates. It is recognised that the interpretability of ANFIS models have reduced due to the "curse of dimensionality". Hence, Non-Dominated Sorting Genetic Algorithm (NSGA-II) technique is implemented to reduce the complexity of these ANFIS models. This is followed by a Fuzzy rule sensitivity analysis, where the impacts of Fuzzy rules on model accuracy are found to be dependent on factors such as communication range and controlled or uncontrolled environment.

Long-term WSN routing stability is measured, taking into account the adaptability and robustness of routing paths in the real-world environments. It is found that routing stability is subjected to the implemented routing protocol, deployed environment and routing options available. More importantly, the probability of link failures can be as high as 29.9% when a next hop's usage rate falls less than 10%. This suggests that a less dominant next hop is subjected to more link failures and is short-lived.

Overall, this thesis brings together diverse WSN test beds in real-world indoor environments and a new data extraction platform to extract link quality parameters

from ZigBee PRO stack for a representative assessment of WSN link quality. This produces realistic perspectives of the interactions between WSN communication reliability and the environmental dynamics, particularly spatial challenges. The outcomes of this work include an in-depth system level understanding of real-world deployed applications and an insightful measure of large-scale WSN communication performance. These findings can be used as building blocks for a reliable and sustainable network architecture built on top of resource–constrained WSN.

Author's Declaration

I declare this thesis is a record of original work carried out by myself, under the supervision of Professor Cindy Goh at the University of Glasgow. The copyright of this thesis belongs to the author under the terms of the United Kingdom Copyrights Acts. As such, due acknowledgment must be made of the use of any material contained or derived from this thesis. This thesis has not been submitted elsewhere in consideration for a higher degree.

Publications

The original work presented in this thesis has been published in following refereed Journals and International Conferences.

[1] C. L. Lim, C. Goh, and Y. Li, "Long-Term Routing Stability of Wireless Sensor Networks in a Real-World Environment," *IEEE Access*, vol. 7, pp. 74351 − 74360, May 2019.

[2] C. L. Lim, M. Bolt, A. Syed, P. Ng, C. Goh, and Y. Li, "Dynamic performance of IEEE 802.15.4 devices under persistent Wi-Fi traffic", *2015 International Conference of Recent Advances in Internet of Things (RIoT)*, IEEE, Singapore, 2015.

[3] C. L. Lim, C. Goh, A. Khan, A. Syed, and Y, Li, "Predicting types of failures in wireless sensor networks using an adaptive Neuro-Fuzzy inference system," *2016 12th International Conference on Wireless and Mobile Computing, Networking and Communications (WiMob)*, IEEE, New York, USA, 2016.

[4] C. L. Lim, C. Goh, A. Khan, and Y. Li, "Understanding spatial related network challenges from physical and network layers," *2017 International Conference on Computing, Networking and Communications (ICNC)*, IEEE, Santa Clara, USA, 2017.

[5] A. Khan, S. Sharma, C. Goh, and C. L. Lim, "A review of network models for internet of vehicles," *The Sixth International Conference on Advances in Vehicular Systems, Technologies and Applications,* pp. 1-6, Nice, France, 2017.

[6] A. Khan, S. Sharma, C. Goh, and C. L. Lim, "QoS assessment and modelling of connected vehicle network within Internet of vehicles," *International Journal on Advances in Software,* vol. 11 (1), 2018.

Acknowledgements

Table of Contents

List of Tables

List of Figures

xvi

List of Abbreviations

4B	Four-Bit Estimator
ACK	Acknowledgement
ACV RSSI	Average Coefficient Of Variation RSSI
ANFIS	Adaptive Network-Based Fuzzy Inference System
ANN	Artificial Neutral Network
AODV	Ad Hoc On Demand Distance Vector
BER	Bit Error Rate
BNTC	Bi-Directional Neighbour Table Connectivity
BRE	Bursty Routing Extensions
CA	Carrier Avoidance
CAP	Contention Access Period
CCA	Clear Channel Assessment
CDF	Conditional Probability Distribution Function
CFP	Contention Free Period
CSMA	Carrier-Sense Multiple Access
CTP	Collection Tree Protocol
CTS	Clear To Send
DB	Decibel
DC	Don't Care
DIFS	Distributed Coordination Function Interframe Space
E2E	End-To-End
ED	Energy Detection
ES	Evolutionary Strategies
ETX	Estimated Number Of Transmission
F-LQE	Fuzzy Link Quality Estimator
FIS	Fuzzy Inference System
FSPL	Free Space Propagation Loss
GA	Genetic Algorithm
HM	Human Movement
ILTP	Intermediate Quality Link Transformation Protocol
IOT	Internet Of Things
IP	Inactive Period

IQ	Intermediate Quality
LEACH	Low Energy Adaptive Clustering Hierarchy
LNS	Log Normal Shadowing
LOO-CV	Leave One Out Cross Validation
LOS	Line Of Sight
LQI	Link Quality Indicator
LR-WPAN	Low Rate-Wireless Person Area Network
MAC	Media Access Control
MF	Membership Function
MOEA	Multi-Objective Evolution Algorithm
NF	No Failure
NI	Network Instrumentation
NLOS	Non-Line Of Slight
NMS	Network Management System
NSGA-II	Non-Dominated Sorting Generic Algorithm II
NT	Neighbour Table
NTC	Neighbour Table Connectivity
PDE	Poorly Deployed Environment
PDR	Packet Delivery Rate
PRR	Packet Reception Rate
QOS	Quality Of Service
RIM	Radio Irregularity Model
RNP	Required Number Of Packet Protocol
RMSE	Root Mean Square Error
RREP	Route Response
RREQ	Route Request
RSSI	Received Signal Strength Indicator
RT	Routing Table
RTS	Request To Send
RX	Receiver
SD	Standard Deviation
SFC	Switching Frequency Count
SIR	Signal to Interference Ratio
SNR	Signal To Noise Ratio

STLE	Short-Term Link Estimation
TDMA	Time-Division Multiple Access
TMCP	Tree-based Multi-Channel Protocol
TS	Takagi-Sugeno
TX	Transmitter
UDP	User Datagram Protocol
WR	Wi-Fi Router
WRE	Weighted Regression Estimator
WSN	Wireless Sensor Network

1 Introduction

1.1 The Surge in Smart Buildings and Wireless Sensor Networks

The push to reduce the energy consumption of buildings and the impact of the built environment on human health and the ecosystem has seen a steady rise in the number of Smart Buildings [1, 2, 3]. Context-aware environments are foreseen as key elements in the control and regulation of multiple applications in Smart Buildings, such as intelligent heating, ventilation and air-conditioning controls, energy management systems, smart health and intruder monitoring system. In addition, the demand for data-driven applications is projected to result in a one to two-fold increase in the number of internet connected devices [4, 5], and this surge will be made possible by the advent of Internet of Things (IoT). The need for large-scale sensing capabilities as well as scalable communication networks with high mobility levels have fuelled the exponential growth in the research of Wireless Sensor Networks (WSNs) [6, 7].

WSN plays an intrinsic role in Smart Buildings, reporting environmental information and surrounding context wirelessly to IoT devices and applications. It has proven to be an attractive and important enabler for accurate sensing in terms of associated low installation cost as well as the flexibility it offers in sensor placements [8, 9]. WSN is made up of clusters of smart wireless sensor nodes that are small, built with limited processing and computing resources, and are designed to sense, measure, and collect information from their surroundings. These nodes are equipped with wireless transceivers, have self-organising capabilities to form a cohesive wireless network to transmit and relay the measured data to a base station. WSN avoids the need for pulling wires at installation, thus allowing for reductions in installation cost and increased flexibility in sensor placements.

While WSN offers numerous benefits, they have yet to realise their full practicality in real-world applications. Optimisation protocols are in place in the software stacks of

wireless sensor nodes to ensure that WSNs operate smoothly without the need for human intervention. These protocols comprise a set of rules that organise routing paths and govern certain behaviours between devices during data exchanges. However, existing optimisation protocols are often found to exhibit poor dependability in the face of a real-world deployment. Studies have shown that a large number of WSN deployments operate with less than 90% throughput [10, 11, 12]. Particularly, WSNs in indoor environments inherit lower efficiency due to the susceptibility to indoor network challenges and the unpredictable radio propagation [13, 14, 15, 16]. For instance, communication across dense environment and frequent physical changes within the environment caused by human movements are known to alter the communication reliability between nodes [17, 18, 19, 20, 21].

Failing to provide precise solutions under the persistent influence of network challenges may lead to further link failures and higher energy consumption of battery-powered devices [15, 16]. Furthermore, due to the scattered deployment of WSN in remote environment, it is challenging to eliminate the source of network failure or to even replace the batteries of energy-depleted devices. With considerable bottlenecks encountered in the WSN field trials testing for network reliability, there has been resistance to adopt these wireless technologies in the commercial market. Therefore, in order to create a sustainable competitive advantage, the need to realise the practicalities of this complex technology with minimal infrastructure change has intensified. It is critical to evaluate the state of WSN communication reliability performances in real-world deployments and to design new networking strategies to effectively improve the performance of WSN services.

1.2 Research Motivation

This thesis is motivated by the following research challenges.

1. Energy constraint wireless sensor nodes

The increased complexity in wireless sensor node application has driven the need for higher energy consumption requirements [22]. This is especially true for data intensive applications that produce large amounts of data. The choice of wireless communication technology to transmit and receive these data therefore needs to be

carefully considered as it impacts both the reliability of data exchange between nodes and the associated energy consumption.

Different types of interferences in the environment can have different impacts on the performance of wireless communication. To mitigate these interferences, additional detection mechanisms need to be put in place [23, 24]. Computational resources such as computing time and memory size necessary to perform the usual arithmetic operations, and operational strategies that match the application's requirements are paramount to an efficient and reliable WSN. However, the option to select WSN components relative to the computational effort required by specific application is not always available.

2. Poor predictability of WSN communication in an indoor environment

The propagation of transmitted signals is determined by the physical medium between communicating wireless sensor nodes. The ways in which the nodes are deployed and the dynamics of the environment have direct influences on the reliability of wireless communication. Objects in physical medium such as walls and cabinets act as reflectors, creating different propagation paths for the transmitted signals [13, 19]. Depending on the position of the nodes and the layout of their surroundings, the receiving node receives superposition of multiple copies of the transmitted signal via differing propagation paths, each arriving at different times and qualities.

In addition, human movements and changes in object placements such as opening and closing of door introduce signal propagation topology change. These factors result in temporal alteration in the propagation paths of a transmitted signal, causing signal qualities to fluctuate [25, 26, 27]. In such situations, signal quality fluctuations of 30 dB are not uncommon [28]. In reality, it is difficult to predict or control these spatial challenges unless the position of all nodes and the geometry of the environment are known, static or uninterrupted at all times. This is also impractical due to the vast number of interactions among all factors in a real-world deployment [29, 30]. As such, the ability to predict these spatial challenges is seen as a critical factor to improve WSN communication reliability.

3. The need for accurate detection of the cause of wireless link failure

Network challenges have different effects on individual WSN communication layers [31, 32, 33]. This is to say that a topology failure could be attributed to either the poor time synchronisation of the MAC layer or poor end-to-end connectivity of the routing layer. A link failure detected at a specific layer should not be representative of the entire stack without knowing the response from other layers [31]. Furthermore, common generalisation of a link performance as good, intermediate or bad does not provide sufficient information for WSN optimisation protocol to execute efficiently [34, 35]. For instance, increasing transmission power may improve the reliability of long distance communicating nodes [13], however, this may not be true for nodes suffering from channel access failures under persistent Wi-Fi interference [36].

Data and computation intensive applications with real-time requirements further add on to existing system limitations such as processing performance and buffer space. These limitations can be confused with network failures if no specific detection mechanisms are in place. The inability to identify the cause of link failure may adversely affect the network's performance [15, 27, 34]. Therefore, in order for WSN optimisation protocol to function optimally, it is crucial to identify the causes of link failures.

4. The need for system-level understanding during WSN communication failures

The absence of system-level understanding to deployed solution, for example in a home and building automation, renders it hard for a network operator to accurately diagnose network issues. WSN nodes are designed with redundancy features for network self-healing and to minimise abrupt changes in a network. These features include retransmissions, consecutive keep-alive messages, channel back offs, which are performed automatically by the communication stack. As such, link failures are often hidden from the user point of view.

Existing WSN simulators designed to approximate the performance of a WSN in a simulated environment is limited [37, 38]. Every simulator has features that work well in the respective domain as they inherit the different approaches and theoretical models to investigate specific problem. However, this has also led to accuracy and authenticity issues when different simulation settings are used. For instance,

simulations and theoretical models may not take into account the different protocol stacks, type of application, characteristics of wireless module used, and antenna polarisation. Due to these, simulation can only be used for performance estimations, but not to be relied for accurate results due to the complexity of radio propagation. For these reasons, understanding how these network challenges impact communication devices, and how they can be detected and measured under diverse real-world environmental settings will be beneficial for accurate network failure diagnosis and prediction of link failure.

1.3 Research Aim and Objectives

The main aims of this thesis are to (1) develop realistic WSN test beds that produce a representative collection of WSN communication performance parameters for realistic investigation of indoor environment challenges, (2) formulate novel strategies to predict and interpret WSN communication failures pertaining to spatial network challenges and their causes and (3) apply developed methods on real-world WSN tests beds and investigate gaps in existing WSN protocol.

The objectives of this research are to:

1. Develop WSN test beds by deploying proprietary NXP semiconductors wireless sensor nodes in real-world environments for realistic investigation of indoor environment challenges. This includes a seamlessly integrated data extraction platform that complies with the implemented WSN protocol to enable a representative collection of WSN communication performance parameters.

2. Evaluate WSN communication performance that are under the influence of both experimental and real-world indoor environmental settings with known types of network faults and hypothesised symptoms. These are for example, persistent Wi-Fi traffic, communication through dense environment and human movements.

3. Using link quality parameters obtained from the operating stacks of wireless sensor nodes deployed in real-world environments to train and evaluate models that accurately classify WSN link failures to the associated spatial network challenges.

4. Classify WSN communication failures into smaller specific areas of inquiry for model interpretation. By doing so, users can comprehend the classification model

by inspecting its functions, providing insights into wireless sensor nodes' behaviour under real-world environmental settings.

5. Formulate methods to investigate the gaps and performance of existing WSN protocols using developed classification models and post-interpretation of WSN communication failures.

1.4 Thesis Novelties and Contributions

The novelties and contributions of this thesis are as follows:

In this thesis, WSN test beds using actual wireless sensor nodes deployed in real-world environments were developed. Proprietary wireless sensor nodes were used, built using NXP's JN5168 wireless modules [39] and implemented on an open standard ZigBee PRO Home Automation [40]. In addition, a data extraction feature called Network Instrumentation (NI) was developed to provide "in-network" monitoring and reporting of information within the ZigBee PRO communication stacks. As opposed to the use of generated simulated data [37, 38], data collected from an under-represented WSN test beds (i.e. controlled [41, 42], one hop network [43, 44]), or data collected from non-proprietary systems (i.e. non-standard network protocol), the novel use of extracted representative ZigBee PRO performance indicators that were collected from diverse real-world environmental settings, provided a realistic investigation and evaluation platform for WSN communication reliability. This data were also used for relevant benchmarking and proof-of-concept purposes, as well as for prediction models training inputs.

It is emphasised in the literature that Wi-Fi and WSN technology do not co-exist well in the same operating environment because the WSN application under simultaneous Wi-Fi traffic suffers from packet distortion [36, 45, 46, 47, 48, 49]. Therefore, an investigation was conducted to evaluate the impact of persistent Wi-Fi traffic and WSN communication on each other. This investigation produced two novel findings. First, it was demonstrated that the IEEE 802.15.4 nodes' transmission failures under persistent Wi-Fi traffic were largely due to channel access failure rather than corrupted data packets. Second, the operating distance between the IEEE 802.15.4 nodes, and between the IEEE 802.15.4 nodes and the interference source were key factors affecting the dynamic co-existence relationship. IEEE 802.15.4 and IEEE

802.11 bgn nodes were found to co-exist well in the same environment as long as they were separated with sufficient spatial distance and operating frequency.

WSN spatial related link failures prediction models were developed using Adaptive Neuro Fuzzy Interference System (ANFIS) technique. These ANFIS models, designed to classify WSN link failures due to poorly deployed environment and human movements, produced an accuracy of 92%. A comparison between multiple prediction models, trained with different inputs combination produced the following key findings. First, physical layer parameters had showed superior results at predicting spatial-related link failures as compared to network layer parameters. This is due to their ability to distinguish poorly deployed environment and human movements. Secondly, the best-produced model mirrors the properties of signal strength, channel fluctuations and communication success rate. This work highlighted the limitations of existing single parameter link quality assessment, and the importance of careful selection of training parameters and the use of cross-layer parameters for prediction of WSN link failures.

Due to the "curse of dimensionality", any increase in input variables generates an exponential number of IF-THEN rules within the ANFIS model. The increasing number of rules becomes difficult for user to interpret (i.e. hard to read and understand). Hence, Non-dominated Sorting Genetic Algorithm II (NSGA-II) technique was implemented to reduce the complexity of generated ANFIS models, whilst sacrificing minimal model accuracy. To our best knowledge, there is limited work that investigates the impact of MOEA technique's settings on minimisation of Fuzzy model rule-base size. Therefore, different NSGA-II settings were experimented to achieve a thorough exploration of input and output space and to avoid premature convergence of all objectives. The influence of individual Fuzzy rule on the different predictive conditions was also evaluated using Fuzzy rules removal sensitivity analysis. It was found that the dominance of rules was dependent on factors such as communication range and controlled or uncontrolled indoor office environments.

Instantaneous assessment of WSN link quality is often preferred in the literature with limited work focuses on long-term WSN routing stability in a real-world indoor environment. In this thesis, long-term routing stability measures of Zigbee PRO using link failure prediction model on real-world WSN test beds were evaluated. These

measures are relative routing path usage count, usage rate of unique next hops and switching frequency counts were introduced to identify potential network bottlenecks and provided an alterative means to monitor WSN communication reliability. It is found that up to 29.9% of the less dominant routing paths in real-world test beds were connected to links with failures. These links were short-lived and had contributed to the undesired phenomenon of network instability.

1.5 Thesis Organisation

In Chapter 2, common causes of WSN link failures and existing detection mechanisms are reviewed. Existing link quality assessments are often insufficient to provide reliability communication because they generalise all types of link failures as a single entity. In order to improve WSN communication reliability, particularly in a dynamic deployed environment, the cause of link failure should be accurately identified.

In Chapter 3, two sets of controlled experiments designed to investigate Wi-Fi interference and spatial network challenges are presented. In the first experiment, wireless sensor nodes, equipped with the fundamental IEEE 802.15.4 standard, are experimented under persistent Wi-Fi traffic generated with User Datagram Protocol (UDP). Results showed that Wi-Fi interference can be mitigated with careful deployment and configurations. In the second experiment, WSN nodes, implemented with ZigBee PRO standard, are configured to communicate under the influence of simulated single human walking profiles and poorly deployed environment (i.e. long distance communication and communication across dense environment). Link quality parameters collected in this experiment are used to train link failure prediction models using ANFIS technique. The performance of these models and training parameters are then compared and evaluated.

In Chapter 4, the interpretability and accuracy trade-offs in Neuro-Fuzzy systems are outlined. NSGA-II is implemented on the initially generated ANFIS models to reduce the complexity of their Fuzzy rule-base resulted from the high number of IF-THEN rules and antecedent used. Due to the unique problem to be optimised, different NSGA-II settings are investigated to ensure thorough exploration of Neuro-Fuzzy solutions in the input and output space.

In Chapter 5, two distinct large-scale WSN test beds are reviewed. These test beds are deployed in actual occupied administration offices in the Solaris building in Singapore and the Vaucanson building located in La Rochelle, France. A decision tool is formulated to select an ideal solution among the Pareto front of optimised Fuzzy models (developed in Chapter 4). Thereafter, Fuzzy rules removal sensitivity analysis is used to evaluate the impact of individual Fuzzy rule on the different predictive conditions. Results showed that the dominance of link quality parameters is dependent on the environmental settings and the communication distance across the network.

In Chapter 6, the long-term routing path stability of ZigBee PRO implemented WSN deployed in real-world environments are investigated. With the application of spatial related link failure prediction models, it is not uncommon to find actual routing paths to operate on link with failures. Relative routing path usage counts, usage rate of unique next hops and switching frequency count are introduced as routing stability indicators. The discovery of potential network bottlenecks highlights the importance of monitoring long-term routing path stability and the need to avoid the use of non-dominant links.

Finally, the conclusions drawn from this research and recommendations for future directions are discussed in Chapter 7.

2 A Review on Wireless Sensor Network Link Failures

Evidence and findings from field trials and literature have shown that WSN in real-world deployments still exhibit communication reliability issues. There is a pressing need to overcome the practical challenges associated with deploying this complex technology. Therefore, Chapter 2 reviews the existing solutions in the literature designed to detect or mitigate commonly found WSN network challenges. In Section 2.1 and Section 2.2, the general functionalities of WSN are discussed, including optimisation protocols and link quality assessment mechanisms respectively. When deployed in real-world environmental settings, nodes are found to exhibit unpredictable behaviours because of their lack of awareness of their surroundings. As such, Section 2.3 reviews the different types of network challenges pertaining to WSN communication reliability and assesses the gaps in WSN link quality estimations in the literature. These network challenges include imperfection operating conditions, spatial network challenges, inter-WSN interference, and Wi-Fi interference. Findings of this chapter highlight that Wi-Fi interference and spatial network challenges are key factors affecting WSN communication reliability.

2.1 Wireless Sensor Networks Optimisation Protocols and their Energy Constraints

WSN consists of spatially distributed autonomous sensor nodes designed to sense, measure and gather information about the physical or environmental conditions. These nodes are usually equipped with devices such as wireless microcontrollers, modular sensors, batteries and energy-harvesting capabilities. Sensor data is collected and transmitted wirelessly from one node to another. Depending on the implemented optimisation protocol and applications [50], sensor nodes can form a reactive network topology with self-organising capabilities so that sensors data can be relayed reliably to the destination nodes. Optimisation protocol ensures that the requirements of WSN

applications are met without the need for human intervention. These requirements, commonly termed as Quality of Service (QoS) help to for example, maintain maximum data throughput for data sensitive applications [14, 51] and reduce end-to-end latency for data critical applications [52, 53].

The requirement of small form factor and bill of material constraints on sensor nodes limit their resources such as energy, memory, computational power and communications bandwidth. In particular, energy in battery-powered WSN is a scarce resource. Given that the longevity of WSN applications depends on the energy consumption rate of sensor nodes [54], energy efficiency becomes one of the prime considerations in designing an optimisation protocol [55, 56]. To avoid energy deficiency in WSN, optimisation protocol must be balanced between energy consumption, system performance, and operational fidelity while relying on a light memory footprint.

2.2 Link Quality Assessment in Real-World Environments

QoS criteria are assessed through link quality assessment, where the quality of a communication link is monitored, measured and evaluated [57]. Optimisation protocol then decides the appropriate solution to mitigate or to reduce any link failures. For example, if a transmitting node senses an occupied or noisy channel, it backs off for a period of time until the channel is cleared before transmission. Doing so minimises potential packet collision. Conversely, a suboptimal decision may lead to excessive channel backoff, which leads to increasing energy wastage in the long run. In this section, some of the limitations of existing link quality assessments are reviewed.

2.2.1 Limitations of Single Parameter Link Quality Assessment

Xu and Lee [58] introduced Weighted Regression Estimator (WRE) to estimate link quality. WRE is a regression model where the weightage for each regression is determined by the spatial distance between a set of nodes. WRE takes into account the characteristics of irregular radio propagation [59] and the link quality of nodes in same geographical region. Authors explained that WRE improves the robustness of link quality assessment since neighbouring nodes in the same region experience

similar link quality. This work assumes that all environmental dynamics affect nodes regionally and the level of impact can be measured with distance, which is not always true. For example, link failures from asymmetrical communications and hidden terminal problems do not affect nodes regionally [15]. Furthermore, received signal strengths measured do not correlate well with distance between communicating nodes, particularly in an indoor environment with the presence of human movements [43].

The quality of a link is commonly classified as poor, intermediate and good [10, 11, 25, 60], as shown in Figure 2.1. Doddavenkatappa, Chan and Leong [60] proposed the use of Intermediate Quality Link Transformation Protocol (ILTP) to alternate communication channels and to improve a link of Intermediate Quality (IQ) into a "good" one. Authors argued that Packet Reception Rate (PRR) varies across different channels and that IQ links can be improved through channel diversity. For instance, there is an 85% chance of finding a better channel for an existing link with 70% PRR. However, this work assumes that all causes of link failures degrade PRR. Authors in [36] has shown that when sharing communication channel with persistent Wi-Fi traffic, only 5% of all losses can be captured using PRR indicator while the rest of the losses can only be detected from channel access failure. This means that Wi-Fi traffic do not influence every link quality metrics equally. Since ILTP determines a link quality using only PRR, network challenges that do not impact PRR (e.g. Wi-Fi traffic) may remain undetected.
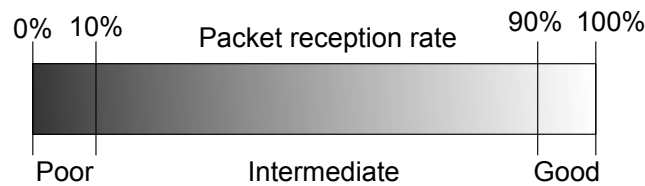
Figure 2.1. The description of link quality based on PRR values. A perfect link is described with PRR of 100%. Poor link has a PRR of less than 10%, PRR of intermediate link is between 10% and 90%, and good link has PRR greater than 90% [10, 11, 25, 60].

Bursty Routing Extensions (BRE) protocol is introduced in [10], which also exploits the characteristics of IQ links. Nodes implemented with BRE actively detect

retransmitted packets in the channel and help to forward them if they failed repeatedly. The authors mentioned that IQ links typically have "bursty" characteristics where link failures are temporal and will also become temporarily reliable after receiving a number of consecutive packets over the same link. Therefore, BRE employs a Short-Term Link Estimation (STLE) mechanism to determine if IQ links are bursty and reuse these links when they are stable, instead of re-routing. Doing so helps to preserve the stability of the network topology. By preventing unnecessary route changes, BRE is said to reduce total overhead over traditional routing by 19% and reduce transmission costs by 40%. In another work, Cerpa et al. [61] tackled the high temporal characteristics of a low-power communication in indoor WSN deployments with Required Number of Packet protocol (RNP). RNP is the average number of packets sent before the receiver receives a packet. RNP is said to be a better measure of link quality than PRR as it takes into account the underlying distribution of losses. For example, a longer period of zero PRR can incur higher RNP values than a shorter period of zero PRR. Although a BRE and RNP implemented nodes can identify the temporal characteristics of link failures, they have not explored identifying the causes of link failures and bottlenecks in the network.

2.2.2 Link Quality Assessment using Cross Layer Parameters

A failure detection mechanism belonging to a specific layer of a protocol stack should not be representative if it does not consider the responses from other layers [31]. For example, a link failure could be potentially attributed to either poor time synchronisation characteristic of MAC layer or poor end-to-end connectivity characteristic of the routing layer. The use of information from multiple layers such as cross-layer parameters can provide more details about the quality of a link.

Four-Bit estimator (4B) proposed in [62], is a cross-layer link quality metric that takes into account of four different link properties. These properties include the probability of decoding error during packet reception at the link layer, relative importance of a link by comparing among the neighbours at the network layer, and confirmation of incoming and outgoing reception through acknowledgement at the physical layer. It is said that the network layer parameters allow relative links comparison with neighbouring nodes, while physical and link layer parameters are more efficient at

estimating the quality of a link at reception. The performance of 4B was then evaluated with Collection Tree Protocol (CTP), which built and maintained a tree network. It is found that a 4B-based CTP produced a better performance in terms of packet delivery than a CTP that uses Estimated number of Transmission (ETX). Through simulation, 4B nodes favoured shorter communication distance between nodes. This is because a shorter communication distance is reasoned to have better quality due to better link budget and lesser chances of link asymmetry at the link layer. As such, the depth counts of routing paths in the network increased and the overall number of retransmissions reduced.

In a similar work, Baccour et al. [35] presented Fuzzy-Link Quality Estimator (F-LQE) that also combined four link properties found in a WSN. F-LQE combined the coefficient of variation of PRR indicating the stability of a link over time, Signal to Noise Ratio (SNR) used to differentiate a bad and good quality channel, Window Mean with Exponential Weightage Moving Average technique [63] to measure data throughput overtime, and the PRR difference between uplink and downlink for link asymmetry measure. Baccour et al. highlighted that WSN communication channel quality is usually assessed with functions of imprecisely measured channel properties such as a link quality threshold of 0.95 packet delivery. Unlike classical logic, Fuzzy logic is used to deal with imprecise information, providing approximate truth of a proposition based on linguistic variables and inference rules. For instance, a channel can be unstable, stable, and highly stable. Using cross-layer information and linguistic representation of link quality assessment, F-LQE nodes are tested extensively in an outdoor simulated experiment and have demonstrated superior network performance by avoiding the use of unstable links and noisy channels.

2.2.3 Generalisation of Links Failures as a Single Entity

It is common for link quality assessment to generalise all causes of link failures as a single entity. For instance, WRE nodes [58] assumed all causes of link failure affect nodes regionally, and ILTP nodes [60] assumed all network challenges impact WSN through packet losses. In F-LQE [35] and 4B [62], multiple link properties are characterised and used as measures to distinguish "good" links from "poor" links. For example, by measuring a link's temporal characteristic and both uplink and downlink reception qualities, a link can be determined as "good" if it is stable and do not

experience link asymmetry. While the ability to identify link failure is important, it is equally critical to differentiate the causes of link failures. This is to say that the ability to measure channel noise is not the same as identifying channel noise caused by inter-network collision or inter-network congestion. While both inter-network collision and inter-network congestion cause packet losses and noisy channels, they require different methods to overcome them. Network congestions should be tackled with traffic re-routing at the routing layer, while collision can be overcome with a more precise transmission synchronisation at the MAC layer (refer to Section 2.3.3). In this case, simply generalising link quality as "good, intermediate or bad" does not provide sufficient information for WSN optimisation protocol to execute optimally [27, 34, 35].

The environment in which the WSN is deployed in is often dynamic and the impact on WSN communication reliability varies according to the types of network challenges. Due to the complex nature of the transmission medium, the ability to characterise link quality precisely is challenging where optimisation protocols have shown to exhibit unpredicted behaviour. For instance, network flooding can result in non-uniform data propagation where packets are relayed further in different directions [15]. This is because at the initial stage of flooding (i.e. network broadcast), packet collisions are more common due to a sudden surge of broadcasted packets. The inability to detect and prevent increasing asymmetrical communications from packet collisions has led to some packets travelling further than others. In this example, a small imperfection has manifested in ways not tested in the simulation. Furthermore, the optimisation protocol is often designed to overcome network challenges without the need for human intervention. When ineffective methods are executed in attempt to overcome persistent network challenges, the lack of link failures notification can pose as a bottleneck to WSN communication reliability. This means that a protocol may opt for unwarranted re-routing to compensate of frequent link failures along routing paths, leading to excessive energy consumption. Therefore, it is critical for link quality assessment to assess the happenings in the environment and to identify the cause of link failure accurately. Doing so allows the upper layers of the optimisation protocol to decide on the appropriate solution to mitigate the source of failures and improve overall network reliability.

2.3 Wireless Sensor Network Link Failures and Existing Detection Models

In Section 2.2, identifying the causes of link failures is explained as essential for the optimisation protocol to function effectively. WSN, being deployed within a dynamic environment may render it difficult to pinpoint the exact causes of link failures. Therefore, in this section, the commonly found network challenges, pertaining to WSN communication reliability are discussed.

2.3.1 Imperfect System and Operating Conditions

WSN and its operating conditions are imperfect. These imperfections include but not limited to, irregular antenna propagation, mismatching of hardware characteristics and even environmental factors such as temperature and humidity conditions [15, 30, 64, 65]. They are known to degrade the assessment of link quality between communicating nodes and are often accounted as probabilistic variables and random factors during modelling [59, 66, 67, 68].

1. Energy depleted wireless sensor nodes

To minimise the overall hardware size and built cost, wireless sensor nodes are often equipped with batteries of small capacity. Batteries replacement in a remote environment and for a large network size is impractical. As such, energy efficiency is seen as one of the primary design goals in a battery-powered WSN. The wireless transceiver is the primary energy consumer in a wireless sensor node [54]. The design of an optimisation protocol should avoid excessive usage of transceiver such as prolonged idle listening where a node listens to a channel for packets that are intended for it or other nodes, and excessive control-packet overhead where a node transmits packets aggressively to maintain a network.

On the contrary, in order for a WSN to be precise, responsive and reliable, additional monitoring activities involving active transceivers are often required. These activities include continuous monitoring of the channels and additional control packets for robust communication, both of which are conflicting goals with minimising the consumption of energy [69, 70]. Therefore, the choice of optimisation protocol must

balance both the reliability of data transfer and the associated energy consumption.

Uneven energy depletion is often caused by limited routing options in the network, which can lead to early death of energy depleted relay node and even network partition [55, 55]. For example, the early death of node forces affected nodes to take alternate routes. This phenomenon is often referred to as network routing hole or coverage hole as shown in Figure 2.2. The energy-depleted node denoted in orange circle leaves a region in the network with no routing option or no sensing coverage [55, 71]. The solid arrows in Figure 2.2 illustrate the original routing paths between the routers and coordinator, as denoted as red circles and yellow triangle respectively. The dashed arrows show the effect of a routing hole leading to a reconfiguration of routing paths of the affected routers. It is noted that a routing hole may not always associate with energy-depleted nodes. In [72], nodes in the same region can be shadowed by large physical obstacles, or affected by frequency jamming, leaving affected nodes unreachable.
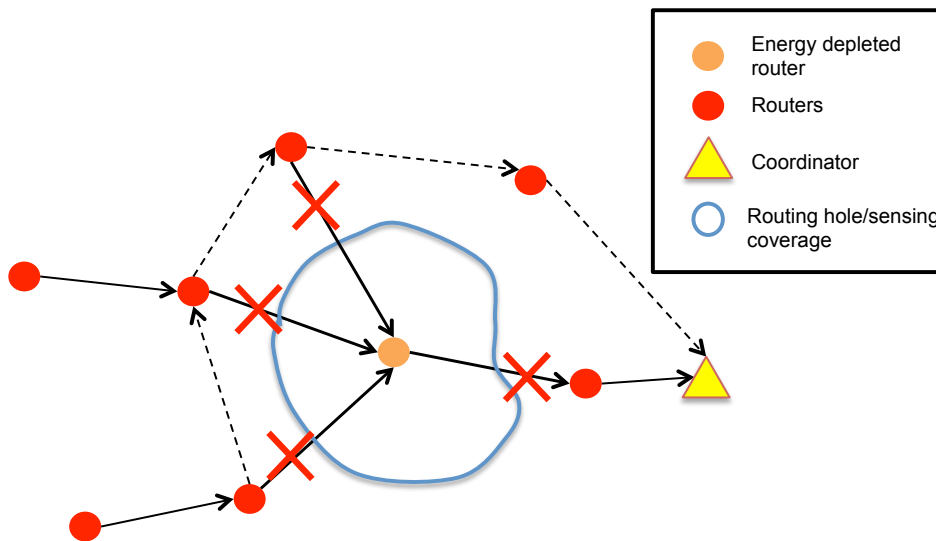
Figure 2.2. Network routing hole – An energy depleted router leaving a routing hole in the network, forcing previously connected routers to take a different and often longer route towards the coordinator.

WSN nodes usually do not have the information of the energy consumption rates or energy residual of neighbouring nodes. The lack of awareness of unreachable energy depleted nodes triggers persistent retransmissions or network probing if an alternate route towards the destination node is unavailable. Detection of routing or coverage

holes is important so that affected nodes can modify their tasks dynamically, according to the energy consumed and estimation of the network lifetime. Energy depleted node arise as a node-level symptom where only the affected node stops transmitting data. A distributed detection of node anomalies can be highly effective [73]. For instance, periodic "keep-alive" broadcast is a common mechanism in ZigBee PRO standard [40] used to inform neighbouring nodes that a node is still "alive" and available.

Minimising individual sensor nodes' energy consumption does not guarantee maximising a network's overall lifetime [74]. To exploit maximum network residual energy, a fair energy consumption of nodes across the network should be prioritised. Low Energy Adaptive Clustering Hierarchy (LEACH) [74, 75, 76] techniques are known to prolong the lifetime of the network by distributing the energy consumption among nodes in clusters. LEACH protocols require all the nodes to share their energy status among neighbouring nodes, including the estimation of the network lifetime based on energy consumption rates. Sharing of this information allows the cluster heads to be rotated based on the remaining energy of the nodes within each cluster. Since a cluster head consumes more energy from longer channel listening and data aggregations, an even consumption of energy among sensor nodes is achieved from rotations.

Duty cycling [77, 78, 79, 80] is another common mechanism known to minimise the energy consumption of individual sensor nodes. This is done via synchronising and scheduling nodes' sleep and wake cycles. Nodes implemented with energy efficient duty cycling protocol are allowed to enter low-power sleep mode whenever possible and activate their transceivers only when data packets are ready to be transmitted or received. The packet transmission or receive time-slots are allocated by a centralised device for a reliable data exchange and to avoid potential packet collision between devices within the shared frequency spectrum.

2. Wireless communication temporal characteristic

The temporal characteristic of a wireless communication is referred as the quality of transmitted signals between two devices that varies with time. Temporal characteristic is often explained with the dynamics of the operating environments, such as noise

level, multipath signals, moving terminals, and human bodies [81, 82]. Due to the impracticality of accounting for all entities in a deployed environment, temporal effect is often observed to be random and referred to as varying probability in path loss models [66, 83]. For instance, the variation in received signal strength between communicating nodes in the lognormal shadowing technique, used to predict signal path loss, is accounted as a Gaussian variable, as shown in Equation 2.3.

Different performance metrics have different temporal characteristics. For example, Srinivasan et al. [66] has found that when measuring the quality of received packets between two nodes, the Link Quality Indicator (LQI) metric varied more than Received Signal Strength Indication (RSSI). LQI provides an additional indicator about the received signals' chip error rate, while RSSI has a smaller operating range, making it less sensitive to PRR variation. In particular, when nodes operate near the sensitivity edge of a receiver at less than -87 dBm, PRR enters a grey transition region. In this transition region, PRR varies radically from 0 to 100% where local noise level is said to be a contributing factor on top of poor signal reception. Zuniga and Krishnamachari [84] have also found that the temporal effect has a direct impact on a node's packet delivery performance, both constructively and destructively. This is to say that a link of poor quality between communicating devices may fluctuate between transitional and disconnected zones, making accurate link quality assessment a difficult task. It is concluded that this variance in PRR is not affected by factors such as modulation, encoding, output power, and frame size. Rather, it is explained by the severity of multipath effects from the environment [84]. To better assess the quality of a link, a transitional coefficient is introduced to estimate the size of the transitional region (amount of poor links) for different environments. The smaller the transitional coefficient, the better the RSSI metric can be translated to PRR.

The temporal characteristic of a link failure is sometimes regarded as a random phenomenon. Unless the quality of network is severely at risk, temporal solutions are implemented to avoid drastic compensation by the optimisation protocol [11, 25, 61]. For instance, upon identifying a highly temporal failure (*bursty* link), an aggressive backoff technique is employed to delay retransmission [25]. Since link failures on a *bursty* link are temporal, retransmission after backoffs has been shown to improve the packet delivery success rate. Srinivasan et al. [25] identified *bursty* links with β

factor, calculated using Conditional Probability Distribution Functions (CDFs). β determines the probability that the next packet will be received after n consecutive successes or failures. In another work, Authors in [10] developed STLE to identify *bursty* links and suggested to use these links when they are stable. By avoiding the need for re-routing, the STLE reduced the total overhead by 19% as compared to traditional routing. STLE determines the temporal characteristics of a neighbour's link by overhearing consecutive packets sent from a sender-node and deriving the probability of successful delivery based on the packet sequence number and failed acknowledgments.

In [85], a Tree-based Multi-Channel Protocol (TMCP) is designed to measure noise in multiple industrial environments. TMCP models noise with parameters from different layers – channel detection, channel assignment and data communication. Despite the use of cross layer parameters, a static TMCP is still insufficient to take into account the varying noise in all industrial environment. Therefore, the use dynamic channel allocation mechanism is suggested where channels are monitored dynamically over time.

3. Hardware imperfections

Hardware imperfections issues are rooted at a single node and can manifest as a bias or a drift throughout the lifetime of a node [86]. These imperfections are for example, different battery statuses and hardware calibration mismatches between nodes leading to non-isotropic propagation.

The phenomenon of radio propagation irregularities is commonly referred as manufacturing hardware dissimilarities [59, 68]. Manufacturing hardware-related factors include differences in hardware calibration and nodes not having the same antenna gain along all directions. Signal propagation is often mistaken to be uniform across all directions in an isotropic manner. However, evidence in the literature shows that irregularity in propagation must be expected [15, 59, 63]. Non-isotropic radio propagation refers to the variation of transmission signal quality with different propagation directions. This effect was demonstrated to be non-repeatable under an uncontrolled environment and is associated with the transitional region due to a high variance in reception rates and asymmetric connectivity between nodes [84].

Even different battery statuses can introduce varying transmission power. Zhou et al. [59] experimented wireless communication between nodes of different battery statuses. It was observed that different battery statuses on the same sender node produce different transmission power where the receiver node received packets of different signal strength. Similar observations were made when different sender nodes, equipped with the same battery, produced packets of different signal strengths when received on the same receiver node. This is classified as a radio heterogeneity property, where different hardware calibration and battery statuses can lead to different signal transmission powers.

Detection of hardware issues can be challenging as the error in reported value can be mistaken for other forms of network challenges [73]. The impact of non-isotropic radio propagation due to hardware imperfection on the performance of upper-layer protocols has demanded a need for realistic WSN propagation models. Therefore, the effective radiated power (peak power) that an isotropic antenna can emit is modelled using the Radio Irregularity Model (RIM) [68]. RIM takes into account the random variance in transmission power that varies with the degree of directional propagation. RIM also considers the impact of different battery statuses on signal strength. During simulation, nodes configured to communicate under RIM settings were found to have frequent signal coverage mismatches, which had further led to asymmetrical links and hidden terminal issues.

4. Severe environmental temperature change

The environmental temperature in which WSN is exposed to vary with different deployed environments such as industrial plant, cold room, and data centre. Severe temperature change is observed to degrade wireless link quality estimators considerably, such as the RSSI [87, 88, 89]. At temperatures ranging from 13 °C to 37 °C, RSSI was seen to have a linear decrement of 1.3 dBm with every increase in 10 °C [88]. Boano et al. [87] has also found a non-negligible impact of temperature on different radio chips, where the RSSI measured on CC2420 radio chip and Scatterweb Modular Sensor Boards dropped over 9 dBm and 6 dBm respectively when the temperature increased from -10 °C to 50 °C.

The effect of temperature also differs for the receiver and sender nodes. As the

temperature increased from 25 °C to 65 °C, authors in [89] observed that the sender node's output power decreased by 5 dBm, while the measured input power on the receiver node decreased by only 3 dBm. The reason for the change in temperature affecting the assessment of link quality is explained not as a malfunction of the RSSI measuring circuitry, but rather a decrease in ability of low-power radio to demodulate signals. It is said that the efficiency of the low noise amplifier stage 2 in a CMOS receiver drops. Due to the inconsistency of RSSI readings at different temperature fluctuation scenarios, RSSI-based protocols do not perform well. Therefore, Luomala and Hakala [88] suggested the use of frequency diversity instead of a single communication channel for a more accurate RSSI estimation. It is recommended to take temperature into account when deciding the transmission power used. For instance, 20% less transmission power is recommended for night operations where environmental temperature is expected to drop.

Quartz crystal's resonant frequency is also affected by the effect of changing environmental temperature [90]. Quartz crystal within a sensor node serves as a clock feature used mainly for time synchronisation activities. It was demonstrated that the change in operating temperature can cause more than 100-ppm difference on the crystal oscillator frequency over time [90]. This clock drift impacts nodes in multiple ways including the accuracy of time stamps produced, sleep and wake schedules of duty-cycle nodes, as well as transmission synchronisation between communicating nodes. The effects of temperature variations on WSN protocols are examined in TempLab [91]. Boano et al. found that the key bottleneck nodes failed at high operating temperature, leading to increasing end-to-end packet latencies and even network partitions (i.e. routing holes). Environmental noise was also measured to be higher when temperature increased, which had led to the following two phenomena. Firstly, link quality assessments on heated nodes were perceived as "weaker" due to elevated noise in the channel. Secondly, the number of packet losses had increased due to increasing Clear Channel Assessment (CCA) failures, where communication channel was occupied or noisy.

Overall, most electronic devices are designed with an optimal temperature operational range [91]. It is common for WSN protocols to assume that the operating temperature is static, and any link failures to be non-temperature-related. However, existing

researches have shown that the temperature effects on WSN operations should not be overlooked, and the role of temperature when assessing link quality should be taken into consideration, in particular for WSN operating under extreme temperature conditions.

2.3.2 Spatial Network Challenges

When a node transmits a packet, the radio signals can travel over multiple different propagation paths dictated by the physical entities within the WSN deployed environment. These signals experience path loss depending on the propagation paths taken. Path loss refers to the decrease in the power density of electromagnetic waves according to the power law function of the distance between the communicating nodes. Particularly in an indoor environment, spatial challenges can alter a signal propagation path, introducing greater path loss and affecting the assessment of link quality. These challenges include, but are not limited to Line-Of-Sight (LOS) or Non-LOS (NLOS) communication, distance communication between nodes, and static and mobile physical attenuators.

Propagation loss models are commonly used in the literature to estimate the reduction of power density of a transmitted electromagnetic wave as it propagates through space. The following path loss models are designed to take into account different power degradation levels caused by the respective spatial challenges.

1. Free space propagation loss

The Free-Space Propagation Loss (FSPL) model is shown in Equation 2.1. FSPL measures the attenuation of signal power between two antennas with the conditions of LOS communication within a free space, no hardware imperfection and effects of antenna gains. This model employs the exponential path loss degradation concept with separation distance d between transmitter and receiver, and operating frequency f. Due to the lack of accounting realistic entities such as terrains, reflectors within the deployed environment, the application of FSPL for general application is impractical. Rather, FSPL is usually only implemented as a basis for propagation situation and as a first approximation for link budgeting.

$$FSPL(d) = 20log_{10}(d) + 20log_{10}(f) + 92.45 \qquad (2.1)$$

where f is the operating frequency measured in units of GHz, and d is the separation distance between transceivers in km.

2. Shadowing effect

Log Normal Shadowing (LNS) is a widely accepted empirical model that estimates the generic path loss encountered over a distance in multiple environments. As shown in Equation 2.2, LNS consists of components rooted from theoretical FSPL model in Equation 2.1, which assumes exponential path loss with separation distance between transmitter and receiver. The inclusion of path loss exponent n allows LNS to be modified for different environments (refer to Table 2.1). On the other hand, zero-mean Gaussian distributed random variable X_σ allows LNS to generically estimate the path loss of nodes in the same test bed. This means that nodes deployed in the same region are expected to experience path losses of similar range.

$$PL(d) = PL(d_0) + 10nlog_{10}\left(\frac{d}{d_0}\right) + X_\sigma \qquad (2.2)$$

where d is the separation distance between transceivers, d_0 is the reference distance, $PL(d_0)$ is the measured reference path loss from the test bed, n is the path loss exponent depending on the operating environment, and X_σ is Gaussian variable based on the level of shadowing effect. Generally, d_0 should be in the far field of the transmitter so that the near-field effects do not alter $PL(d_0)$.

X_σ accounts for the shadowing effect from the environment in decibel (dB). Shadowing involves average large-scale probabilistic attenuation on received signals due to factors such as the direct obstruction of propagation path between communicating objects and multipath. In a situation where there is no shadowing effect, variable X_σ is zero. Site-specific values n and X_σ are determined from the empirical data.

Path loss exponent n, presented in Table 2.1 [92], varies depending on the environment conditions of signal propagation. The rule of thumb for path loss

exponent is 2 denoting free space and greater exponent for a denser environment [30, 92]. Determination of path loss exponent requires extensive channel measurement and modelling of the same environment by sampling both RSSI and distance between devices. A deterministic path loss exponent is usually limited to specific deployments. For instance, a path loss exponent in an indoor office environment is different from an indoor industrial environment [85, 93, 94].

Table 2.1 Path loss exponent for different WSN operating environments [92].

WSN operating environment	Path loss exponent n
Free space	2
Urban area cellular radio	2.7 to 3.5
Shadowed urban cellular radio	3 to 5
In building line-of-sight	1.6 to 1.8
Obstructed in buildings	4 to 6
Obstructed in factories	2 to 3

LNS model is used to estimate the signal strength of a received signal [95, 96, 77]. The relationship between path loss exponents and reference distances on long distance communication between GSM base-stations is investigated in [95]. Path loss exponents are calculated using least squares method where reference distances varied from 65 to 1560 meters. It is demonstrated that the path loss exponents reduce with increasing reference distance. This is because longer reference distance is less likely to be affected by near-field obstruction. In addition, the influence of a reference distance on path loss exponent weakens if the transceiver's antenna height increases. This is because there is lesser near-field obstruction on signal propagation with the use of a taller antenna. This phenomenon is also observed in [97, 98]. In other words, a higher antenna generally requires a smaller path loss exponent and the reference distance should always be in the far field of the antenna such that the near-field effects have less impact on the reference path loss.

Experimental path loss modelling for outdoor empty plaza, straight sidewalk, and

open grass field at 2.4 GHz is performed in [97]. It is concluded that a two-slope lognormal model is preferred over a one-slope model to account for the different signal degradation in different test sites. Similar observations are made in [99, 100] where two-slope log-distance models are superior in terms of the path loss estimation and applicability for wireless channel modelling. In particular, transmission at a low height is affected by environmental dynamics such as the irregular reflection, absorption, and scattering effects from crops.

Marinda et al. [93] conducted a LOS path loss approximation experiment on communicating nodes in an indoor environment. She found that depending on the communication channels, the measured signal strength fluctuates from 11 dB to 14 dB between static nodes. This range increased from 14 dB to 18 dB when conducted in an indoor industrial environment. The variation of received signal strength is explained with the real-world environmental factors like noise floor, radio interference and physical obstructions. Larger physical obstacles for example, in an industrial environment setting create higher signal attenuation and deeper deviation effects on received signals [85]. This phenomenon of substantial deviation of signal strength is referred to as the shadowing effect.

Tsai [101] examined the impact of the shadowing effects on the WSN sensing coverage and found that the sensing radius of a node is non-uniform. This is because the transmitted signals corresponded to different propagation paths at different directions and suffered dissimilar amounts of shadowing loss. An increase in shadowing effect by 2 dB was found to degrade sensing coverage by 10%. Furthermore, a node experiencing 8 dB X_σ will only perform at 66% of its full sensing coverage capability. As such, if a specific sensing coverage is desired, an increase in the number of nodes in the network is recommended.

3. Multipath fading

Similar to a shadowing effect, multipath fading is a spatial-related phenomenon that causes signal attenuation and deviation [30, 102, 103]. Puccinelli and Haenggi [30] conducted an experiment between two communicating nodes deployed in a room with no external disturbances. It was found that the RSSI measured did not fluctuate over time. Rather, RSSI only fluctuates when the entities in the deployed environment

were moved. The multipath fading level was uniquely determined by the topology of the deployed environment and was deterministic under static conditions without external interference. The change in environment had led to the change in multipath effect, where transmitted packets travel through different propagation paths depending on the transmitters' positions relative to the receiver.

The following factors are known to alter a propagation path:

1. Reflection – The phenomenon that occurs when a radio signal meets an obstacle surface and the angle of incidence is equal to the angle of reflection. Signal power is lost through absorption of the surface. Highly reflective surfaces include wet surfaces, metallic objects and mirrors.

2. Refraction – The phenomenon that occurs when a radio signal passes through an obstacle surface, causing a change in its direction and speed. Signal power is lost from reflection off the medium surface and absorption from the medium. The refraction level depends on the change of speed and angle of radio signal, which varies with the material of the medium.

3. Diffraction – The phenomenon that occurs when a radio signal meets an obstacle and travels around it. Diffraction loss is higher when the radio signal meets a sharp edged corner, and lower on smoother spherical surfaces.
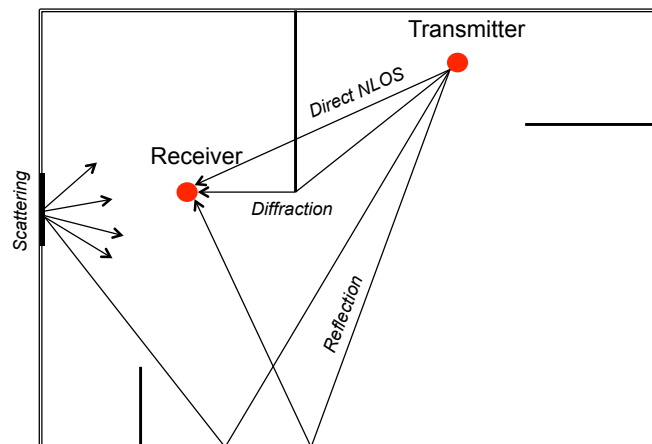
Figure 2.3. Simplified 2D multipath effects in an indoor environment.

Particularly in an indoor environment, every physical entity acts as a potential radio signal reflector. As a result, a node receives multiple copies of the transmitted signal

that are reflected off different parts of the environment [30, 65]. Figure 2.3 illustrates a simplified 2D multipath effect of a transmitted packet travelling along multiple propagation paths in an indoor environment. The transmission distance of reflected paths are longer than the direct LOS/NLOS path, thus causing the reflected signals to be weaker due to path loss, and are delayed by several nanoseconds. This delay in reception produces finer variance of channel impulse within the reception symbol duration due to the small coherence time of the channel relative to the application requirement. This phenomenon is referred to as short-term fading or fast fading [65, 104].

Mobile attenuators such as human bodies in the real-world environment are common. The multipath-fading phenomenon exhibits a linear dependency with increasing human density, while shadowing (long-term fading) is a direct consequence of human presence [41]. Authors in [81] measured the fading levels of communicating nodes under the presence of human movements and concluded that the movement of human bodies do not obstruct LOS as much as NLOS communication. Under NLOS conditions, fading levels ranges from 15 to 25 dB, while in LOS conditions, the range of fading levels reduced from 4 to 11 dB. The higher fading level under NLOS conditions is explained with the rarely completely shadowed dominant ray of LOS signal propagation.

Han and Abu-Ghazaleh [104] investigated the effects of fading level on IEEE 802.11 standard's optimisation protocol that overcomes link failures with increasing channel backoffs. Typically, the CCA at the MAC layer assumes that the link failures are caused by channel contention (i.e. simultaneous transmission by neighbouring nodes). However, this assumption is not true in distributed wireless network. The packet losses due to fading have led to an increase in backoff timer even without experiencing packet collisions. This creates unfairness in sharing of wireless medium, where the affected nodes are slower to compete for channels due to the increased in backoff duration. Hence to address this issue, a backoff algorithm that can discriminate between collisions and transmission losses due to fading is recommended. The phenomenon of multipath is also experienced differently on different channels [65, 105]. The estimation of distance can be misplaced by up to 20 meters between the best and the worse channel, in particular long-distance

communication [105]. In order to minimise the influence of fading levels on the measured signal power, measuring signal quality on multiple channels is also suggested to provide better link quality assessments.

Lognormal path loss models are superior over deterministic models (i.e. Rayleigh and Nakagami) due to their generality [106]. However, despite their popularity, they are not optimised for a dynamic environment. Lognormal path loss models rely on distance-based estimation, which can be affected by environmental changes such as seasonal and temperature change [96]. The need to measure the probability distribution of inter-sensor distance is also unrealistic to be obtained in real-world applications. Furthermore, such techniques do not take into consideration the three-dimension nature of a WSN deployment; nodes deployed at different heights and orientations will experience different path loss to distance relationships. It is to note that the lognormal path loss models in [85, 97, 99] are modelled for point-to-point communications, which is not representative for the entire deployment ground. This is to say when nodes are deployed in regions of the deployment ground that are subjected to different environmental dynamics, re-calibration of models is necessary.

Fading effect cannot be deterministically calculated unless the local positions of the communicating nodes, the geometry of the deployed environment, and the movements of mobile attenuators are known at all times. In reality, accounting for all these factors is impractical. Probabilistic approach such as LNS is therefore useful for tractability and link quality estimation. A node is typically unaware of the impact of fading level only until a link failure occurs or if the information about the received signals qualities is shared among neighbouring nodes. Furthermore, the effect of fading can also be mistaken as non-spatial network challenges, such as signal quality variation from a change in communication channel [30, 65, 105], or the constructive and destructive distortion during reception from concurrent transmissions [12]. Therefore, a node that has no knowledge of the spatial network challenges in its deployed environment may experience persistent degradation in communication reliability, particularly in an indoor environment.

2.3.3 Inter-WSN Interference

The complicated routing and reporting structures of a distributed wireless network

and the lack of centralised routing control render it hard for an optimisation protocol to predict traffic intersection points as well as concurrent transmissions. A dense arrangement of wireless sensor nodes without precise synchronisation for spectrum sharing can lead to inter-WSN interference. In this section, inter-WSN interferences are explained in terms of contention-based and congestion-based link failures.

1. Contention-based link failures

Contention-based link failures are referred to as packet losses caused by simultaneous transmissions from nodes within neighbouring range. The receiver node unknowingly receives and demodulates more than one packet at a time, resulting in packet corruption and subsequently discarded packets. Whitehouse et al. [107] suggested that a packet collision can be detected through a continuing search for a new preamble during packet reception. A collision is confirmed if a second preamble is identified during the reception of the first packet. However, to perform this technique would require the data layer to anticipate and compare the preamble of the second packet.

Contention to communicate in the shared spectrum usually occurs on a first come, first served basis. To avoid simultaneous transmissions, transmission synchronisation at the MAC layer, known as duty cycling, is commonly implemented. Nodes implemented with duty cycling protocol possessed the ability to access the channel, where it transmits only at a dedicated channel access periods (time-slots). Doing so minimises packet collisions and optimises nodes' sleep and wake operations for energy saving purposes [77, 78, 80 108, 109, 110].

There are two common types of duty cycling protocols. They are based on Carrier-Sense Multiple Access - Carrier Avoidance (CSMA-CA) and Time - Division Multiple Access (TDMA) technique. In the CSMA-CA (slotted) mode, beacons used to synchronise nodes are transmitted periodically. The period bounded by the beacons, called Superframe, is divided into 16 time-slots. These time-slots are grouped into Contention Access Period (CAP), Contention Free Period (CFP), and Inactive Period (IP). When the nodes need to transmit their data, they have to compete for the channel access during CAP. Prioritised nodes can request for guaranteed time-slot for transmission during CFP. All devices can put to sleep during the IP. A Optionally, Request to Send (RTS) and Clear to Send (CTS) messages are exchanged

to further mediate access to the shared spectrum. On the other hand, in TDMA mode, the time frame is divided into a fixed number of time-slots. Every time-slot is allocated for individual node to transmit only at a specific time, preventing concurrent transmissions. When nodes are not required to transmit, their radio interfaces can be switched down for power saving. Global synchronisation of TDMA mode among all nodes is possible if there is sufficient time frame length to be allocated. However, this would require the use of maximum time-slots throughout the network, and may introduce transmission latency. Synchronisation of time frame among nodes in the same region is a challenging task, as spatial reuse of a time-slot is possible. This is to say that a node outside of another's radio range can still transmit at the same time-slot if scheduled by different systems. This is known as the hidden terminal problem [110].

CSMA-CA and TDMA protocols also introduce non-negligible overheads required to organise spectrum sharing among nodes. These overheads involve specifying nodes' sleep and wake cycles, and dedicating transmitter-initiated (RTS) and receiver-initiated (CTS) roles [77]. Woo and Culler [108] highlighted that spectrum synchronisation packets constitute a significant overhead and should be implemented only when the media contention level is high. For example, additional Acknowledgement (ACK) packets may not be necessary if the sender node overheard the transmission of the same packet by the receiver, which implies that the receiver has already received and forwarded the packet. In network implemented using CSMA-CA (slotted) mode, seeking for channel access permissions may degrade channel utilisation if there are increasing number of nodes. Furthermore, the constant probing of channel and exchange of control packets may escalate energy consumption if not implemented optimally.

The effectiveness of collision avoidance depends on the location of the interferer from the source node. Han and Abu-Ghazaleh [104] demonstrated that as long as the measured signal power of the potential interferer at the sender node is above the carrier sense threshold, packet collision can be avoided. However, Whitehouse et al. [107] explained that the use of technique such as CSMA-CA, TDMA, RTS/CTS and ACKs are often assumed to be symmetrical. In practice this is not always true. Han and Abu-Ghazaleh [104] also highlighted that the additional RTS and CTS on top of

CSMA do not necessarily reduce packet collisions more than CSMA. Four successive transmissions (RTS, CTS, data and ACK) are more likely to fail compared to only data and ACK. However, upon link failures, the use of RTS and CTS loses only control packets while CSMA loses the data packet.

2. Congestion-based link failures

Congestion-based link failures are referred to as buffer overflow triggered by the inability to handle higher than expected network traffic. Buffers are blocks of memory set aside within a programme to hold data. When the buffer size is smaller than the data a programme attempts to write into, system congestion and memory access errors can occur [111, 112, 113]. As parts of the memory have to be reserved for processing the sensed data and maintaining network information, the remaining buffer for withholding of packets is limited. Limiting buffer size improves end-to-end packet latency while traveling on multi-hop routes. However, this may restrict the capabilities of the WSN application and protocol to handle high network loads [113, 114].

The detection of buffer congestion can be measured with abnormal packet losses, increasing length of buffer queue, overloading of channel noise, scheduling time, and packet delay [112]. The selection of congestion detection mechanism is dependent on the application and routing method implemented. For instance, a network operating in an industrial environment is expected to have high noise level [85]. As such, to detect network congestion with elevated channel noise may not be suitable.

A node may stick to one routing path consistently that it perceives to have the best quality such as the shortest routing path. Without prior knowledge of network traffic flow, imbalance-merging load at network intersection points can cause packet congestions [112]. If not promptly managed, stubborn congestion can further introduce more packets in the region due to persistent retransmissions. In this case, the traffic diversion technique to alternative paths is recommended to prevent congestions of packets in specific network regions [115]. Kang et al. [116] introduced Topology Aware Resource Adaptation (TARA) protocol to alleviate traffic congestions at network intersection points. It was pointed out that a fully utilised buffer space does not always translate to congestion and hence, TARA also measures

channel loading to detect elevated noise that may be caused by potential interferers. In TARA, an alternate path is generated between the distributor and the merger nodes. When congestion is detected, traffic is diverted through the distributor node along the alternate route and eventually merged at the merger node.

Network traffic estimation is as important as the reactiveness of the traffic diversion technique [115]. Traffic control strategies such as additive increase and multiplicative decrease of regional packets are often not efficient and reactive enough to resolve congestion issues. Combining network traffic estimation with traffic diversion technique is necessary to avoid congestions at all. The estimation of traffic is based on the affected nodes' buffer capacities as well as the number of packets expected at the interaction points. Upon expecting high network traffic, affected nodes are prompted in advance to divert their traffic to an alternative route or drop packets along the congested paths even before data is lost.

The potential inter-WSN congestions can be minimised with the reduction of network traffic using data aggregation technique. In data aggregation implemented protocol, a node combines data coming from different sources before forwarding the packet, thereby reduces the packets being transmitted [117, 118]. The number of traffic reduced depends on the number of clusters and the number of nodes in each cluster. The representative node (i.e. the clusters head) combines the received data from nodes in its clusters into a single packet, avoiding the need to forward all packets to the subsequent next hop. Data aggregation may also involve data fusion where sensory data are combined to produce a new but more accurate signal. By reducing the number of transmission, energy consumption is also minimised. This is provided that the energy consumed for data aggregation is less than the energy consumed for the transmission process. It is noted that data aggregation techniques do not take into account the impact of lossy links in real-world deployment. By grouping nodes into clusters, it fixates the parent and children relationships within the network and the limiting routing paths options between nodes. Any poor link in the network may become a bottleneck for all nodes in the lower depth of the network.

Overall, the organisation of spectrum usage to minimise inter-WSN interference requires an efficient use of existing information. This includes the estimation of the network traffic based on the application type, knowledge about the neighbouring

nodes' traffic flow to anticipate inter-WSN interference, and the ability to distinguish inter-WSN interference from other network challenges.

2.3.4 Wi-Fi Interference

Wi-Fi devices (IEEE 802.11) are commonly known to interfere the communication reliability of WSN nodes (IEEE 802.15.4) [36, 45, 46, 47, 48, 49]. Guo, Healy and Zhou [49] observed that IEEE 802.11 devices cause significant increase in link failures ranging from 2% to 25% on IEEE 802.15.4 nodes depending on the separation distances between the receptive nodes and interferers. It was highlighted that with optimal positioning of sensor nodes, these sporadic outages could be avoided. Yun et al. [119] emphasised that the ZigBee specification (network layer on top of IEEE 802.15.4 standard) relies on duty cycling and CSMA-CA mechanism to minimise packet losses from simultaneous transmissions. However, its inability to switch channels without human intervention means that it cannot effectively avoid Wi-Fi interferences that overpower WSN nodes communication.

Adequate frequency separation through channel diversity can avoid the impact of external interference on IEEE 802.15.4 networks [119, 120]. Wi-Fi interference is observed to be detectable with the combination of Energy Detection (ED) (received signal power estimation within channel), LQI and SNR of a received packet [120]. The combination of these metrics is said to be able to differentiate a packet failure due to poor receptive strength from a packet failure that experienced high environmental noise (i.e. higher chance of channel interference). Srinivasan et al. [66] also highlighted that regular Wi-Fi beacons are prominent and stand out from environmental noise. WSN nodes could distinguish IEEE 802.11 traffic even without decoding the signal, provided that the Wi-Fi's operating channel is known. However, the need for excessive channel monitoring for external interference can lead to increasing energy wastage [109].

Authors in [121] evaluated the impact of Wi-Fi traffic on ZigBee devices' communication quality in terms of SNR in a Judo training venue. They have showed that the SNR have degraded under concurrently transmitting Wi-Fi devices and the level of degradation depends on the position relative to the Wi-Fi access point. The increase of transmission power of ZigBee nodes is found to improve SNR level but

has limited impact if the interference source is too near. Therefore, an optimal deployment of WSN nodes is recommended to avoid Wi-Fi interference in a Wi-Fi dominant environment.

2.4 Persistent Wi-Fi Traffic and Spatial Challenges in an Indoor Environment

A summary of network challenges discussed in Section 2.3 is shown in Table 2.2. Existing literature have found that these network challenges can impose various impact on WSN communication reliability and each requires a different solution. In particular, Wi-Fi interference and spatial challenges are identified as two key network challenges in an indoor environment that pose as long-term and persistent issues to WSN communication reliability.

Numerous Wi-Fi access points can be found in a typical indoor work environment, deployed in a scattered manner to provide sufficient Wi-Fi coverage to "data-hungry" consumer devices such as smart phones, computers and mobile terminals. It is notable that Wi-Fi interference can spread widely and inconsistently in the frequency spectrum (occupying multiple channels) across the deployed environment. With high data uploading and video streaming applications becoming a trend in digital marketing, the need to improve WSN and Wi-Fi co-existence in the same operating environment becomes critical [16].

Wi-Fi interference does not influence all link quality metrics equally. Under Wi-Fi interference, signal strength-related WSN link quality parameters such as RSSI and LQI values are found not to coincide with the packet error-related link quality parameters such as Bit Error Rate (BER) and PRR [36, 49]. Wi-Fi interference is also known to degrade signal quality due to excessive noise in the communication channel and also distorts packets during reception. This in turn has introduced receiver-to-transmitter turnaround latency on IEEE 802.15.4 communications, resulting in further partial CCA detection and higher probability of a transmission failure [45].

CSMA-CA technique is commonly adopted as a standard feature for the resolution of contention in computer networks. However, fair channel access between different standards is not always achievable due to the differences in application requirements,

operating procedures and hardware capabilities. A Wi-Fi device with higher transmission power, greater bandwidth occupancy, higher transmission duty cycle and shorter backoff period than IEEE 802.15.4 devices, tend to occupy the channel more often. This poses as a persistent interference for the weaker low-power WSN devices, if not managed well.

On the other hand, spatial challenges such as environment path loss, long distance communications and mobile physical attenuators were found to introduce constant varying path loss between WSN nodes. Given that the indoor environments consist of varying object densities made up of different building materials, the interactions between real-world environments and the scattered WSN nodes are hard to model. Furthermore, a node often assumes symmetrical communication with its neighbour upon overhearing a packet. However, due to the signals travelling along different propagation paths, bi-directional connection is not always guaranteed.

The inability to accurately measure the impact of spatial challenges has further impacted on the performance of optimisation protocols. For instance, the irregular propagation due to the environmental path loss affects the ability of localisation protocols to estimate distances between communicating nodes. In [51, 68], receiver nodes measured packets of -90 dBm RSSI value at both distances of 7 m and 26 m. Even with calibration techniques such as moving average method, curve fitting and weighted average to map RSSI to distance, localisation errors cannot be disregarded [51]. The inaccuracies observed between RSSI and distance estimation rendered RSSI as an unsuitable single parameter to determine the location of a mobile node in an indoor environment.

Table 2.2. A summary of network challenges pertaining to WSN communication reliability.

Network challenges	Impact on WSN reliability	Solutions or detection mechanisms
	Imperfection operating conditions	
Energy depleted nodes	Early death of routers leaving routing holes in the network [55, 71, 72]	Duty cycling – Fair energy depletion through synchronisation transmission [78, 79] LEACH – Fair depletion through rotation of cluster heads [74, 75]
Hardware imperfection (battery status, hardware calibration)	Irregular transmission power leading to large transition region and asymmetrical communication [15, 27, 59, 63]	RIM – Propagation model that takes into account the random transmit power across all directions [68]
Temporal effect	Short-term link failure due to elevated channel noise, multipath and presence of human bodies [11, 25, 61, 81, 82, 83]	STLE – Monitors neighbours consecutive link failures and determine the reusability of lossy link [25] B-factor – Monitors consecutive link failures and adopts aggressive back off to delay transmission on lossy links [25]
Drastic change in environmental temperature	Degrade reception signal quality due to the inability to decode packets [87, 88, 89, 91]	Frequency diversity on multiple channels for a more accurate link quality assessment [88]

Spatial challenges		
Environmental path loss (attenuation, multipath fading)	Degrade reception quality leading to asymmetrical connectivity and packet loss [30, 51, 65, 68, 93, 101, 102, 104]	Propagation models that take into account the variability of received signal power due to the environment [82, 84]
	Increase channel access backoff timer [104]	Frequency diversity on multiple channels for a more accurate link quality assessment [65, 105]
Path loss due to mobile attenuators	Degrade reception quality due to the presence of human bodies [41, 51, 81]	Propagation models that take into account the variability of received signal power caused by the human movement [41, 51, 81]
Inter-WSN interference		
Contention-based	Elevated noise level [12]	Transmission synchronisation and energy detection with CSMA-CA and TDMA [77, 104, 108, 109]
	Distortion packet during reception [107, 110]	Detecting of second preamble during packet reception [107]
Congestion based	Buffer overflow, turnover latency, channel noise, abnormal packet loss [111, 112, 114]	Traffic diversion [115, 116] LEACH - Traffic reduction [574, 117, 118, 122]
Wi-Fi interference		
Contention-based	Degrading throughput, noise level [48, 82, 83, 121]	Adequate frequency separation [82, 119, 120]
	Affecting channel accessibility [36, 45, 49]	Adequate distance separation [48, 121]

2.5 Chapter Summary

This chapter reviewed the network challenges in an indoor environment that have an impact on WSN communication reliability. They are the imperfect operating conditions, spatial challenges, inter-WSN interference and Wi-Fi interference.

WSN nodes have limited lifespan and computational capability. For nodes to monitor the dynamics within the operating environment require constant energy draining operations such as the detection of second preamble to identify packet collision, monitoring of multipath effects on multiple channels, and overhearing neighbouring node's transmitted packets to determine temporal links. Unless the local positions of the communicating nodes and interferers, the geometry of the deployed environment, and the movements of mobile attenuators are known at all times, it is impractical for the nodes to anticipate and react to all kinds of network challenges.

Wi-Fi interference and spatial related network challenges (i.e. physical changes in the environment altering multipath and shadowing effects) are identified as two key network challenges that pose as long-term and persistent issues to WSN communication reliability. Particularly in an indoor environment, they degrade WSN communication in many ways. Since each of them requires a different solution, distinguishing them from other forms of network challenges is critical. Thus in Chapter 3, a series of controlled experiments is conducted to investigate the impact of Wi-Fi interference and spatial network challenges on WSN communication reliability.

3 WSN Performance Under Persistent Wi-Fi Traffic and Spatial Challenges

Chapter 3 investigates the influence of persistent Wi-Fi traffic and spatial challenges on WSN's communication reliability. Separate experiments are conducted using NXP's proprietary wireless sensor nodes deployed in controlled indoor environments under simulated network challenges. In Section 3.1, the impact of persistent Wi-Fi traffic on concurrently transmitting WSN nodes is investigated at the lower layers of a Low-Rate-Wireless Personal Area Network (LR-WPAN), IEEE 802.15.4 standard. In this experiment, the distance between WSN communicating nodes and distance between WSN nodes and Wi-Fi transmitting source are varied. Their dynamic relationships are evaluated from link quality parameters including Bit Error Rate (BER), LQI, CCA count and PRR.

In Section 3.2, a novel data extraction platform called Network Instrumentation (NI) is developed within node's Zigbee PRO stacks, to extract unique Neighbour Table (NT) and Routing Table (RT) information from experimented nodes. Section 3.3 describes the experiment set up of nodes in an indoor office under the influence of simulated (1) poorly deployed environment and (2) human movement. Adaptive Network-based Fuzzy Inference System (ANFIS) technique is also introduced in Section 3.3 to model spatial-related link failures. The generated models trained with different combinations of inputs are compared and analysed in Sections 3.4 and 3.5, which highlighted the importance of cross-layer parameters and careful selection of training parameters to better predict link failures. Lastly, Section 3.6 concludes the chapter.

3.1 Investigation of WSN Performance Under Persistent Wi-Fi Traffic

In Section 2.3.4, WiFi devices are reviewed to have higher transmission power, greater bandwidth occupancy and higher transmission duty cycles, which often overpowered "weaker" WSN nodes when competing for channel access. This creates an unfair spectrum-sharing phenomenon. Therefore, in this section, the ability of WSN nodes to communicate in the same spectrum as a persistent Wi-Fi traffic is studied from the IEEE 802.15.4 standard perspective.

3.1.1 IEEE 802.15.4 and IEEE 802.11 bgn Standard Experimental Setup

1. IEEE 802.15.4 standard

IEEE 802.15.4 standard is defined as the physical and MAC layers for LR-WPAN devices. The physical layer is responsible for a WSN node's data transmission and reception. Its main functions include carrier sensing, carrier frequency selection, encryption and decryption, and modulation and demodulation. The MAC layer offers channel management capabilities such as accessing control to a shared spectrum, detection of channel's availability, protection of transmission from interference, and providing services for nodes to associate/disassociate the network.

Experimental node's configuration

Two JN5168 development test boards [39] manufactured by NXP Semiconductors are used to simulate two communicating WSN nodes. Nodes equipped with IEEE 802.15.4 standards are configured to exchange data packets of 100 bytes size every 10 ms at a data rate of 250 kbps on channel 20 (2.45 GHz). The transmission power is set at 0 dBm. Every transmission is independent from the previous one such that the transmission failure due to buffer overflow is avoided [46]. The maximum retransmission and maximum CSMA backoff are set to zero. This is done so that whenever the node fails to access the channel during transmission, the entire process is considered to have failed. Lastly, if no ACK were received after a data packet is transmitted, the transmission is also considered to have failed. All exchanged data are recorded on Dell Latitude E6330 laptops connected via USB, from which the

following parameters are extracted.

1. Link Quality Indicator (LQI) – LQI is determined over the first four bytes of a correctly received data packet. It represents the number of chip errors and the average energy detected over the four bytes. In the JN5168 implementation, a LQI value of 250 indicates a maximum quality frame and a value of 0 is assigned to the lowest quality.

2. Bit Error Rate (BER) – Unlike LQI, BER is formulated from both correctly received and corrupted data packets. The received data packet is compared to the known frame structure and BER represents the number of incorrect bits in a received packet. Incorrect bits can be caused by noise, interference, or bit synchronisation errors. The higher the BER, the poorer the quality of frames.

3. Packet Reception Rate (PRR) – PRR in Equation 3.1 is defined as the success rate for a node to transmit a data packet to its destination node and to receive an ACK in return. 100% PRR indicates a perfect reception of all data packets. Here, PRR only accounts for packets that are transmitted across the channel and does not include CCA failure.

$$PRR = 1 - \frac{Number\, of\ transmission\ without\ ACK}{Number\ of\ successful\ CCA\ that\ leads\ to\ transmission} * 100 \qquad (3.1)$$

4. Unsuccessful Clear Channel Assessment (CCA) count – +1 CCA count increment relates to a channel access failure, where energy is detected above a threshold. The number of CCA count relates to the amount of noise in the transmission channel such that a higher CCA count represents a consistently noisy channel.

2. IEEE 802.11 bgn standard

IEEE 802.11 b, IEEE 802.11 g and IEEE 802.11 n standards specify the physical and MAC for WLAN. IEEE 802.11 bgn standard has been widely adopted in Wi-Fi networks. They operate on 13 overlapping 22 MHz wide frequency channels in the 2.4 GHz ISM band. The different versions of IEEE 802.11 standards employ the same CSMA/CA mechanism defined in the original IEEE 802.11 standard, but are enhancements from the previous version that has a higher data rate and transmission

range.

Similar to IEEE 802.15.4, an IEEE 802.11 bgn node is required to sense for noise and concurrently transmitting devices in the channel before initiating a transmission. If the channel is detected idle for Distributed coordination function Inter-Frame Space (DIFS) time, the transmission will proceed. Otherwise, the Wi-Fi device will initiate a backoff timer with a randomly chosen interval. The decrement of the backoff timer will happen only when the channel is detected to be idle for a backoff time-slot. The backoff timer will also pause when a concurrent transmission is detected and resume when the channel is idle again. The Wi-Fi device is allowed to transmit only after the backoff timer reaches zero.

Experimental device's configuration

Wi-Fi traffic is generated using the Linksys Wireless-N Router (WR) (WRT160NL) [123] connected to a Dell Latitude E6330 laptop via an Ethernet port. Iperf programme [124] running on the laptop generates User Datagram Protocol (UDP) packets of 1500 bytes size to a mobile device, Samsung Galaxy Note II N7100. The WR transmits at a data rate of about 130 Mbps, depending on network conditions. The WR transmission power is capped at 21 dBm and is configured to transmit on either channel 9 or 11 to simulate a frequency offset of 2 MHz and 12 MHz respectively from IEEE 802.15.4 channel 20.

3.1.2 Design of Experiment to Simulate the Impact of Persistent Wi-Fi Interference

Experiments are conducted in an office aisle during non-working hours in the absence of human movements except the experimenter. A sanity check is performed using an IQ analyser, Rohde & Schwarz FSV30 [125] and confirmed that no dominant uncontrolled interference was present in the operating channels. In addition, the BER and PRR of the WSN nodes were recorded as majority 0 and 100% respectively before the commencement of experiments.

The objective of this section is to understand the performance of WSN communication under the three different deployment settings; they are operating without Wi-Fi interference, frequency offsets from WiFi operating channel and

varying operating distance between WSN nodes. Table 3.1 illustrates six test conditions, 1A to 1F, categorised into "with or without Wi-Fi interference", "Wi-Fi interference frequency offset" and "IEEE 802.15.4 nodes operating distance". The different frequency offsets between the operating channels between different wireless standards is to understand if a larger frequency offsets can minimise or avoid Wi-Fi interference. On the other hand, the different operating distances of IEEE 802.15.4 communicating nodes are used to vary the impact of Signal to Interference Ratio (SIR) with varying IEEE 802.15.4 signal strengths. For instance, in test conditions 1B, 1D and 1F, the receiver node operating at a greater distance from sender node has a lower SIR than 1A, 1C and 1E. It is noted that in test conditions 1A to 1D, the WR acting as the Wi-Fi interference is placed 5 m away from the IEEE 802.15.4 sender node. Test conditions 1E and 1F, without Wi-Fi interference are used as reference conditions.

Table 3.1. Experiment 1 - Test conditions. IEEE 802.15.4 nodes operating with varying distances to simulate the different impact of Wi-Fi interference on WSN communication reliability.

Test conditions	Wi-Fi and IEEE 802.15.4 nodes frequency offset	IEEE 802.15.4 nodes distance apart	Experiment setup
1A	2 MHz Wi-Fi channel 9	1 m	
1B	2 MHz Wi-Fi channel 9	10 m	
1C	12 MHz Wi-Fi channel 11	1 m	
1D	12 MHz Wi-Fi channel 11	10 m	
1E	-	1 m	
1F	-	10 m	

3.1.3 The Impact of Persistent Wi-Fi Traffic on WSN Link Quality Parameters

Figure 3.1 shows the LQI performance of IEEE 802.15.4 nodes in test conditions 1A to 1F. Each test condition provides 80 LQI samples. LQI outliers are observed to be inconsistent among the test conditions. Note that LQI is based on a correctly received data packet. Hence, these outliers are correctly decoded data packets with varying chip correlation, which can be caused by the background noise and multipath effects from the environment.

It is observed that LQI does not provide a significant difference (P value < 0.05) between test conditions with and without WiFi interference. Instead, LQI varies

according to the operating distance between IEEE 802.15.4 nodes, acting much like a signal strength indicator. For test conditions with 1 m and 10 m operating distance between IEEE 802.15.4 nodes, the LQI are approximately 179 and 102 respectively. The maximum LQI mean difference between test conditions of 1 m and 10 m are only 3.525 and 1.089 respectively.

 Figure 3.2 shows the BER performance of IEEE 802.15.4 nodes under test conditions 1A to 1F. Under test conditions 1A to 1D, the WR is deployed statically, such that the channel occupancy for IEEE 802.15.4 sender node is kept constant [48]. It is observed that BER is found only in test conditions 1B and 1D. The higher BER can be explained by the concurrent Wi-Fi traffic leading to wrongly decoded packets. Under test conditions 1A and 1C where IEEE 802.15.4 nodes have a better SIR (due to a stronger IEEE 802.15.4 signal at 1 m operating distance), bit errors are not found.
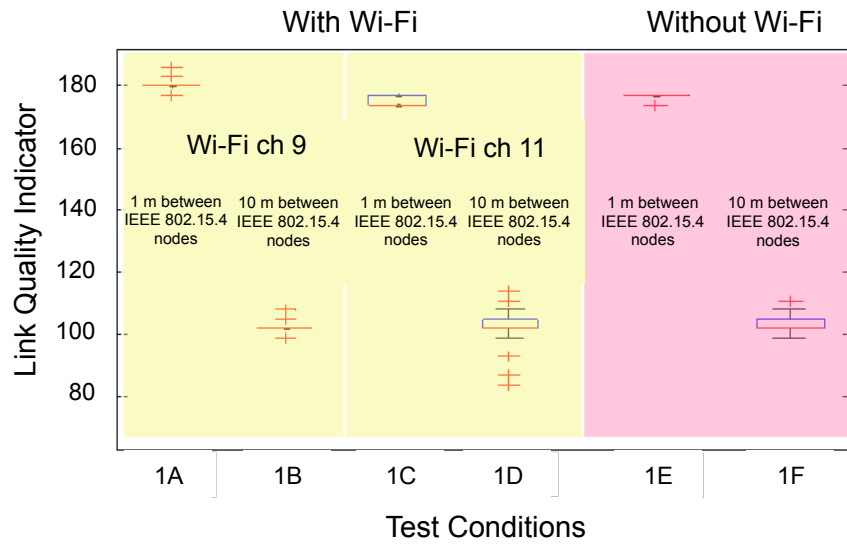
Figure 3.1. Collective LQI of IEEE 802.15.4 nodes under persistent Wi-Fi traffic in test conditions 1A to 1F.
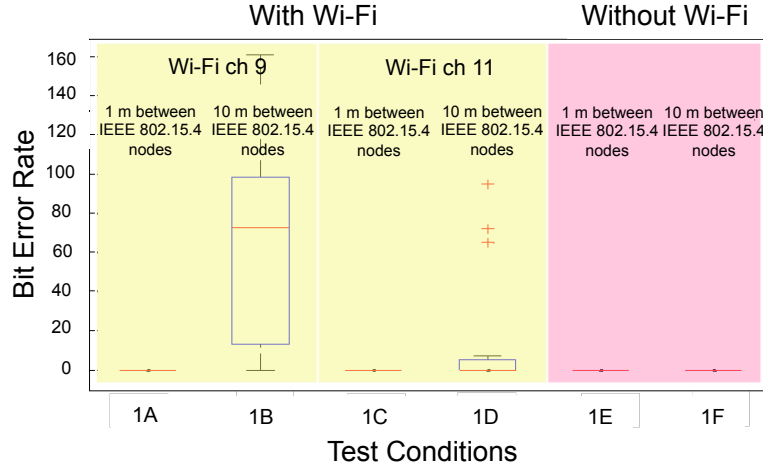
Figure 3.2. Collective BER of IEEE 802.15.4 nodes under persistent Wi-Fi traffic in test conditions 1A to 1F.

Every transmission attempts will begin with a CCA attempt as explained in Equation 3.2. The total CCA attempts combine the number of failed and successful CCA attempts as shown in Equation 3.3. A CCA attempt may fail if the node senses noise in channel 20. Otherwise, a successful CCA indicates a clear channel and commencement of packet transmission. Referring to Equation 3.4, a successful CCA can result in either a successful transmissions or failed transmissions, depending if an ACK is received within the maximum MAC ACK waiting period.

$$Total\ TX\ attempts = Total\ CCA\ attempts \qquad (3.2)$$

$$Total\ CCA\ attempts = Total\ failed\ CCA + Total\ successful\ CCA \qquad (3.3)$$

$$Total\ successful\ CCA = Total\ successful\ TX + Total\ failed\ TX \qquad (3.4)$$

Table 3.2 shows the results of 20480 transmission attempts for test conditions 1A to 1F. It is clear that the transmission failures, if any, are negligible as long as there is sufficient frequency separation from the interferer. As expected, the lowest PRR was recorded in test condition 1B at 91.05 %. Under test condition 1B, the IEEE 802.15.4 nodes are expected to have the lowest SIR with the Wi-Fi interference operating at

only 2 MHz frequency offset. It is observed that the measured PRR corresponds to BER, where the highest BER (most bit errors) is also found in test condition 1B.

Table 3.2. The breakdown of 20480 transmission attempts.

Test conditions	1A	1B	1C	1D	1E	1F
Total TX attempts	20480	20480	20480	20480	20480	20480
Total failed CCA	11907	13350	10215	10744	1	1
Total TX (successful CCA)	8573	7130	10265	9736	20479	20479
Total failed TX	8	638	0	278	0	0
Total successful TX	8565	6492	10265	9458	20479	20479
PRR%	99.9	91	100	97.9	100	100

The Wi-Fi interference is reflected in the number of CCA failures. A higher CCA count is observed in test conditions 1A to 1D regardless of the operating distance between the WR and IEEE 802.15.4 sender node. While under test conditions 1E and 1F, the CCA failures are negligible. This finding confirms that the majority of the IEEE 802.15.4 transmission failures are due to the inability to access the communication channel rather than corrupted packets.

Communication robustness between IEEE 802.15.4 nodes is achieved via the CSMA/CA mechanism, where a node is denied channel access if the channel is occupied. By default, the IEEE 802.15.4 standard defines the maximum number of CCA backoff as four. Since CCA failures do not dominate in PRR calculations, PRR may not reflect the actual amount of Wi-Fi interference. For instance, a node operating in a "noisy" environment may still achieve a relatively good PRR of more than 97.9%.

In this experiment, UDP transmission does not use flow control. UDP packets are flooded into the medium without checking if the spectrum is occupied, simulating an extreme case of Wi-Fi interference. This experiment shows that even under persistent Wi-Fi interference, careful channel configuration and deployment of WSN nodes can

minimise or avoid the impact of Wi-Fi traffic. WSN nodes that are deployed at 10 m apart should operate at least 12 MHz frequency apart from Wi-Fi operating channels.

3.2 Extraction of Zigbee PRO Parameters using Network Instrumentation

Typically, external sniffers have to be deployed throughout the WSN's lifetime to obtain information on link quality of communicating devices. However, the use of sniffers is impractical due to two factors. Firstly, the resources needed are significant and grow exponentially with increasing network size. Secondly, the information collected on the sniffers may not be representative, as sniffers are subjected to packet distortion from interference. For instance, other devices operating in the same spectrum may transmit at the same time, and cause the sniffer to receive a distorted packet. Therefore, in order to extract link quality parameters from WSN nodes deployed in real-world environment, a new component called Network Instrumentation (NI) is developed into the Zigbee PRO stack of the WSN nodes.

3.2.1 Network Instrumentation Architecture

1. ZigBee PRO

ZigBee PRO [40] is a wireless communication specification based on the IEEE 802.15.4 standard. ZigBee typically operates in the 2.4 GHz ISM radio bands with data rates up to 250 Kbit/s. Figure 3.3 illustrates the ZigBee protocol stack architecture, where its operations and features are built on top of the IEEE 802.15.4 standard. The ZigBee specification further includes the network layer and application layer. Their purposes include keeping track of the roles of devices, managing network requests, de-multiplexing of incoming messages to the appropriate applications, and triggering activities in the MAC layer such as initiating the network and assigning network addresses.

Figure 3.3. ZigBee protocol stack.

2. Network instrumentation

NI, as shown in Figure 3.4, is designed to extract Neighbour Table (NT) and Routing Table (RT) periodically. A WSN router's NT contains communication information about its neighbouring nodes that are within reception range. This information includes network addresses of neighbouring nodes, their respective RSSI, depth, relationship to the neighbour, and device type. If node B is found in node A's NT, node B and A are assumed to have established communication in the past 60 seconds. Similarly, if a previously existing node B is no longer found in node A's NT, communication between them is assumed to have failed. A WSN router also holds information about the state of route discovery and already established routes. This information is stored as entries in the RT, consisting of the addresses of destination and next hops. Querying the NT and RT of all routers in the network allows us to obtain the actual routing paths in which packets are relayed between nodes.

Information from the NT and RT entries provide link quality knowledge about the local environment around a router, and the communication reliability of the selected routing paths towards a destination node. Variations in entries within NT and RT are indicators of link stability and routing path stability respectively. Link stability is defined as the rate in which a node drops out from an existing link and re-joins it.

Poor link stability suggests a node is deployed with a substandard connection with a neighbouring node where packets transmitted to it have a higher chance of failure. On the other hand, routing path stability is defined as the rate in which a selected next hop towards the destination node changes, leading to a variation along the existing routing path. Poor routing path stability indicates that a routing path is unstable due to frequent failing/ re-joining of connection or frequent changes of parent node towards the destination node.
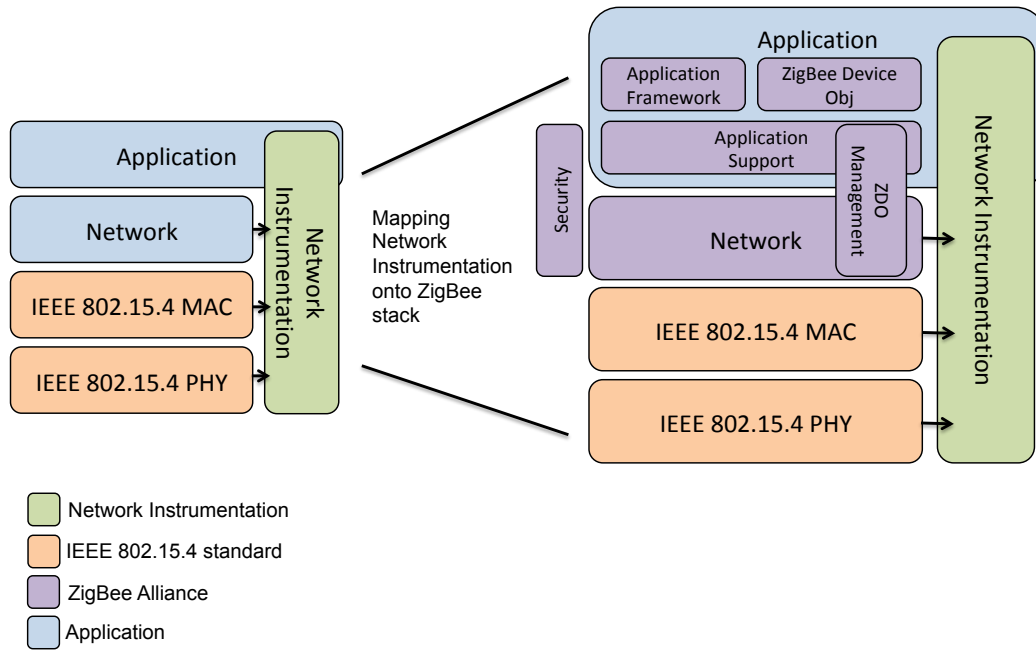
Figure 3.4. Mapping of Network Instrumentation onto ZigBee stack.

For NI to function seamlessly, three design considerations were derived.

1. Minimal packet overhead – To minimise the impact of energy cost and application latency of the WSN application, only necessary link quality parameters at a sufficient granularity should be extracted.

2. Maintain full standard compliancy – NI should maintain full ZigBee PRO HA compatibility where only standard API is used. This allows seamless interoperability with newly added ZigBee PRO devices.

3. Future proof – Information extracted from the nodes should be interpretable in similar protocols. Extraction features of NI should also be applicable for non-ZigBee devices.
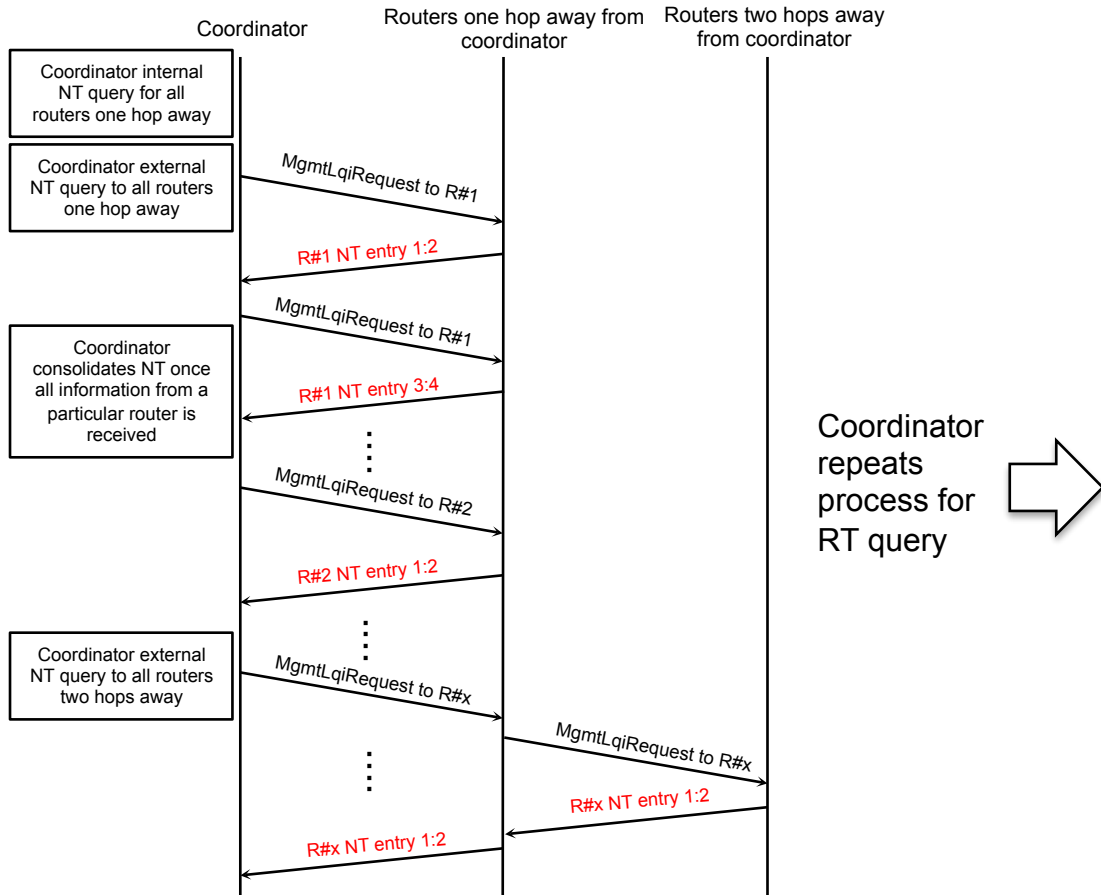
Figure 3.5. Flow diagram – Network Instrumentation to extract NT and RT from WSN routing devices in the network.

Figure 3.5 shows the NI flow diagram to extract NT and RT information from WSN routing devices. Table 3.3 illustrates the code execution for the coordinator to query NT and RT periodically from all routers. The query interval depends on the size of the network.

Table 3.3. Code execution flow – Coordinator to query NT and RT information from all routing devices in the network.

Events	Execution
Coordinator to access its own NT	1) Coordinator shall access its own NT by executing "ZPS_eAplZdpMgmtLqiRequest" command and selecting itself as the destined node. a. Coordinator has access to the addresses of all routers that are one hop away
Coordinator to access NT of all routers	2) Coordinator shall access the NT of routers that are one hop away by executing "ZPS_eAplZdpMgmtLqiRequest" command with the targeted router as destined node. a. Coordinator has access to the addresses of all routers that are two hops away 3) Step 2 shall be repeated for routers in the subsequent hops (relative to coordinator) until all routers are covered.
Coordinators to repeat step 1 to 3 to query Routers' RT	4) Once, all router's NT are obtained, coordinator shall repeat step 1 to 3 to query routers' RT using the "ZPS_eAplZdpMgmtRtgRequest" command.

3.2.2 WSN Parameters to be Monitored

Information from NT and RT is post-processed into the following four parameters.

1. Neighbour Table Connectivity (*NTC*)

Table 3.4 illustrates an example of four consecutive NTs of node A, queried at 15 minutes intervals. NT consists of information about its neighbouring nodes B, C and D at the time of data query. Neighbour Table Connectivity (NTC_{AB}), similar to PRR, is the percentage of node B captured in node A's NT, observed over a number of NT windows. NTC_{AB} indicates the consistency of node B connected to node A in percentage. The calculation of NTC_{XY} is shown in Equation 3.5. 100% NTC_{XY} indicates that node Y is consistently found in node X's NT and packets transmitted from node Y is well received on node X. Conversely, 0% NTC_{XY} indicates that node Y is not found in node X's NT and node X has not received any packets transmitted from node Y.

Table 3.4. An example of four consecutive Neighbour Tables of node *A* at 15 minutes intervals.

NT *A* (t = x)		NT *A* (t = x + 15)		NT *A* (t = x + 30)		NT *A* (t = x + 45)	
Entry	RSSI (dBm)	Entry	RSSI (dBm)	Entry	RSSI (dBm)	Entry	RSSI (dBm)
B	-88	-	-	*B*	-87	-	-
C	-62	*C*	-62	*C*	-63	*C*	-63
D	-78	*D*	-80	-	-	*D*	-82

2. Bi-direction Neighbour Table Connectivity (*BNTC*)

Similar to *NTC*, *BNTC* can be explained as the rate of connectivity between two nodes in percentage. Both $BNTC_{AB}$ and NTC_{AB} represent the outgoing and incoming communication success rates between nodes *A* and *B* respectively, and are calculated in a similar manner (Equation 3.5). In other words, $BNTC_{AB}$ is equivalent to NTC_{BA}. Associating both *NTC* and *BNTC* indicates the likelihood of link asymmetry between two nodes. An imbalance in *NTC* and *BNTC* highlights irregularity in receptive quality where one node can receive packets from the other but not the other way around.

$$NTC_{XY} = \frac{Total\ appearance\ of\ node\ Y\ in\ all\ NT_x\ collected}{Total\ NT_x\ collected} * 100 \qquad (3.5)$$

3. Mean Received Signal Strength Indicator (*mean RSSI*)

Mean RSSI$_{XY}$ as stated in Equation 3.6 is the average RSSI in dBm of node *Y* measured at node *X* over a number of NTs window. *Mean RSSI* is a measure of average power present in received packets. Mean RSSI$_{AB}$ suggests how well node *B* is received by node *A* in terms of signal strength over an observed period.

$$Mean\ RSSI_{XY} = \frac{1}{n}\sum_{i=1}^{n} RSSI_{XYi} \qquad (3.6)$$

4. **Average Coefficient of Variation RSSI (*ACV RSSI*)**

ACV RSSI$_A$ is the average coefficient of variation of RSSI in dBm of all links found in node A's NT. ACV RSSI$_A$ can be explained as a measure of relative variability of received signal strength between all neighbouring nodes around node A during the observed windows. A high *ACV RSSI$_A$* value indicates that the RSSI measured from all neighbouring nodes are subjected to high dispersion or high channel variability.

The calculation of ACV RSSI$_A$ is expressed as:

$$ACVRSSI_{XY} = \frac{1}{n}\sum_{i=1}^{n}\frac{SD\ RSSI_{XYi}}{Mean\ RSSI_{XYi}} \qquad (3.7)$$

where n is the number of neighbouring nodes around node X. *SD RSSI* and *Mean RSSI* is the standard deviation of RSSI and mean of RSSI of the neighbouring node i over the same observed windows respectively.

3.3 Modelling of Spatial-Related Link Failures using ANFIS

It can be seen from the literature review in Chapter 2 that WSN link quality parameters are imprecise at detecting the causes of link failures, and the network challenges in the deployed environment can impose different influences on WSN communication. Given that spatial challenges in an indoor environment cause persistent uncertainties in link quality assessment, the need to take them into consideration is critical to optimise WSN communication reliability. Therefore in this section, controlled experiments are conducted to extract link quality performance parameters from ZigBee PRO nodes under the influence of simulated spatial challenges. As illustrated in Figure 3.6, parameters – *NTC, BNTC, mean RSSI* and *ACV RSSI* – are used as training inputs to model three link failure conditions using Adaptive Network-based Fuzzy Inference System (ANFIS) technique. ANFIS (explained in Sections 3.3.2 and 3.3.3) is chosen to leverage on its tolerances for imprecision and partial truth to achieve robustness and accuracy, particularly in real-world systems. The link failure conditions are as follow:

- Link failure due to poorly deployed environment – Link failures that are influenced by the dense and static physical obstructions between nodes or if

nodes are located too far apart.

- Link failure due to human movements – Link failures that are influenced by the physical obstruction of a human in close proximity.

- No failure – Best-case scenario where a node is not subjected to any influence of spatial challenges. Any failures under such conditions are considered negligible.
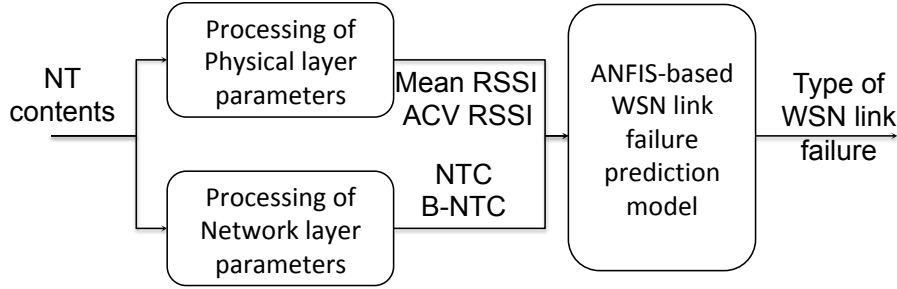
Figure 3.6. Block diagram – ANFIS-based model to predict spatial challenges.

3.3.1 Design of Controlled Experiment to Simulate Spatial Challenges

In this section, experiments simulating poorly deployed environment and human movement are described. Experiments are conducted during non-working hours (i.e. in the absence of human movements except the experimenter). A sanity check was performed using an IQ analyser, Rohde & Schwarz FSV30 [125] and confirmed that no dominant uncontrolled interference was present in the operating channels.

1. Experiment 1 – Poorly deployed environment

Experiment 1 illustrated in Figure 3.7, consists of four ZigBee PRO [39] nodes uniformly deployed in an open office environment, 5 m apart from one another. The experimental layout simulates WSN nodes communicating with each other under the influence of reception signal decay and increasing signal attenuation, which mimics long distance communication and static physical obstructions respectively. All nodes were mounted in the same orientation and at a height of 1.3 m on desk partitions. It is important to note that due to the difference in the local operating environment around individual nodes, the propagation paths of transmitted signals are different. As such, uniform signal strength decay between nodes cannot be expected. This means that despite the similar operating distance between node *A* to node *B* and node *B* to node

C, their link quality measurements may not be the same. By doing so, a more realistic set of measurements as compared to computer-simulated data is produced.
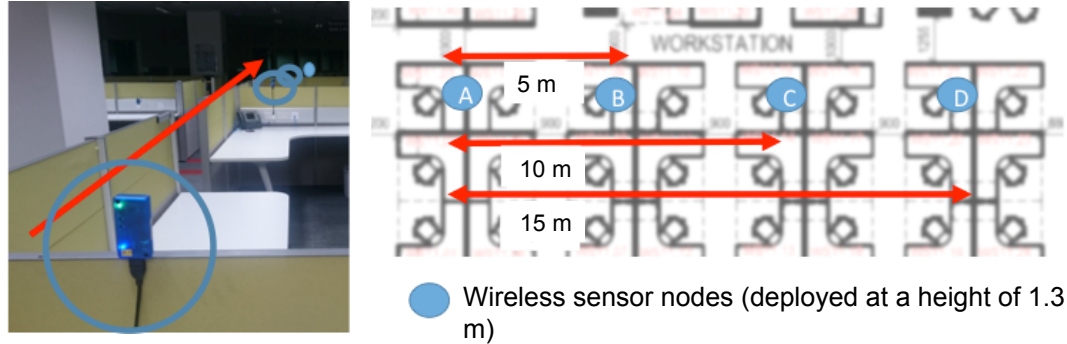
Figure 3.7. Experiment layout – Simulation of wireless sensor nodes communicating under progressively poor deployed environment conditions in an open office.

2. Experiment 2 – Human movement

Experiment 2 as shown in Figure 3.8 consists of two ZigBee PRO nodes [39] deployed 4.5 m apart with LOS communication. The nodes were mounted on tripods, elevated 1.3 m from the ground. Prescribed human walking sequences with LOS obstruction were introduced to simulate nodes communicating under the influence of a single human movement profile. Experiment 2 was conducted in both an open space laboratory and open office, where different multipath and fading effects are expected.
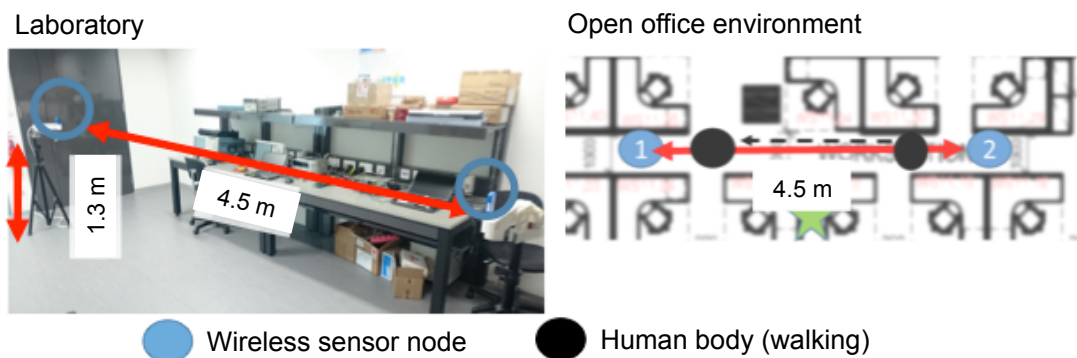
Figure 3.8. Experiment layout – Simulation of wireless sensor nodes communicating under the obstruction of a single human movement profile in a laboratory and open office.

3.3.2 Fuzzy Inference System and Artificial Neural Network

There has been a constant debate about whether the Artificial Neural Network (ANN) or Fuzzy Inference System (FIS) is more optimal for modelling complex and non-linear systems [126, 127, 128, 129]. ANN mimics the biological neural networks of animal brains, is known for its ability to approximate any function. However, ANN technique is often viewed as a black box. Analysing the trained network is difficult due to the complex knowledge representation where model structures used to map the input and output spaces are driven by a data-based objective functions and layers of mathematical processes [126]. The framework of an ANN consists of a collection of processing neurons called units that are arranged in a series of layers, interconnected with connection weights. Units of individual layers receive inputs from the previous units multiplied by the connections weights, and the outputs are computed by non-linear functions of the sum of its inputs. Connection weights, representing the learnt relations between units, are adjusted iteratively according to the differences between the targeted and actual output. This mapping process is repeated until a desired accuracy of the model is met.

On the contrary, FIS mimics the concept of human reasoning and decision-making. Users can comprehend the developed model intuitively through the Fuzzy sets theory that maps inputs to outputs. For instance, the Mamdani-type FIS [130] models a system by synthesising a set of linguistic control rules obtained from domain experts, such as an engineer describing a cooling system.

$$\textit{Room Temperature of 39 degree} \text{ is translated into } \textit{Room Temperature is Very Warm} \tag{3.8}$$

An element in a Fuzzy set (*Room Temperature*) is mapped onto Membership Functions (MFs) (i.e. either *Very Cold, Cold, Warm* or *Very Warm*), where a grade of a set is given. Multiple elements can be combined to form a list of IF-THEN rules, where the relationship between elements (antecedents) can be translated into a decision (consequents) as shown in Equations 3.10 and 3.11.

$$\textit{IF antecedents(s) THEN consequents} \tag{3.9}$$

$$IF \text{ “Temperature is Very Warm” THEN “Turn on AC”} \qquad (3.10)$$

$$IF \text{ “Temperature is Cold” THEN “Turn on Heater”} \qquad (3.11)$$

Both ANN and FIS techniques have their advantages and disadvantages. ANN possesses high fault tolerance of incomplete and noisy data, while FIS allows the incorporation of expert knowledge into the model as Fuzzy rules [126]. Chapter 2 discusses the imprecise-ness of WSN link quality parameters mainly due to the nature of low-power radio propagations under the influence of environmental dynamics. The ability to describe the training inputs parameters' behaviours under different conditions is highly valued. Unlike ANN where network structure lacks physical significance, the construction of Fuzzy rule-base in FIS can be viewed as grey-box modelling. FIS combines verbal modelling where parts of the system are modelled with linguistic control rules. This is done in a way prior knowledge can be instilled to the inferred behaviour of the system. In addition, the linguistic representations of model structures provide users the ability to interpret information within the model, and estimate the unknown in a semantic manner.

3.3.3 Adaptive Network-based Fuzzy Inference System Architecture

Researchers have progressed to incorporate soft computing with Fuzzy rule-based classifiers. Neuro-Fuzzy classifier such as ANFIS [131] is one of the most researched topics at this juncture. ANFIS, a Takagi-Sugeno (TS) technique [132], combines the approximate reasoning of FIS with the learning features of ANN into a single data learning technique.

1. Grid partitioning

Functionally, ANFIS divides the input and output space using the grid partitioning technique, where each partition represents a set of IF-THEN rule corresponding to a linear state equation (Equation 3.12). Figure 3.9 shows the combination of premises represented as nine partitions that are generated form two inputs with three MFs each. Grid partitions are constructed from enumerating all possible combinations of MFs of all input variables forming the IF-THEN rules. By doing so, the non-linear system being modelled is described as a weighted sum of these linear state equations.
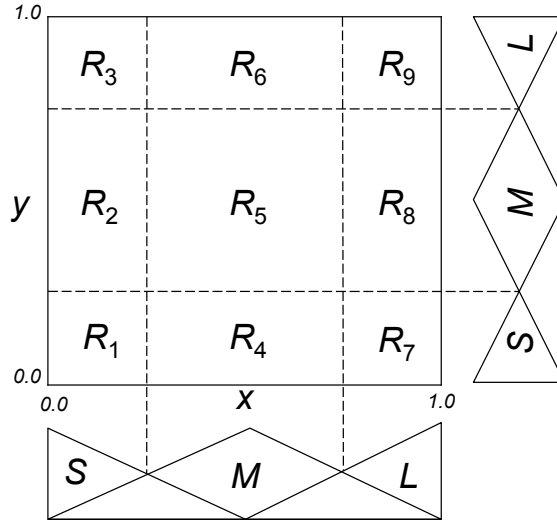
Figure 3.9. Training input parameters *x* and *y* with three MFs each {*S, M, L*}. Enumerating them produces nine combinations of IF-THEN rules, constructing a uniform grid coverage for the input and output space.

To deal with a complex problem with small error tolerance (i.e. with a large number of intricately related input and output variables), more Fuzzy sets and rules are required. The number of correctly classified patterns in grid partitioning is associated with the accuracy of the model. Increasing the number of intervals (the total number of partitioning generated from increasing inputs) produces a model of finer-grain that is better able to approximate a non-linear system. However, the number of rules increases exponentially with an increasing number of inputs. The number of IF-THEN rules is of order $O(T^k)$, where *T* is the number of inputs and *k* is the number of MFs.

2. ANFIS architecture

An Fuzzy IF-THEN rule *i* of an two rules ANFIS model can be illustrated as follows:

$$Rule\ i: If\ x\ is\ A_i\ and\ y\ is\ B_i, then\ f_i = p_i x + q_i y + r_i\ , i = 1, 2. \qquad (3.12)$$

where *i* denotes the rule index, *x* and *y* are crisp values of the training inputs, A_i, B_i are corresponding linguistic values, also known as the MFs, and p_i, q_i, and r_i are the consequent parameters of the linear state equation, f_i.

ANFIS network architecture with two input and two MFs each is shown in Figure

60

3.10. This network architecture is an adaptive multilayer feed-forward network, consisting of five layers, namely, a Fuzzy layer, product layer, a normalising layer, de-Fuzzy layer and a total output layer. In each layer, network nodes perform individual functions on incoming signals.

Layer 1 is the Fuzzy layer where each node i generates a membership grade of a MF relationship based on input x. This membership grade can be expressed as:

$$O_{1,i} = \mu_{A_i}(x) , i = 1, \dots, 4. \tag{3.13}$$

where $O_{1,i}$ denotes the membership grade of i-th node of layer 1, and μ_{A_i} denotes the MF, which is explained in Equation 3.18.

Layer 2 is the product layer where each node i corresponds to a single TS-type Fuzzy rule and calculates the firing strength w_i based on the product of input signals. This relationship can be written as:

$$O_{2,i} = w_i = \mu_{A_i}(x) * \mu_{B_i}(y), i = 1, 2. \tag{3.14}$$

where $O_{2,i}$ denotes the output of i-*th* node of layer 2.

Layer 3 is the normalising layer where each node i calculates a normalised firing strength $\overline{w}_i$ for a given rule-base on inputs w_i. The normalising function can be represented by:

$$O_{3,i} = \overline{w}_i = \frac{w_i}{w_1 + w_2} , i = 1, 2. \tag{3.15}$$

where $O_{3,i}$ denotes the output of i-*th* node of layer 3.

Layer 4 is the de-Fuzzy layer where each node i calculates the weighted consequent value of a given rule using a linear combination of the inputs multiplied by the normalised firing strength $\overline{w}_i$. This defuzzication relationship can be expressed as:

$$O_{4,i} = \overline{w}_i f_i = \overline{w}_i (p_i x + q_i y + r_i) \,, i = 1, 2. \tag{3.16}$$

where $O_{4,i}$ denotes the output of *i-th* node of layer 4, and p_i, q_i, and r_i are consequent parameters.

Layer 5 is the total output layer, where node *i* calculates the output of all defuzzication neurons and produces an overall ANFIS output. The results can be written as:

$$
\begin{aligned}
O_{5,1} &= overall\ output \\
&= \sum_i \overline{w}_i f_i \,, i = 1, 2. \\
&= \sum_i \frac{w_i}{w_1 + w_2} * f_i \,, i = 1, 2. \\
&= \frac{w_1 f_1 + w_2 f_2}{w_1 + w_2}
\end{aligned} \tag{3.17}
$$

where $O_{5,1}$ denotes the layer 5 output.
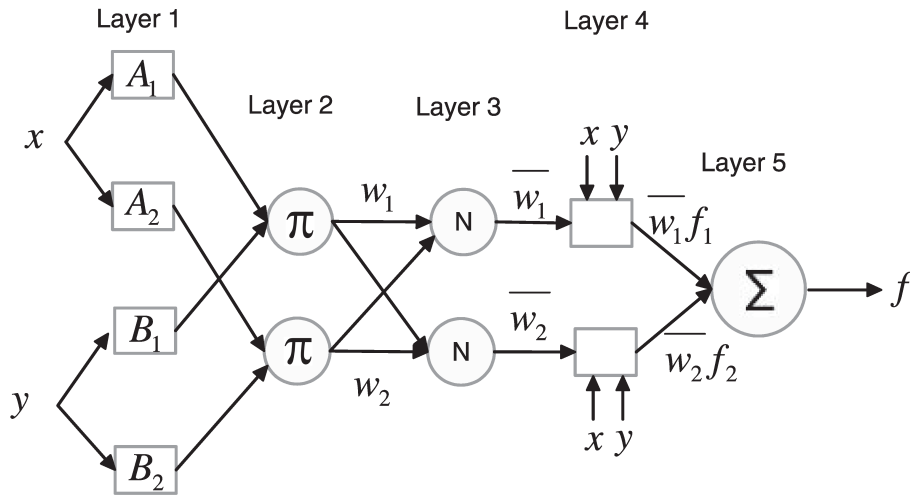
Figure 3.10. ANFIS architecture [131].

3.3.4 ANFIS Models Training

The flow diagram of ANFIS to model link failures caused by spatial related network challenges is shown in Figure 3.11. Firstly, the model training inputs – *NTC, BNTC,*

mean RSSI and *ACV RSSI* – and training output – "0", "1" or "2", which classifies as "no link failure", "link failure caused by human movements" and "link failure caused by poorly deployed environment" respectively – of 2100 samples size are normalised and divided into *k* subsets using *k*-fold validation. At any point of the model training process, one *k* subset is used as the test set while the other *k-1* subsets are combined to form one training set. The accuracies across all *k* trials are then computed. In this manner, every data point will be in a test set once and training set *k-1* times. The use of *k*-fold validation minimises misleading results where a model based on a single training data set may underperform, giving no indication to the model's performance under unseen data.
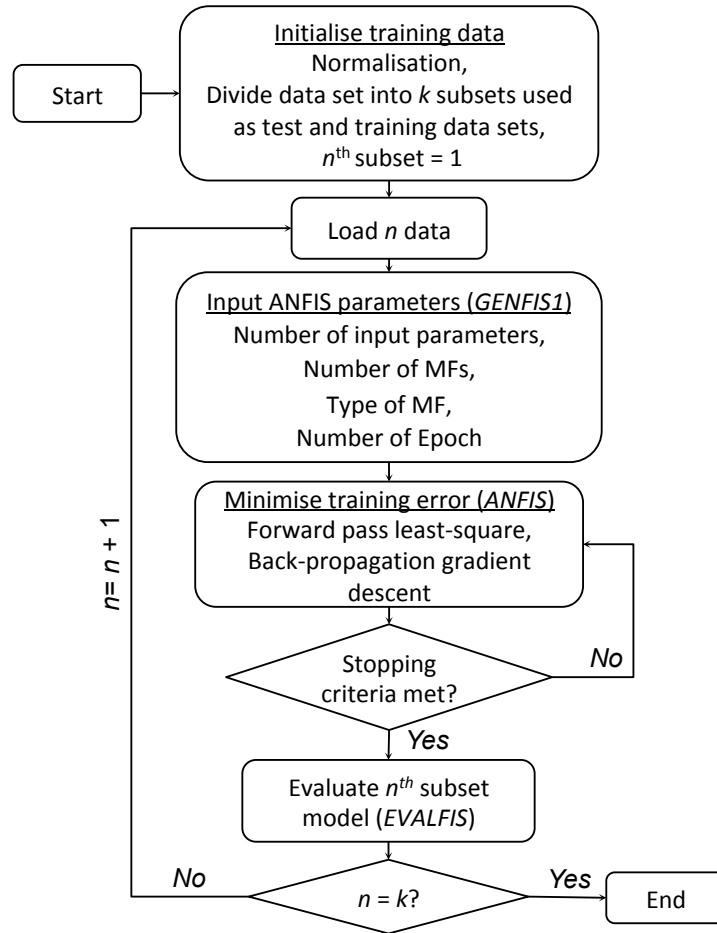
Figure 3.11. ANFIS application flow diagram

Three key functions – *GENFIS1*, *ANFIS* and *EVALFIS* – are used to develop the ANFIS models in MATLAB v2015b. *GENFIS1* function is used to generate the initial TS-type ANFIS network structure as shown in Figure 3.12. This network structure is

63

an extension of the basic network structure from Figure 3.10, consisting of 81 rules, constructed by four inputs and three input MFs each. In this work, the MFs are described in the form of a Gaussian function as shown in Equation 3.18.

$$\text{Gaussian}(x; \sigma, c) = \exp\left(\frac{-(c_i - x)^2}{2\sigma_i^2}\right) \tag{3.18}$$

where the x is the input value, c_i denotes the mean of the *i-th* fuzzy set and σ_i is the associated variance. The membership grades in Equation 3.13 is computed with Gaussian MF.
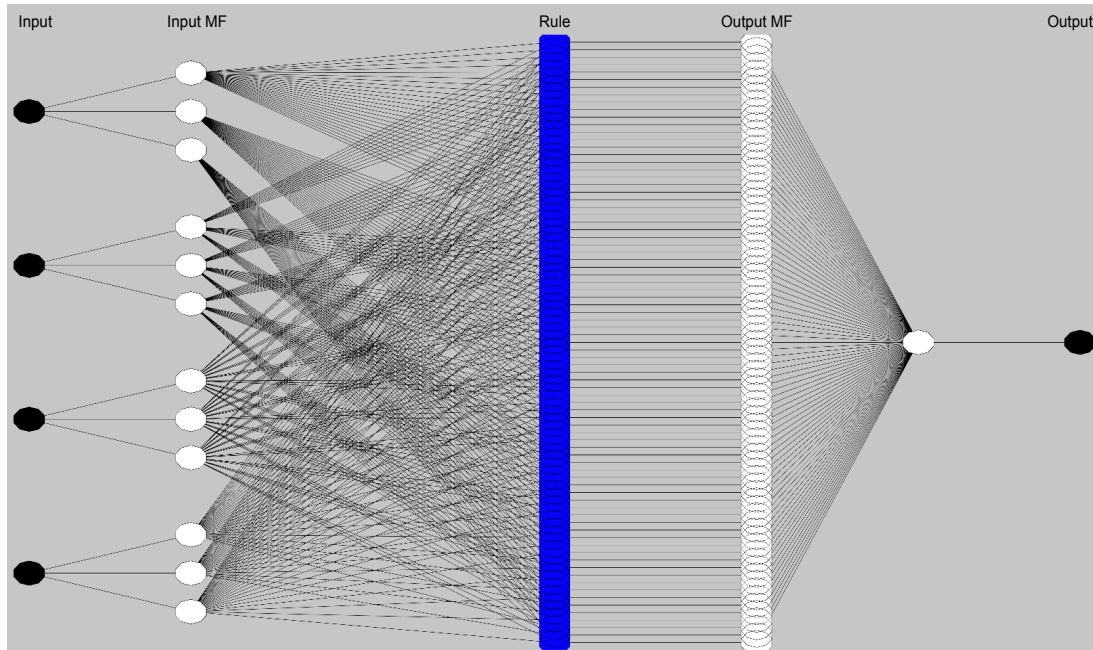
Figure 3.12. TS-type ANFIS network architecture of 81 rules made up from four inputs and three input MFs each (MATLAB v2015b).

Subsequently, *ANFIS* function is used for model training using n^{th} training data subset. The network learns the non-linear system in two phases. First, in the forward phase, the consequent parameters, p_i, q_i and r_i in Equation 3.16 are identified using the least squares method. Second, in the backward pass, the error signals propagate backward from the output layer, where the premise parameters, c_i and σ_i in Equations 3.13 and 3.18 are updated by gradient descent. This learning process is repeated for 100 Epoch as the premise and consequent parameters are adjusted according to the training errors. Lastly, the developed model is evaluated based on Root Mean Square

Error (RMSE) with test data set using the *EVALFIS* function and the entire process is repeated for *k* number of times.

3.3.5 Training with Parameters Combinations

The ANFIS models are trained 15 times with 15 different sets of input parameters combinations as presented in Table 3.5. The purpose of using multiple parameters combinations is to understand the behaviour of different inputs and their combinations thereof under different link failures to ascertain which layer (i.e. physical and network layer) has a greater impact on the predictive conditions.

ANFIS models' prediction accuracies are used as performance index for comparison and ranking. The models are analysed with the help of box-plot diagrams generated in MATLAB using *BOXPLOT* function. On every boxplot, a central red mark indicates the median accuracy of the ANFIS models trained by the respective parameter combination. The bottom and top edges of the box indicate the 25th and 75th percentile respectively, while whiskers extended beyond the box are the extreme data points. Outliers, if any, are represented with '+' symbol, where they are more than 1.5 times of the interquartile range. Boxplots are used to describe the value spread from the median.

Table 3.5. Parameter combinations used to train ANFIS models.

Sets	1	2	3	4	5	6	7	8	9	10	11	12	13	14	15
Mean RSSI	✔				✔	✔	✔				✔	✔	✔		✔
ACV RSSI		✔			✔			✔	✔		✔	✔		✔	✔
NTC			✔			✔		✔		✔	✔		✔	✔	✔
BNTC				✔			✔		✔	✔		✔	✔	✔	✔

3.4 Influence of WSN Parameters on Spatial Challenges Predictability

1. Comparison between combination sets with one parameter

This section presents the comparison results of single parameter combination sets (set $1 - 4$). Referring to Figure 3.10, it is clear that *mean RSSI* (set 1) as single parameter performed significantly better than *ACV RSSI*, *NTC*, and *BNTC* (sets $2 - 4$) with a prediction accuracy of 81.8%. This suggests that *mean RSSI,* which represents the average reception signal strength, is suitable for link failure detection caused by spatial challenges. An explanation is that physical LOS obstructions such as human bodies, walls, and desk partitions can attenuate or distort the transmitted signals; this degrades the strength of received signals and leads to a higher chance of link failures [17, 21], or which are detectable with *mean RSSI*.

ACV RSSI (set 2) produced the worst accuracy of only 6.5%. It is observed that under the conditions of "no failure" and "failure due to poorly deployed environment (experiment 1)", multipath and fading effects are subjected to minimal variations due to the static experimental environment. *ACV RSSI* measures channel variability, taking into account the dispersion of reception signal of all connecting links (temporal fading and multipath fluctuation). From the experiment 1, *mean RSSI* between nodes is also found to be relatively constant throughout the experiments having no more than 1.1 dBm variation. This explanation echoes the poor performance of *ACV RSSI*, which was not able to detect between different conditions distinctively i.e. link failures from no failures.

On the other hand, network layer parameters, *NTC* and *BNTC* (sets 3 and 4) as single parameter produced a relatively poor prediction accuracy of only 40.4% and 39.2% respectively. *NTC* and *BNTC* represent the connectivity between communicating nodes, and are capable of differentiating a link with and without failure. However they are insufficient to distinguish between human movements and poor deployed environment. This will be further explained in the following sections.
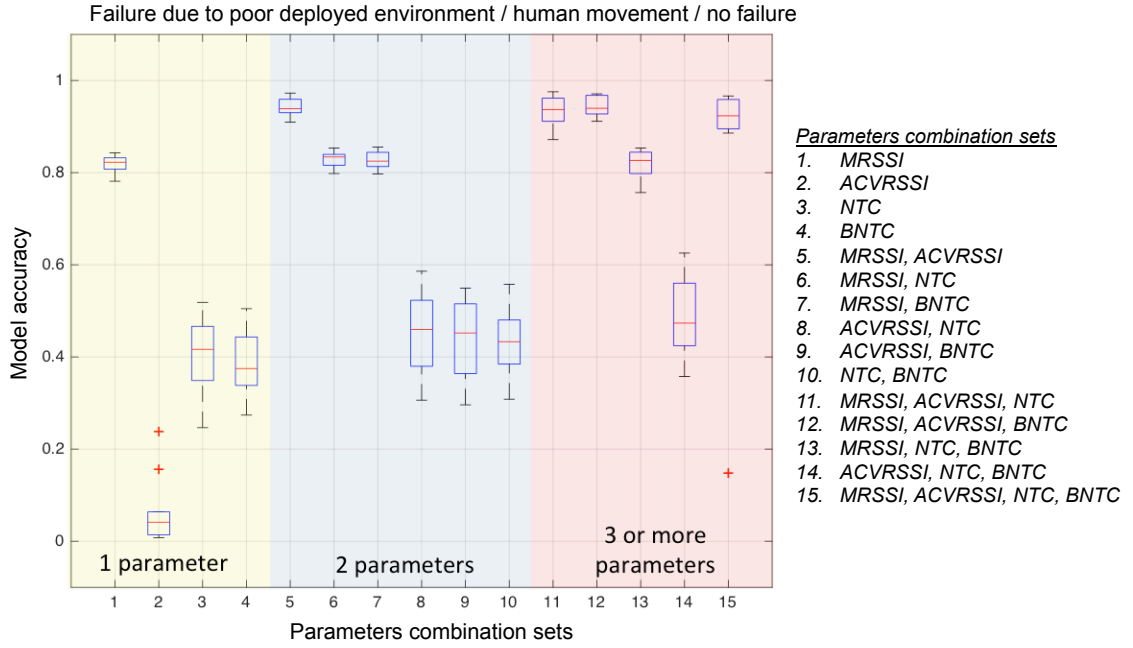
Figure 3.13. ANFIS models' prediction accuracy – Link failure due to poor deployed environment vs. human movement vs. no failure.

2. Comparison between combination sets with two parameters

The mean prediction accuracies of combination sets with two parameters (sets 5 – 10) in Figure 3.10 are compared. It is obvious that any parameter combination sets containing *mean RSSI* (sets 5 – 7) performed well, producing an average accuracy greater than 80%. This is also highlighted in the previous section where *mean RSSI* as a single parameter performed well.

It is observed that the prediction accuracy of *mean RSSI* improved with *ACV RSSI* (set 5) as compared to with *NTC* or *BNTC* (sets 6 or 7). This phenomenon can be explained with the degradation of reception strength measurements due to physical obstructions, while the introduction of human movements also inflict temporal changes from the multipath and fading effects. *Mean RSSI* and *ACV RSSI* represent reception strength and reception fluctuation respectively. The combination of both physical layer parameters not only improved the detection of link failures, they also enhanced the model's ability to distinguish the causes of failure (i.e. human movements or poorly deployed environment) with an accuracy of 94.2%. In contrast to the poor results of set 2, it emphasised that a single parameter alone (*only ACV*

RSSI) may have insignificant impact on the model's performance but could still be useful if more information is provided.

The ANFIS model's training samples with *mean RSSI* poorer than -86 dBm (300 samples) and links with *NTC* and *BNTC* poorer than 80% take up only 59% and 51% of the entire population respectively. This suggests that *NTC* and *BNTC* may have wrongly indicated a particular condition. This false positive prediction can be explained with nodes communicates at reception sensitivity edge (poor *mean RSSI*), may not always lead to link failures. As a result, *NTC* and *BNTC* representing connection success rate, and link asymmetry performed poorly when it comes to differentiating spatial challenges.

3. Comparison between combination sets with three or four parameters

The mean prediction accuracies of combination sets with three or more parameters (sets 11 – 15) in Figure 3.10 are compared. Once again, it is observed from sets 11 – 13 and 15 that combination sets that contain *mean RSSI* produced good prediction accuracies greater than 80%. Amongst them, sets that contain *ACV RSSI* (sets 11, 12 and 15) performed even better, producing prediction accuracies of more than 90%. Clearly, this strongly suggests that poor reception strength and high relative signal variation are key characteristics of a link failure caused by spatial challenges.

The comparison between set 15 (highest number of parameters of four) and combination sets 5, 11 and 12 (less parameters yet similar prediction accuracies) demonstrates that having more training parameters does not necessarily translate to a better prediction accuracy. In other words, adding more training inputs may not necessary produce a more accurate prediction. Instead careful selection of training parameters may achieve higher prediction performance.

3.5 Comparison of the Parameter Combinations

1. Physical layer

From Table 3.6, it is clear that the *mean RSSI* stands out among all parameters where the top eight models contain *mean RSSI* as one of their training inputs. Whether used alone or as a joint parameter, *mean RSSI* is a strong influencer when it comes to

detecting link failures due to a poorly deployed environment and human movements. On the other hand, *ACV RSSI* appears in the top 4 best predictors, while *ACV RSSI* as a single parameter performed poorly. This is attributed to the minimal variations of multipath and fading effects in a static environment, thus leading to poor detectability of link fluctuation. However, when *ACV RSSI* is combined with other parameters, the overall prediction accuracy has showed improvement. For example, prediction accuracy of set 6 with *mean RSSI* and *BNTC* improved from 82.7% to 94.5% with the addition of *ACV RSSI* (set 1). In this work, *ACV RSSI,* representing reception fluctuation, is poor at detecting link failures from no failures. However, it is still able to differentiate link failures due to a poorly deployed environment or human movement.

2. Network layer

NTC and *BNTC* as single parameters, and as joint parameter represent both link connectivity and link asymmetry. Our findings show that both parameters are insufficient to predict link failures caused by spatial challenges. It is observed that sets trained with mainly network parameters and without *mean RSSI* have larger spread of model accuracy (sets 3, 4, 8-10, 13), as shown in Figure 3.10. These spreads can vary up to 30%. This can be explained with the grey transitional region phenomenon [84], where network level parameters alone can produce false positive predictions, which have wrongly indicated the presence of a particular condition.

Additionally, it is observed that network layer parameters are only useful under the conditions where *mean RSSI* is absent. For instance, the prediction accuracy of set 2 (*ACV RSSI*) improved from 6.6% to 48.6% with addition of *NTC* and *BNTC* (set 14). This phenomenon reinforces that network parameters are useful at detecting a link failure but are not able to distinguish between failures caused by human movements and a poorly deployed environment.

Table 3.6. Training input parameter combinations ranked according to mean prediction accuracies from most to least accurate.

S/N	Combination Set	Parameters Used	Mean Accuracy (%)
1	12	*Mean RSSI, ACV RSSI, BNTC*	94.5
2	5	*Mean RSSI, ACV RSSI*	94.3
3	11	*Mean RSSI, ACV RSSI, NTC*	93.5
4	15	*Mean RSSI, ACV RSSI, NTC, BNTC*	92
5	6	*Mean RSSI, NTC*	82.9
6	7	*Mean RSSI, BNTC*	82.7
7	1	*Mean RSSI*	81.9
8	13	*Mean RSSI, NTC, BNTC*	81.8
9	14	*ACV RSSI, NTC, BNTC*	48.6
10	8	*ACV RSSI, NTC*	45.4
11	10	*NTC, BNTC*	43.6
12	9	*ACV RSSI, BNTC*	43.5
13	3	*NTC*	40.4
14	4	*BNTC*	39.2
15	2	*ACV RSSI*	6.6

3.6 Chapter Summary

In this chapter, the impact of persistent Wi-Fi traffic and spatial challenges on WSN communication reliability is thoroughly investigated through the conduct of controlled experiments. A novel data extraction platform, NI, is introduced to extract representative Zigbee PRO parameters from experimented nodes deployed in real-world environments. Subsequently, ANFIS is used to model link failures caused by spatial-related network challenges. Given that the communication reliability of a WSN is known to be imprecise in real world application, ANFIS technique is chosen for its tolerance for partial truth in training data.

From the controlled experiments, three key conclusions are made. First, minimising Wi-Fi interference is possible with sufficient operating frequency separation. Second, the physical layer parameters have shown to be more useful in predicting spatial-related link failures than the network layer parameters. This is contributed by the abilities of *mean RSSI* and *ACV RSSI* to distinguish poorly deployed environment and human movements. Lastly, individual parameters are observed to behave differently under varying conditions. Thus, there is a need for a better selection of parameters to achieve higher model prediction performance and better model interpretation.

4 Interpretability and Accuracy Trade-Offs in Fuzzy Modelling for Wireless Sensor Networks

In Chapter 3, ANFIS models were developed to predict WSN link failures caused by spatial challenges. These models, trained by different combinations of inputs, were ranked and analysed based on the models' accuracies. ANFIS prioritises classification accuracy and due to the curse of dimensionality, the interpretability on these Fuzzy models is challenging (exponential increase in the number of Fuzzy rules).

The aim of Chapter 4 is to derive a strategy to optimise the ANFIS models' interpretability and accuracy trade-offs specifically for WSN link failure prediction. The importance of model interpretability and its conflicting trade-offs with model accuracy are discussed in Section 4.1. In Section 4.2, the Non-dominated Sorting Genetic Algorithm–II (NSGA-II) technique is introduced to search for non-dominated IF-THEN rules within the ANFIS model's Fuzzy rule-base. The objectives of NSGA-II are to maximise the link failure prediction accuracy, and minimise the total number of IF-THEN rules and the total combined IF-THEN rule length. The implementation of different NSGA-II design heuristics and the influence of different optimisation objectives on model convergence are discussed in Section 4.3. The design heuristics include the initial population with different chromosome diversity, different mutation rates for active and inactive genes, and the use of "don't care" conditions to represent no antecedent conditions of the IF-THEN rules. Lastly, Section 4.4 concludes the chapter.

4.1 Interpretability and Accuracy Trade-Offs in Neuro-Fuzzy System

4.1.1 What is Model Interpretability?

The interpretability of the Fuzzy rule-based classifier distinguishes it from other classification methods. The term interpretability refers to the ability of a classification model to allow users to comprehend the system's behaviour by inspecting its functions. Unlike model accuracy that is determined based on the number of correctly classified training patterns, model interpretation is not as straightforward.

There are different interpretability measures in the existing interpretability-oriented design of Fuzzy rule-based classifiers, such as model complexity, readability, completeness and consistency [133, 134, 135]. Two types of interpretability measures are commonly used. First, the complexity-based interpretability measure is designed to reduce the complexity of a Fuzzy model usually through a reduction of the number of rules and their respective antecedents. Second, the semantic-based interpretability measure, which preserves the semantics of a Fuzzy model, is often associated with the adjustment of MFs. Although these measures are adopted, there is still no universally accepted benchmark within the research community [136]. This is primarily due to the subjectivity of human intuition and the preference for linguistic values when interpreting results [136].

An unbounded number of rules are required to achieve arbitrary model accuracy [138, 139] and a Fuzzy model can become extremely complex when modelling a highly non-linear system. In other words, a complexity-oriented model that is made up of fewer rules and input variables is regarded as easier to comprehend than a model with more rules, hence less complex. In [140], the complexity of an ANFIS model, designed to predict the surface roughness of end milling model, is reduced using Leave One Out Cross Validation (LOO-CV) technique. LOO-CV is a top-down rule reduction approach used to filter less relevant IF-THEN rules from the Fuzzy rule-base. Iteratively, individual rule is removed from the rule-base and the RMSE of the adjusted ANFIS model is computed. The rule corresponds to the greatest RMSE is then removed because it has the lowest contribution to the prediction model. The removal of lowest contribution rule is repeated until RMSE cannot be further reduced.

It is said that the removal of unnecessary rules avoids the over-fitting phenomenon in large rule-base models. As a result, Dong and Wang [140] have showed that ANFIS with LOO-CV outperforms the classic ANFIS model and ANFIS with clustering approach in terms of test data-set model accuracy.

On the other hand, a semantic-oriented model fine-tunes the linguistic hedges (i.e. the shape of a MF) of the original MF, so that the rules can be "self-explanatory" [141, 142]. The semantic-based interpretability measure is introduced by Dubois and Prade [143]. They mentioned that, "the more similar is the observation to an antecedent, the more similar the conclusion should be to the corresponding consequent of the given antecedent". This means that a rule is self-explanatory if its antecedent parts clearly indicate the characteristics of a classified pattern. For instance, a similarity measure is used to identify Fuzzy sets with highly overlapping positions [141]. During the Fuzzy model training, an overlapping of Fuzzy sets creates redundancy in the rule-base where the coverage of IF-THEN rules in the data space becomes highly similar. By merging similar Fuzzy sets and creating a common Fuzzy set in the rule-base improve the distinguishability between IF-THEN rules as well as reduce the total number of rules [141].

4.1.2 The Search for Relevant IF-THEN Rules using Multi-objective Evolutionary Algorithms

Multi-Objective Evolutionary Algorithm (MOEA) techniques have been widely adopted to search for multiple Pareto-optimal along the trade-off surface of a Fuzzy Rule-Based System (FRBS) [137, 144, 145]. MOEA techniques simulate the concept of Genetic Algorithms (GAs) and Evolutionary Strategies (ES) to provide continuous and combinatorial optimisation of Fuzzy properties relating to accuracy and interpretability. As shown in Figure 4.1, the Pareto front (denoted as black circles) is a set of solutions that are superior to the rest of the population (blue circles) in at least one criterion. No solution among the Pareto front is more superior to another in all criterions; an improvement in one property (i.e. increase in the number of rules) degrades the other (i.e. decrease in model accuracy). The common optimisation properties of a FRBS are for example, the total number of Fuzzy rules, total length of Fuzzy rules, number of correctly classified rules, distinguishability between MFs and granularity of the uniform partition [145],
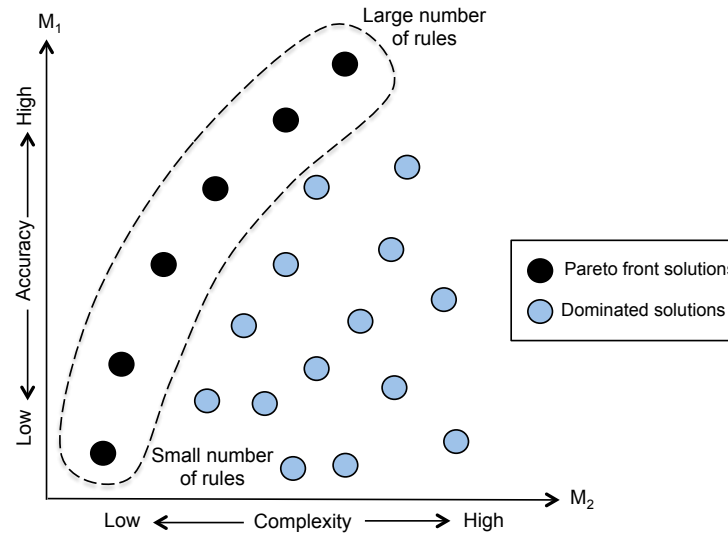
Figure 4.1 Two-objective problem and Pareto front - Trade-off between accuracy maximisation and complexity minimisation of rules sets

Alcala et al. [146] experimented MOEA techniques such as SPEA2 and NSGA-II to simultaneously reduce the rule-base size of FRBS and improve the models' accuracy. During the MOEA search, binary encoded Fuzzy IF-THEN rules are turned on and off, and the corresponding attributes of triangular-shaped MFs are adjusted randomly. Two optimisation objectives are considered; model's accuracy maximisation and complexity minimisation, computed as the RMSE and the total number of active Fuzzy rules respectively (i.e. rules that are turned on). It is found that through exhaustive selection of Fuzzy rules and tuning of corresponding MFs based on training error, a smaller and more accurate Fuzzy rule-base is achieved. However, through the adjustments of MFs, similar to a semantic-oriented model, the homogenous quality of a Fuzzy model is lost. Even if a new pattern in an input space is fully compatible with fine-tuned rules, multiple rules with different MFs are difficult to compare and the ability to interpret the rules is reduced [147]. Therefore, the ability to reduce the number of rules while preserving the homogenous quality of a Fuzzy model is necessary for model interpretation.

The removal of Fuzzy rules without degrading model's accuracy can be explained with a Fuzzy rule-base that contains potential contradictions in its premises combinations. For example, it is contradicting to say, "IF the sun is bright AND the cloud is heavy" [148]. As such, contradictory rules are present where they may be

associated with the empty areas of the input and output space [141]. Optimising a Fuzzy rule-base means the exclusion of rules with little relevance from the model, and the decision to remove them can be based on its approximation contribution [149].

4.2 Fuzzy Rule-Base Optimisation of ANFIS models using NSGA-II

4.2.1 Non-dominated Sorting Genetic Algorithm-II

Non-dominated Sorting Genetic Algorithm II (NSGA-II) has emerged as one of the most adopted MOEA techniques to tackle interpretability-accuracy trade-off in FRBS [145]. NSGA-II is known for its ability to preserve non-dominated and diverse solutions in the Pareto-front with fast non- dominated sorting with elitism approach [150].

Fast non-dominated sorting in NSGA-II evaluates the solutions using Pareto ranking. For instance, in the current population, all solutions that are not dominated by others in terms of optimisation objectives (i.e. non-dominated solutions) are ranked 1. Solutions of rank 1 are then removed from the population. This allows a new set of non-dominated solutions to be selected among the reduced population. These new non-dominated solutions are ranked 2 and are removed from the reduced population. The selection and removal of non-dominated solutions are repeated until a rank is assigned to all solutions. As a result, solutions ranked first and last are regarded as fittest and weakest respectively. Furthermore, among the solutions of the same rank, a crowding measure is used to determine the distance between its adjacent solutions in the objective space. Less crowded solutions with larger crowding measure are viewed as better than crowded solutions with smaller crowding measure. The distinction between crowded and less crowded solutions allows the selection of diverse Pareto front. Lastly, elitism approach in NSGA-II refers to the selection of solutions from the same rank and incorporating them into the next generation. The selection of solutions from the same rank speeds up the GA search without further re-evaluation of fitness. In addition, the preservation of neighbouring solutions of the same rank prevents the loss of good solutions.

NSGA-II is also regarded as superior over other MOEA techniques, particularly in a

noisy environment [151, 152]. Bui et al. mentioned that solutions in a noisy environment tend to be generated close to each other (crowded). It is highlighted that noise in real-world application cannot be discounted. Noise can come from different sources such as data inputting or sampling error from sensors and actuators in a multi–agent simulation. Hence, the ability of NSGA-II to preserve a broader range of solutions with greater crowding distance along the Pareto front allows better distinction from noise.

4.2.2 Problem Formulation

NSGA-II is used to optimise the ANFIS model (refer to Chapter 3.3) and search for non-dominated IF-THEN rules within its rule-base. The flow diagram is illustrated in Figure 4.2. The ANFIS model, initially generated with the four training link quality parameters – mean *RSSI, ACV RSSI, NTC* and *BNTC* – is optimised with the objectives of minimising the total number of IF-THEN rules and the total combined rule length, and maximising the model's prediction accuracy.
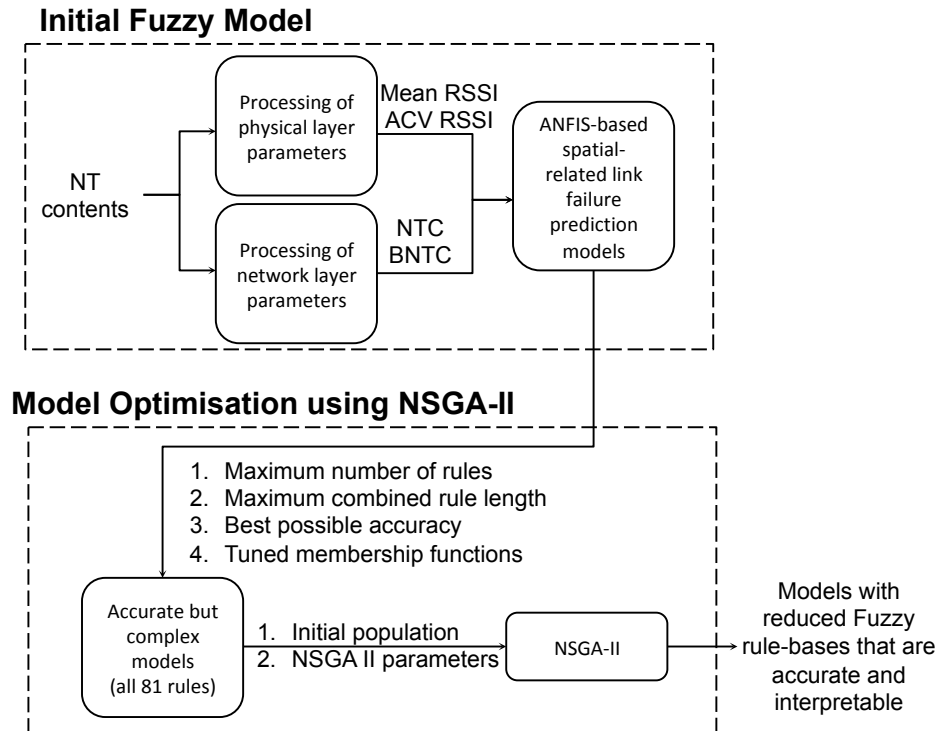
Figure 4.2. Flow diagram – Fuzzy model optimisation using NSGA-II.

1. Chromosome representation

Given that an attribute i has l_i number of linguistic values (i.e. total number of MFs), the total number of possible combination of rules is $\prod_{i=1}^{d} l_i$ for a d-number of attributes. Figure 4.3 shows an ANFIS model represented by chromosomes and genes. A total of 81 binary encoded chromosomes are used to describe the ANFIS model, developed from four attributes – *mean RSSI*, *ACV RSSI*, *NTC* and *BNTC* – and three MFs each, constructing a maximum number of 81 IF-THEN rules. A chromosome of '1' denotes that the respective rule within the rule-base is activated, and '0' denotes that the rule is inactive. All active rules are used to compute the overall model accuracy. Vice versa, inactive rules are not utilised for model accuracy computation.

A chromosome can be further represented with four genes, denoting the corresponding antecedent conditions of the respectively rule (Equation 3.12). '1' being the antecedent part is mapped on a Gaussian MF (Equation 3.18), and '0' being "don't care (DC)" [153]. Given that there are four antecedent parts per rule, the maximum combined rule length of all 81 rules is 324. An attribute that is mapped with DC does not contribute to the membership degree calculations in the classification phase (Equation 3.14) [154].

81 chromosomes representing 81 IF-THEN rules

R_1	R_2	R_3	...	R_{80}	R_{81}

4 genes representing 4 input parameters of each rule

$R_{1,1}$ $R_{1,2}$ $R_{1,3}$ $R_{1,4}$	$R_{2,1}$ $R_{2,2}$ $R_{2,3}$ $R_{2,4}$	$R_{3,1}$ $R_{3,2}$ $R_{3,3}$ $R_{3,4}$

1 0 0 1	**0 1 1 1**	**0 0 0 0**
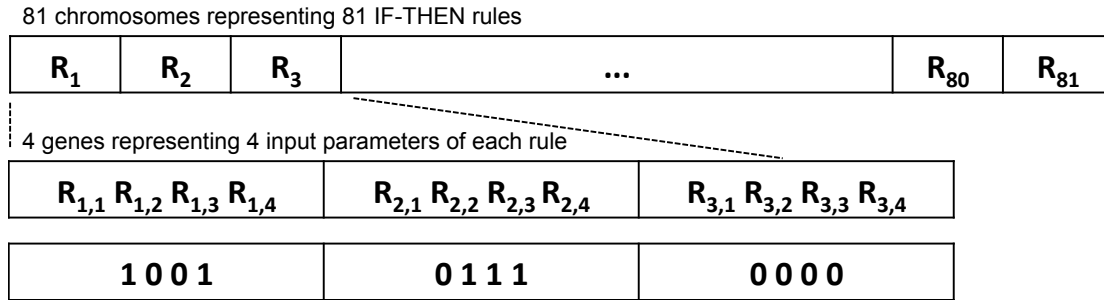
Figure 4.3. Chromosome representation of individual Fuzzy IF-THEN rules and their respective genes.

The antecedent condition of DC is represented by a linguistic value of unity. This means that an attribute mapped with DC have a degree of 1. For example, if the domain of the i-th attribute has an unit interval between [0,1], the membership grade of antecedent condition DC can be written as Equation 4.1.

$$\mu_{DC}(x_i) = \begin{cases} 1, & \text{if } 0 \le x_i \le 1, \\ 0, & \text{otherwise} \end{cases} \tag{4.1}$$

where μ_{DC} is the MF relation of DC type based on input x. When DC antecedent condition is used, the membership grade to the input x is always 1.

2. Objective functions

Three objective functions implemented to optimise the Fuzzy rule-bases of the initially generated ANFIS models are shown in Equations 4.2, 4.3 and 4.4. The objective functions are (1) minimisation of the total activated IF-THEN rules in the optimised Fuzzy rule-base (M_1), (2) minimisation of the combined of rule length of all activated antecedent conditions in all IF-THEN rules in the optimised Fuzzy rule-base (M_2), and (3) maximisation of the classification accuracy based on the optimised Fuzzy rule-base (M_3).

$$\text{Min } (M_1) = \text{Min (Total activated IF-THEN rules)} \tag{4.2}$$

$$\text{Min } (M_2) = \text{Min (Combined rule length for all activated antecedents} \\ \text{conditions in all IF-THEN rules } (M_1)) \tag{4.3}$$

$$\text{Max } (M_3) = \text{Max (Classification accuracy based on the optimised Fuzzy} \\ \text{rule-base)} \tag{4.4}$$

Both M_1 and M_2 are measures of the ANFIS model's interpretability. A simpler Fuzzy rule-base has fewer and shorter rules [147, 155]. M_3 is an accuracy measure between the ANFIS model's predicted output and the training output data (refer to Section 3.3). The greater the M_3, the better the model is at predicting spatial-related link failures.

Every rule in the rule-base specifies a subspace within the input space. These subspaces are dictated by the antecedent conditions of the Fuzzy rules (refer to Section 3.3.3). Figures 4.4 and 4.5 illustrate the differences between Fuzzy partitions incorporating without and with antecedent conditions DC respectively. In Figure 4.4, a 2-D input space is divided into 25 Fuzzy subspaces, constructed by attributes x and y with five linguistic values each. On the other hand, the introduction of DC in Figure

4.5 reduces the total number of Fuzzy partitions to 5. Each partition is partially defined with DC linguistic value, providing a greater coverage within the input space. In this case, a non-linear model can be represented with lesser number of grids, translating to lesser number of Fuzzy IF-THEN rules [156].
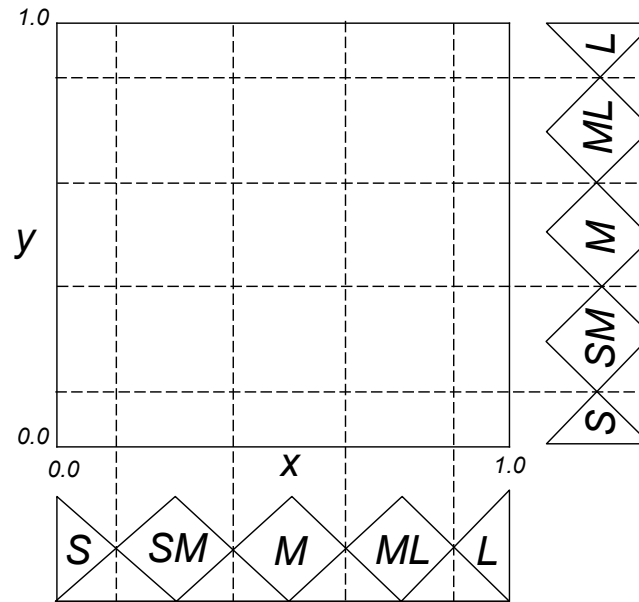
Figure 4.4. Example of Fuzzy partitioning of a 2-D input space [0,1] × [0,1] with five linguistic values for attribute *x* and *y*.
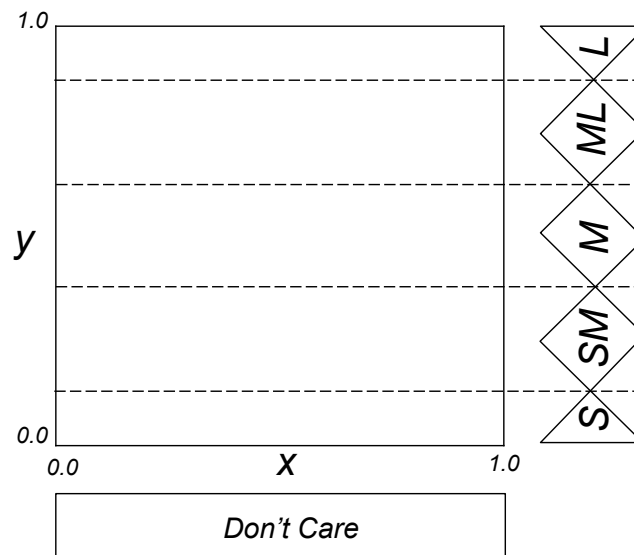
Figure 4.5. Example of Fuzzy partitioning of the 2-D input space [0,1] × [0,1] with "don't care" as an antecedent Fuzzy set.

3. Fuzzy rule-base optimisation of ANFIS models

Figure 4.6 illustrates the flow diagram of NSGA-II used to optimise the developed ANFIS model based on objective functions M_1, M_2 and M_3. In the first step, NSGA-II begins the search for optimal solutions with a number of randomly chosen chromosomes forming the initial population. An initial population P_0 of size N is initialised. Every solution p_i represents an ANFIS model that contains up to a potential maximum of 81 IF-THEN rules and 324 combined Fuzzy rule length.
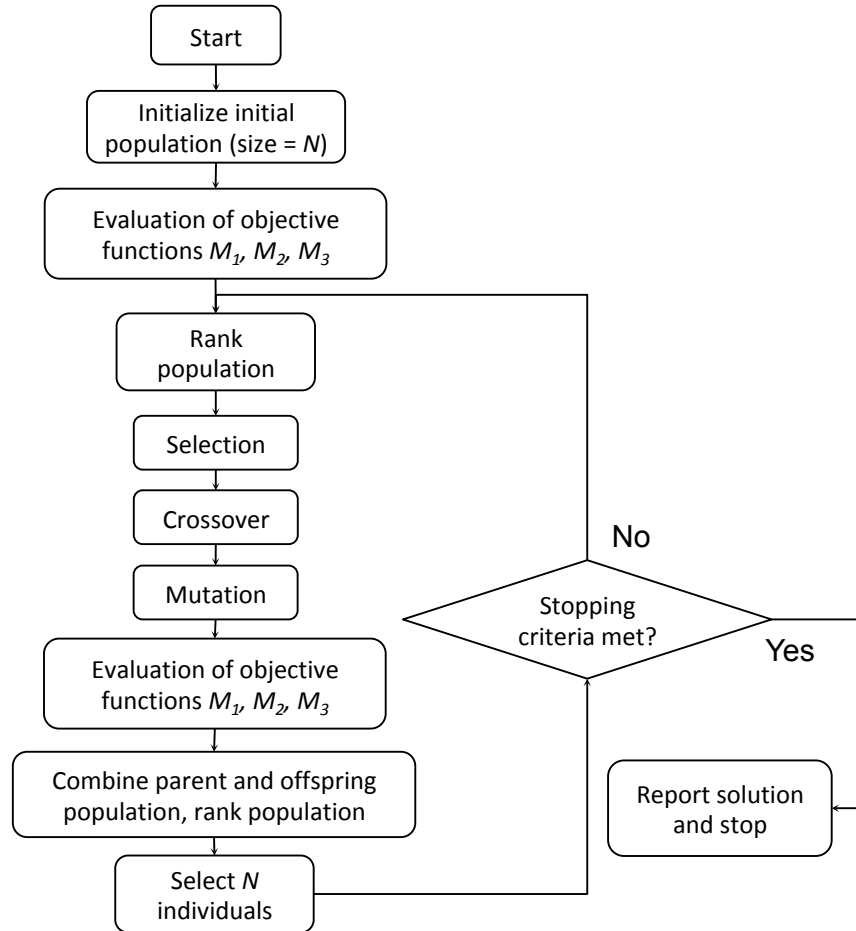
Figure 4.6. Flow diagram – The application of NSGA-II to generate offspring, rank individuals based on objective functions, and carry forward the fittest solutions over 300 generations.

In the second step, solutions in P_0 are ranked using fast non-dominated sorting. For every solution p_i in P_0, the fitness measures – M_1, M_2 and M_3 – are computed and a domination count n_i of zero is assigned. n_i is the number of solution within the P_0 that

p_i got dominated based on the M_1, M_2 and M_3. Solution p_1 dominates solution p_2 if p_1 is better than p_2 in at least one of the fitness measures and is not worse in any of them. This way, a solution with zero n_i is regarded as the fittest solution among P_0 and the n_i of any solution is at most N-1. Once the domination counts of all solutions in P_0 are computed, they are ranked in layers based on the n_i. For instance, all solutions with zero n_i are assigned to front F_1, and all solutions that are only dominated by front F_1 are assigned to front F_2. This ranking process is repeated until every solution p_i is ranked.
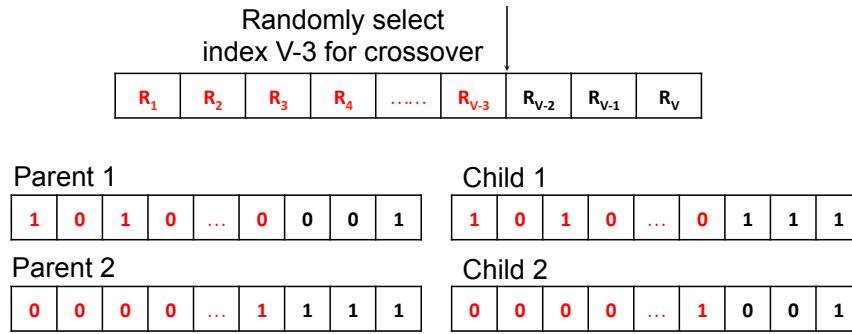
Figure 4.7. Single-point crossover at a random index between 1 and 81 performed on two winning solutions (i.e. parent) to produce two new offspring (i.e. child).

In the third step, for every generation t, $N/2$ pairs of individual solutions are randomly selected from the current population P_t for tournament selection, crossbreeding and potential mutation. The selected pairs will compete for fitness based on M_1, M_2 and M_3. The two winning solutions, also known as parents, will undergo crossbreeding to form two new offspring. Figure 4.7 illustrates two winning parents exchanging their chromosomes at a randomly selected index V-3, where V is the maximum number of chromosomes. In this work, the maximum number of chromsomes V is 81. A single-point crossover is picked at a random index between 1 and 81, from which the winning solutions will exchange their chromosomes. Next, a chromosome can be selected for mutation depending on a mutation rate. Different mutation rates are used for turning on and off the genes. If selected, an activated gene will be deactivated (i.e. from '1' to '0'). Vice versa, an inactivated gene will be activated (i.e. from '0' to '1'). If all four antecedent parts within a rule are switched off by chance (i.e. '0 1 0 0' to '0 0 0 0'), the particular chromosome (i.e. IF-THEN rule) is considered unutilised. On the other hand, a rule is considered active if any one of the four genes is activated.

In the forth step, once every parent pair in P_t has competed, an offspring population Q_t of size N will be generated. P_t and Q_t are then combined to form an intermediate population R_t of size $2N$ and is ranked using fast non-dominated sorting. Figure 4.8 shows the rankings of solutions and the non-dominated sorting procedure to carry the fittest solutions over to the next generation. This time, non-dominated sorting is performed on a $2N$ size population R_t. Similar to the second step, non-dominated solutions with zero n_i are assigned with front F_1. F_2 is assigned to solutions that are only dominated by solutions of F_1. This ranking (i.e. F_1, F_2...F_r, where r is the total number of fronts) process is repeated until every solution p in R_t is ranked.
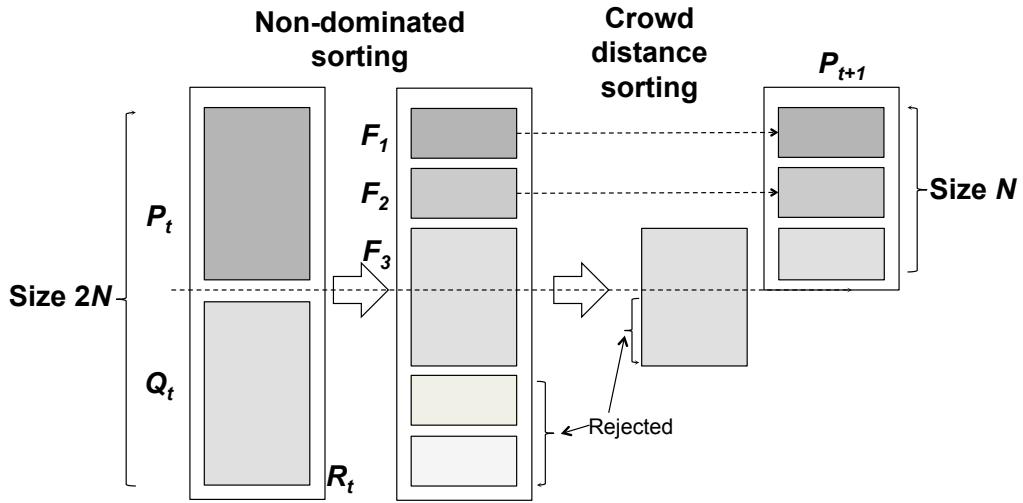
Figure 4.8. Non-dominated sorting procedure with crowd distance measure in NSGA-II used to select the fittest solutions of size N among the population of size $2N$ ($P_t +$ Q_t) based on rankings [150].

In preparation for the next generation, the intermediate population R_t is reduced to size N to form a new population P_{t+1}. This reduction of population size is based on ranking, so that P_{t+1} is made up of fitter solutions of better rankings. When the population size has exceeded N (i.e. with F_3 in Figure 4.8), the remaining individuals in F_3 to be carried forward are chosen based on crowding distance measure. As shown in Figure 4.9, the crowding distance of the solution in orange is the average cuboids side length formed using the nearest neighbours as the vertices (illustrated with dashed boxes). Crowding distance is the average distance of the two points on the side of a solution along each objective. For instance, the crowding distance of solution in orange (Figure 4.9) between its closest neighbours in objective M_1 is $x_2 + x_3$. The

larger the crowding distance relatively to its nearest neighbours, the more diverse is the solution. In other words, solutions within F_3 with the largest average crowding distance in terms of M_1, M_2 and M_3 will be selected to be in P_{t+1}.

Lastly, steps 3 to 4 are repeated until the stop criterion is reached. The stop criterion refers to the maximum number of generations.
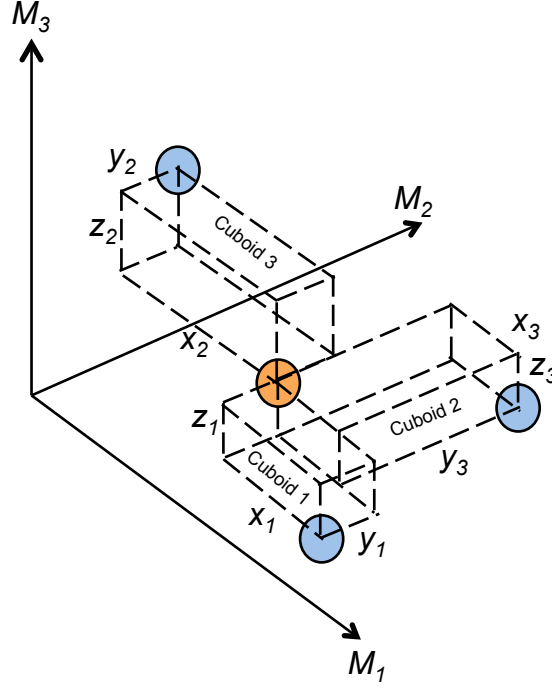
Figure 4.9. Crowding-distance calculation between solutions in the form of cuboids perimeters.

4.3 Exploration of Input and Output Space

The search for non-dominated solutions is iteratively guided by the fitness of the current parent generation [157], and the flexibility of solutions to explore the search space [158]. One drawback of a fitness proportionate selection is that excessive domination by an individual can occur [159]. An individual with the greatest fitness can suppress and dominate the current generation, where its genes are replicated and brought forward to subsequent generations. This leads to a premature convergence towards a local optimum, leaving the rest of the search space unexplored. In addition, a low number of generations (i.e. GA search iterations) can lead inadequate search space exploration. Contrarily, too high a generation requires excessive computations.

In order to allow test cases of contrasting properties to evolve sufficiently, a total of 300 generations is used.

Population diversity and selection pressure are key factors to prevent the exploration of solutions in the wrong direction (i.e. population is trapped in the local maxima or minima) [157]. Population diversity refers to the average distance between individuals based on M_1, M_2 and M_3 values at the population-level. On the other hand, selection pressure is the tendency to pick the fittest solution of the current generation. An overly high selection pressure reduces the population diversity, while an overly low selection pressure prohibits convergence to an optima in a reasonable time. In the next sections, the influence of NSGA-II's design heuristics on population diversity and selection pressure is discussed.

Boxplots are used to describe the evolutions of solutions among the population for the different test cases. Boxplots as explained in Section 3.3.5, described the manner in which the solutions among the respective population are spread out from the median. Outliers, denoted with '+ in these boxplots, highlight the values that are outside of the 1.5 interquartile range from the median.

4.3.1 The impact of Initial Population on Premature Convergence

Table 4.1. NSGA-II design properties for test case A_1, A_2 and A_3, with densely deactiviated, evenly distributed and densely activated initial populations respectively.

Test case	A_1	A_2	A_3
Number of generations	300	300	300
Population size	200	200	200
Mutation rate	0.01	0.01	0.01
Crossover	Single-point crossover	Single-point crossover	Single-point crossover
Initial population diversity	Densely deactivated	Evenly distributed	Densely activated

Three test cases, namely A_1, A_2, A_3 and their respective design properties are illustrated in Table 4.1. Their design properties are the same except for the differences in diversities of initial populations. Different initial population diversities in terms of Fuzzy rule-base size are experimented for their impact on the solutions' ability to explore the search space over the generations. They are (A_1) densely inactive number of rules (a mix of solutions randomly generated with maximum of 40 IF-THEN rules), (A_2) evenly distributed number of rules (a mixed of solutions randomly generated with a minimum and maximum of 1 and 81 IF-THEN rules respectively, and (A_3) densely active number of rules (a mixed with solutions randomly generated with a minimum of 45 IF-THEN rules).

Figures 4.10 a to 4.10 d show the fitness evolution of solutions in test case A_1 over 300 generations with a population size of 200 individuals. From Figures 4.10 a and 4.10 b, an initial population of densely deactivated rules has guided the GA search to evolve quickly towards a small Fuzzy rule-base. Solutions with Fuzzy rule-bases of 10 rules dominated the population even from the 10th generation. A growth in rule-base size is also observed from generation 70 onwards. Subsequently, the population converged with a median of less than 10 rules after generation 150. Figure 4.10 d illustrates the explorations of solutions in the search space. It shows the manner in which all 200 individual solutions (i.e. different ANFIS models) evolved over the generations (i.e. 1st, 5th, 15th, 20th…150th, 300th generation). The solutions of different generations are distinguished by different colour codes. Solutions in the initial population (1st generation) are randomly generated between 1 and 40 rules. They are found to have varying model accuracy performance, ranging from 0 to no more than 80% (Figure 4.10 c). It is clear that the populations have evolved prematurely in the region of small Fuzzy rule-bases, leaving the input and output space largely unexplored.

The solutions' model accuracies of test case A_1 are also observed to converge quickly, as shown in Figure 4.10 c. The randomly generated initial population in terms of Fuzzy rules and their antecedent parts have an overall poor median model accuracy of less than 25%. This suggests that a randomly generated solution is unlikely to have good model accuracy. Thus, solutions with optimal model accuracy require careful configurations of rule-base (i.e. activated IF-THEN rules and antecedent parts).

Fitness evolution of solutions in test case A_1 for objective function M_1

Figure 4.10 a. Test case A_1 - Convergence of objective function, M_1 (initial population - densely deactivated, population size = 200, generations = 300, mutation rate = {0.01, 0.01}).

Fitness evolution of solutions in test case A_1 for objective function M_2

Figure 4.10 b. Test case A_1 - Convergence of objective function, M_2 (initial population - densely deactivated, population size = 200, generations = 300, mutation rate = {0.01, 0.01}).

Figure 4.10 c. Test case A_1 - Convergence of objective function, M_3 (initial population - densely deactivated, population size = 200, generations = 300, mutation rate = {0.01, 0.01}).

Figure 4.10 d. Initial population with densely deactivated Fuzzy rule-base influences the manner in which solutions evolve over 300 generations (initial population - densely deactivated, population size = 200, generations = 300, mutation rate = {0.01, 0.01}).

Figures 4.11 a to 4.11 d illustrate the fitness evolution of solutions in test case A_2 evolved over 300 generations with population size of 200. It is observed from Figures 4.11 a and 4.10 b that the objectives M_1 and M_2 have failed to converge from an initial population of evenly distributed Fuzzy rule-bases. From Figure 4.11 d, the number of solutions with more than 70 Fuzzy rules is observed to have grown from the 80th generation onwards. These solutions are observed as outliers in terms of Fuzzy rule-base size and model accuracy in Figures 4.11 a, b and c. Despite being anomalies, their dominance in model accuracy is maintained, thus allowing them the opportunity to reproduce into the subsequent generations. This phenomenon has led to two local optima as shown in Figure 4.11 d. First is the region of small Fuzzy rule-base and second is the region of solutions with high model accuracy and large Fuzzy rule-base. This signifies that the innovation time taken to generate local optima is possible and these solutions can take over the population as long as they can remain non-dominated.

In test case A_2, majority of the solutions are found to converge towards a small Fuzzy rule-base in the early generations. This phenomenon is also observed in test case A_1 and can be explained by the following two factors. First is the tournament selection. An evenly distributed initial population has about half of the population with 50% of their rules inactive. Competing for fitness between individuals of different rule-base size is unfair. This is because solutions with smaller Fuzzy rule-bases will be selected since it is uncommon to generate an initial population with good model accuracy. Such large diversity in Fuzzy rule-base size during competition can lead to vanishing selection pressure. Elimination of unfit solutions is due to a larger Fuzzy rule-base size rather than the IF-THEN rules being incompetent. The second factor is the crossover between solutions of different rule-base sizes. The winning solutions will undergo crossover and the chances for the solutions with a large rule-base to reproduce with solutions of a small rules-base will increase. This further increases the rate of reproducing an offspring with much smaller Fuzzy rule-base.
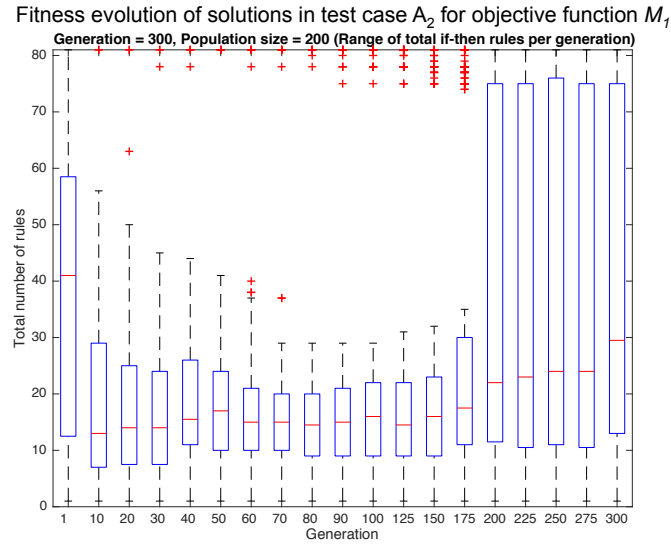
Figure 4.11 a. Test case A_2 - Convergence of objective function, M_1 (initial population - evenly distributed, population size = 200, generations = 300, mutation rate = {0.01, 0.01}).
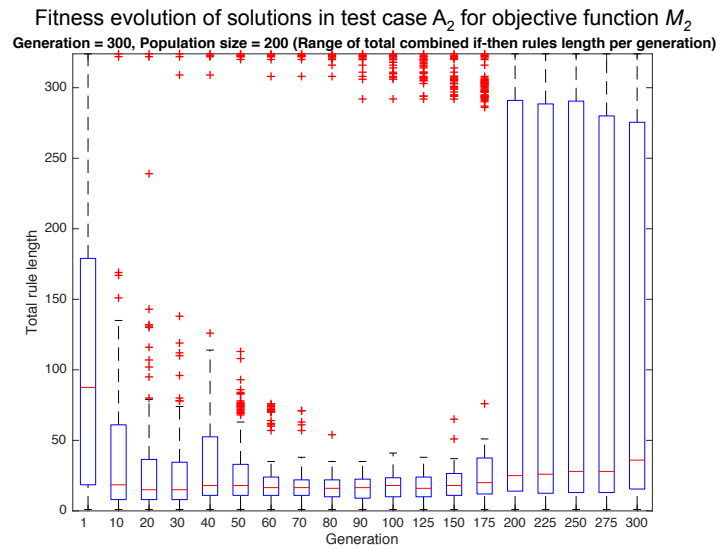
Figure 4.11 b. Test case A_2 - Convergence of objective function, M_2 (initial population - evenly distributed, population size = 200, generations = 300, mutation rate = {0.01, 0.01}).
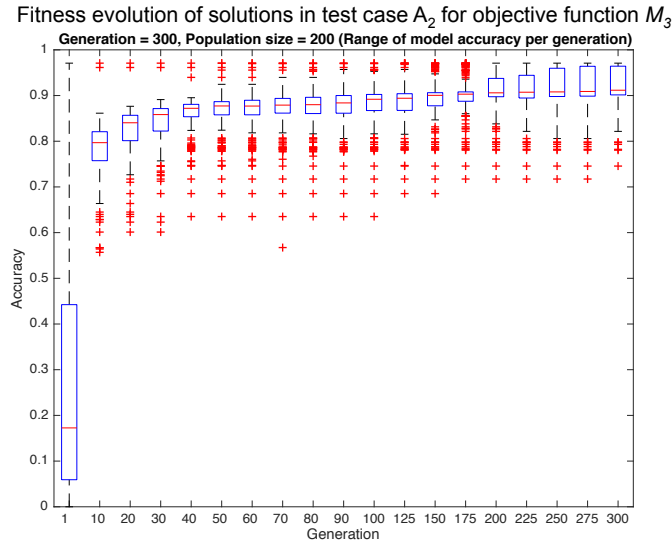
Figure 4.11 c. Test case A_2 - Convergence of objective function, M_3 (initial population - evenly distributed, population size = 200, generations = 300, mutation rate = {0.01, 0.01}).

Figure 4.11 d. Initial population with evenly distributed Fuzzy rule-base influences the manner in which solutions evolve over 300 generations (initial population - evenly distributed, population size = 200, generations = 300, mutation rate = {0.01, 0.01}).

Figure 4.12 a to Figure 4.12 d illustrate the fitness evolution of solutions in test case A_3 evolved over 300 generations with a population size of 200. It is clear that an initial population of densely activated rule-base effectively slows down the convergence of objective functions M_1 and M_2. This can be explained by the choice of solutions during tournament selections. Tournament selections are conducted between solutions of similar rule-base size, providing selection pressure on solutions with better model accuracies. For example, the solution with a better accuracy will be selected between two individuals with 70 rules. Referring to Figure 4.12 d, the slower convergence towards a smaller rule-base has led to a more thorough exploration of solution space.

In addition, the slower reduction of Fuzzy rule-base size in test case A_3 is likely performed through mutation, rather than through crossover as observed in test cases A_1 and A_2. The removal of rules through mutation has led to a subtle reduction in Fuzzy rule-base size. Despite the slower convergence of solutions towards smaller rule-bases, M_3 outliers in Figure 4.12 c still remains. Again, this can be explained with the difficulty to randomly generate a solution with good model accuracy.

Fitness evolution of solutions in test case A_3 for objective function M_1
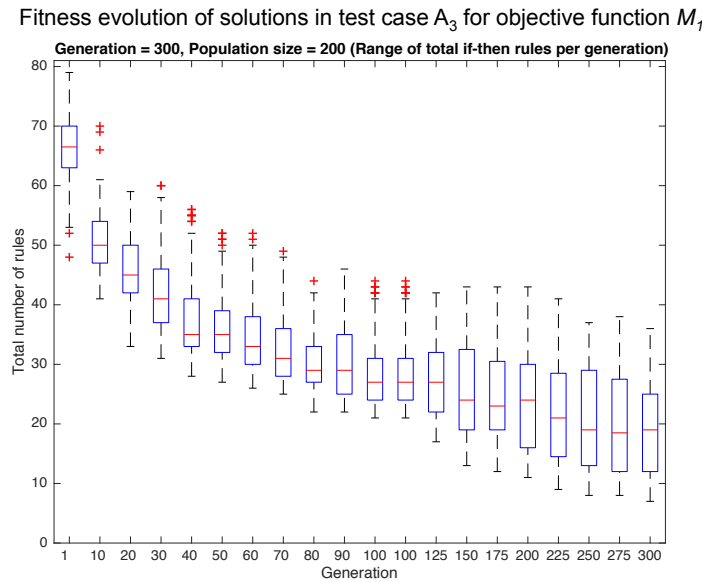
Figure 4.12 a. Test case A_3 - Convergence of objective function, M_1 (initial population - densely activated, population size = 200, generations = 300, mutation rate = {0.01, 0.01}).

Fitness evolution of solutions in test case A_3 for objective function M_2
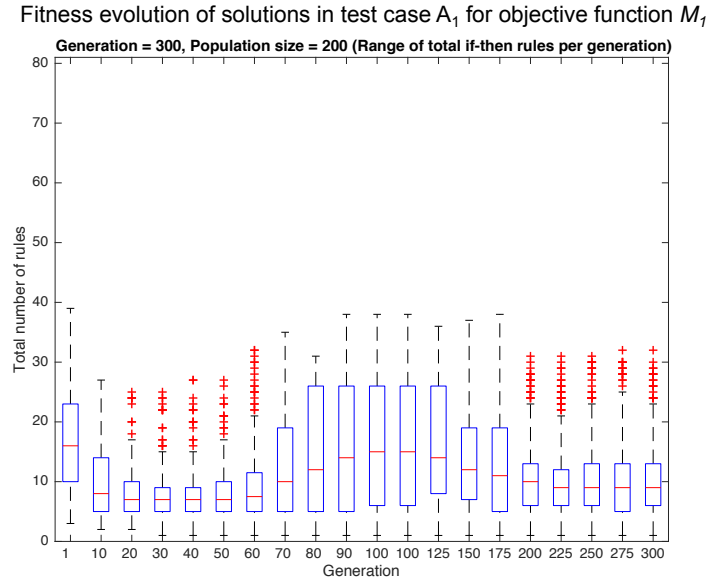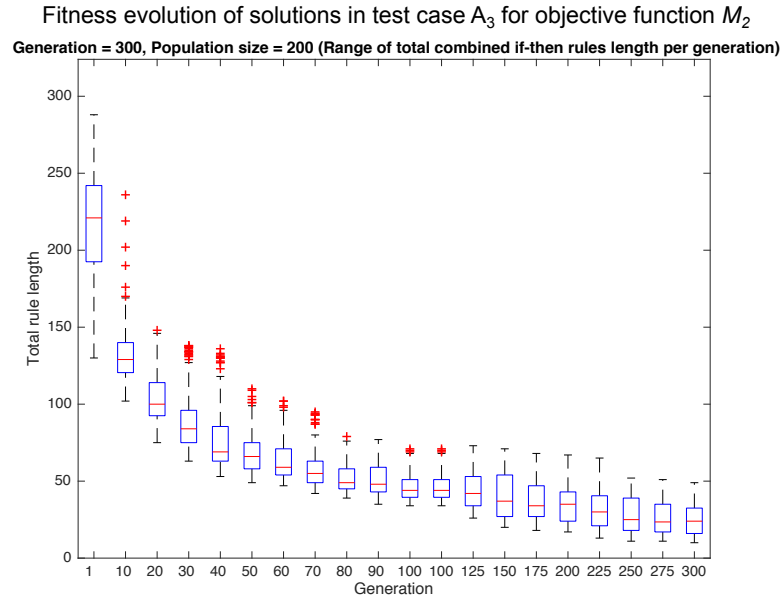

Figure 4.12 b. Test case A_3 - Convergence of objective function, M_2 (initial population - densely activated, population size = 200, generations = 300, mutation rate = {0.01, 0.01}).

Fitness evolution of solutions in test case A_3 for objective function M_3
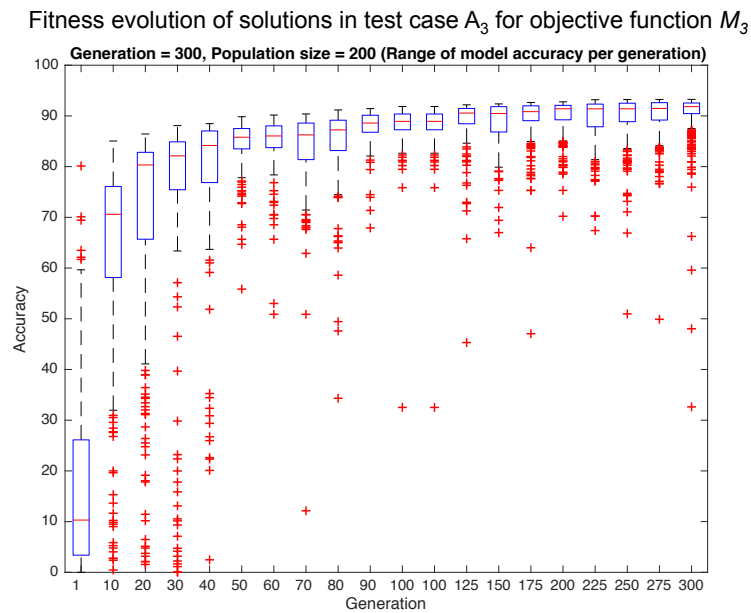
Figure 4.12 c. Test case A_3 - Convergence of objective function, M_3 (initial population - densely activated, population size = 200, generations = 300, mutation rate = {0.01, 0.01}).
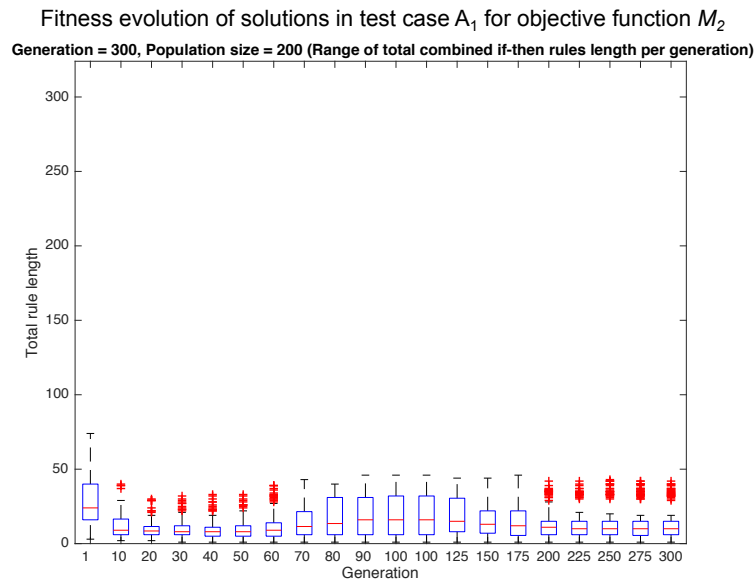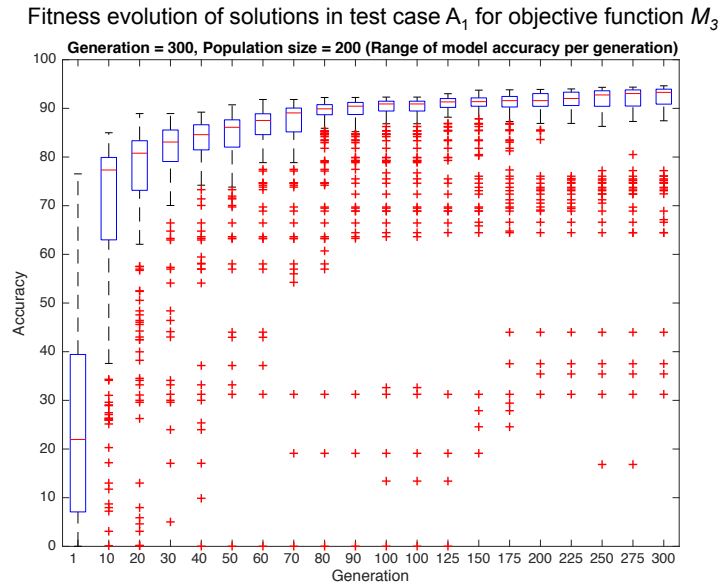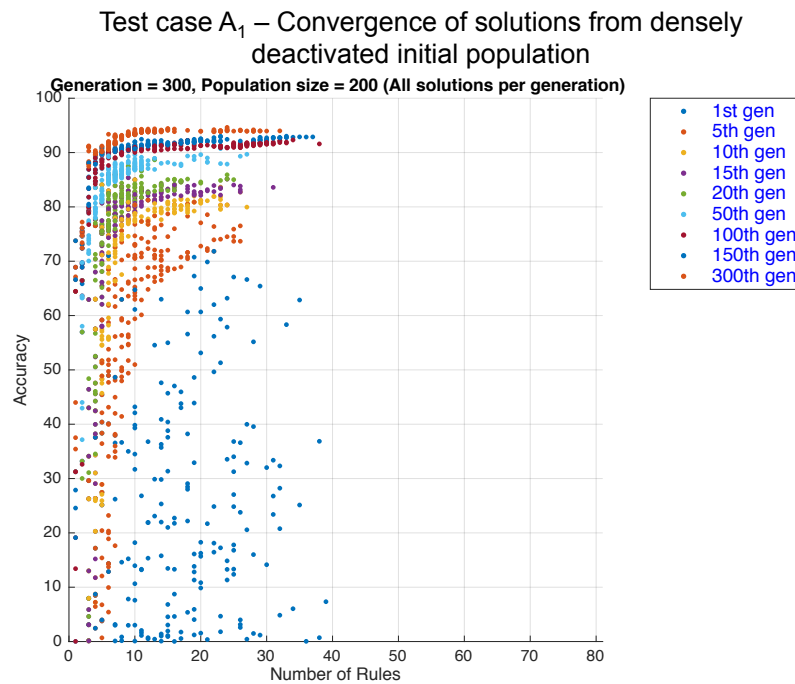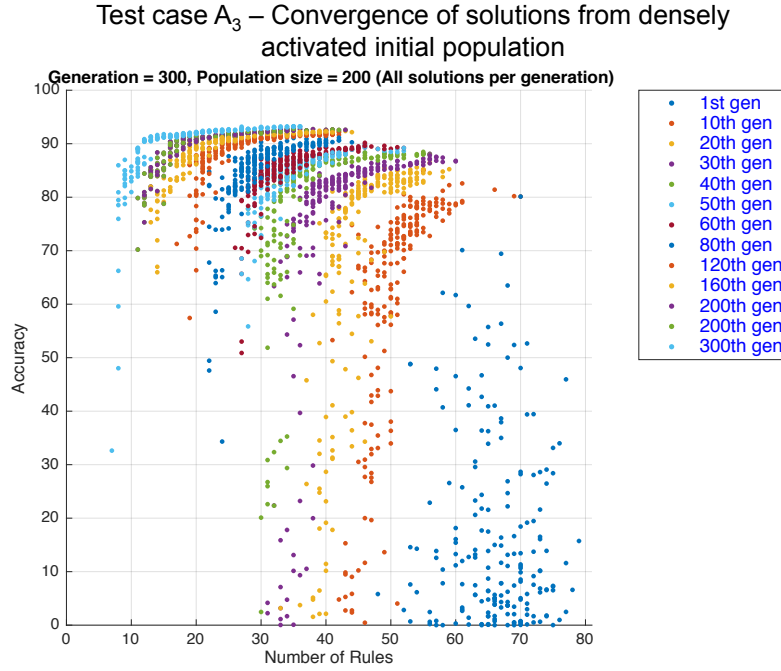
Figure 4.12 d. Initial population with densely activated Fuzzy rule-base influences the manner in which solutions evolve over 300 generations (initial population - densely activated, population size = 200, generations = 300, mutation rate = {0.01, 0.01}).

4.3.2 A Comparison of Impact of Population Diversity on Selection Pressure

Figure 4.13 a illustrates the comparison of mean M_1 of test cases A_1 and A_3 over 300 generations. It is evident that at the start of the GA search, there is a drastic difference in the means for the two test cases. Test case A_1, with densely deactivated initial population, converged to less than 10 rules after the 10th generation, which grew and subsided after 50th and 150th generations respectively. After which, the majority of the solutions did not go beyond 10 IF-THEN rules. On the other hand, test case A_3, which has a densely activated initial population, begins the GA search with a mean rule-base size of more than 65 and converged at a slower rate.

More importantly, an increase in the size of the Fuzzy rule-base in test case A_1 at the later generation is caused by the premature convergence of Fuzzy rule-base size. The selection pressure on better model accuracy occurs only after the population has evolved to a similar M_1 and M_2 fitness. Moreover, as observed from Figure 4.13 b, the quick convergence of mean model accuracy and the reduction mean rule-base size

94

earlier on in the GA search suggest that the parent solutions can be easily dominated by a new offspring.

Test case A_3, with a densely activated initial population, has also guided the solutions to a quick convergence in M_3. This is because individuals with similar rule-base sizes will compete for M_3 in the earlier generations. Unlikely in test cases A_1 and A_2, the populations search for better model accuracy only at the later generations. However, despite the progressive convergence, test case A_3 struggles to produce solutions with less than 20 IF-THEN rules. This signifies a long "takeover time" for a fitter solution to take over the population [159], which suggests a need for a greater selection pressure towards a smaller Fuzzy rule-base.
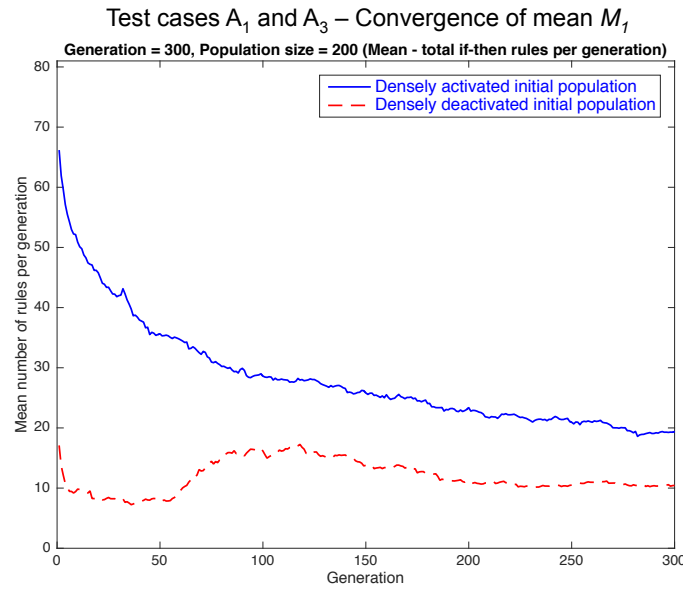
Figure 4.13 a. A comparison of mean number of IF-THEN rules, M_1, between (A_1) initial population - densely deactivated and (A_3) initial population - densely activated (population size = 200, generations = 300, mutation rate = {0.01, 0.01}).
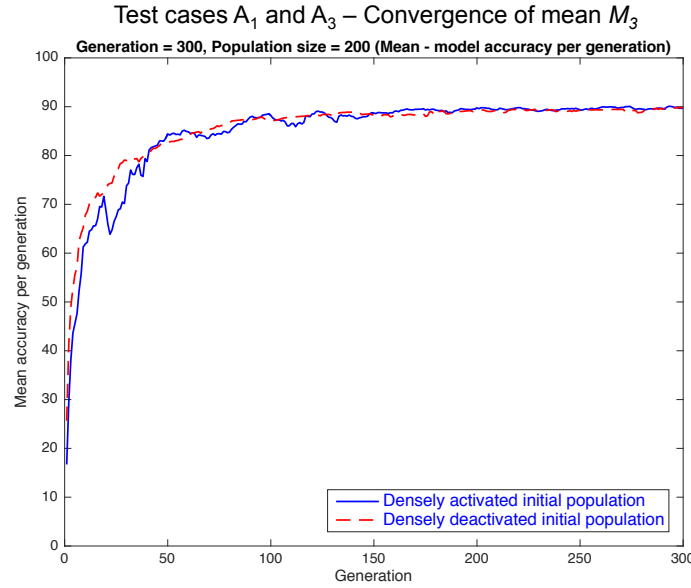
Figure 4.13 b. A comparison of mean model accuracy, M_3, between (A$_1$) initial population - densely deactivated and (A$_3$) initial population - densely activated (population size = 200, generations = 300, nutation rate = {0.01, 0.01}).

The standard deviations of M_1 and M_3 of the populations in test cases A$_1$ and A$_3$ are illustrated in Figures 4.14 a and b. Referring to Figure 4.14 a, test case A$_3$ maintains a Fuzzy rule-base diversity of about 4 to 9 rules over the generations. In test case A$_1$, the GA began with wider range of Fuzzy rule-base sizes of about 9 rules, and this reduced rapidly to 5 rules before the 10th generation. An increase in rule-base diversity is also observed after the 50th generations, corresponding to the increase in overall mean rule-base size of A$_1$ observed in Figure 4.10 a. This is because the populations have a limited exploration space for non-dominated solutions after it converged prematurely into a small rule-base.

The increase in standard deviation of M_1 in test cases A$_1$ and A$_3$ (Figure 4.14 a) at the later generations can be explained by the search of non-dominated solutions over multimodal search space. A multimodal search space is defined as multiple local optima acting as attractors in the search dynamics. Searching for models with a small, yet accurate Fuzzy rule-base at the later generations is increasingly challenging due to similar-looking solutions. This highlights the importance of maintaining M_1 diversity when searching for non-dominated solutions.

This finding further emphasises the importance of a thorough exploration of GA search towards a global optimum [157]. Premature convergence can be prevented when the "innovation time" is longer than the "takeover time" [159]. For instance, the time taken for the best individual to take over the population is longer than that needed to generate a new best individual. Therefore, the ability to maintain diversity among strong individuals without abrupt changes is critical for the creation of exploration opportunities. From Figure 4.12 d, the thorough exploration of search space in test case A_3 can be observed from the variation in M_3 diversity as compared to test case A_1. It is clear that when exploring non-dominated solutions before global convergence, it is necessary to maintain a right diversity in all objectives.
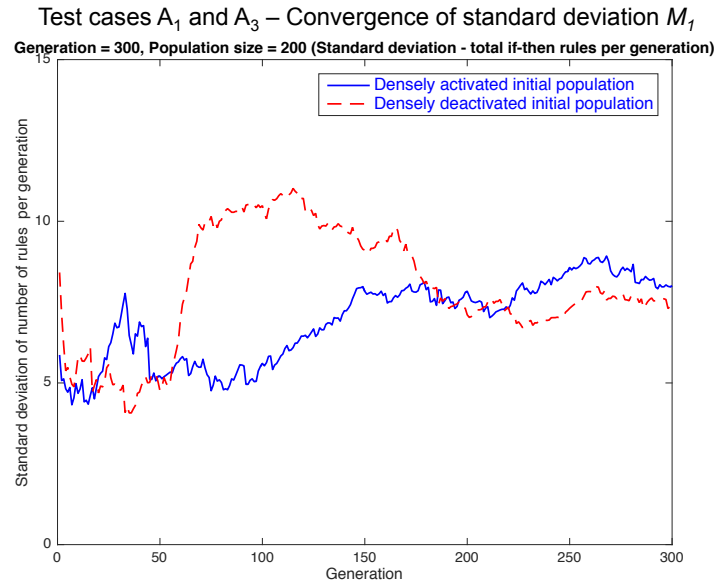
Figure 4.14 a. A comparison of standard deviation of total number of IF-THEN rules, M_1, between (A_1) initial population - densely deactivated and (A_3) initial population - densely activated (population size = 200, generations = 300, mutation rate = {0.01, 0.01}).
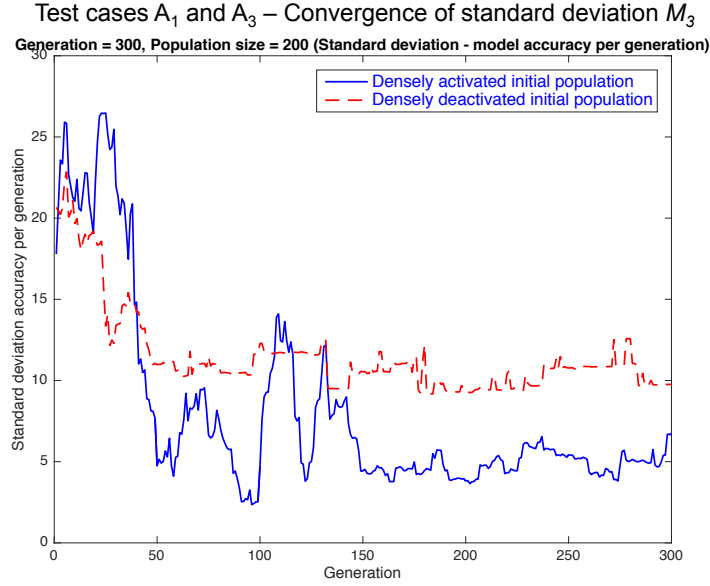
Figure 4.14 b. A comparison of standard deviation of model accuracies, M_3, between (A_1) initial population - densely deactivated and (A_3) initial population - densely activated (population size = 200, generations = 300, mutation rate = {0.01, 0.01}).

4.3.3 Improving Selection Pressure through Different Mutation Rates

In this section, GA search with different mutation rates, used to activate and deactivate the genes (antecedent parts of the IF-THEN rules) of a solution, are experimented to understand their influence on search space exploration. Table 4.2 illustrates the NSGA-II properties for test cases B_1, B_2 and B_3. Their properties are the same except for the mutation rates. In test case B_1, the mutation rate to activate and deactivate the genes is 0.03. The higher mutation rates in contrast to test case A_1 (0.01 mutation rates for both gene activation and deactivation) allows greater chance to generate offspring solutions that have different rule-base from their parent solutions. In test case B_2, mutation rates of 0.03 and 0.01 are used for activating and deactivating of genes respectively. Contrarily, test case B_3 has the opposite mutation rates of 0.01 and 0.03 for activating and deactivating of genes. The purpose of this configuration is to understand the impact of contrastingly different mutation rates on the search space exploration.

Table 4.2. NSGA-II design properties for test case B_1, B_2 and B_3, with mutation rates for activation and deactivation of antecedent parts of IF-THEN rules.

Test case	B_1	B_2	B_3
Number of generations	300	300	300
Population size	200	200	200
Mutation rate	0.03 (Parameter deactivation)	0.01 (Parameter deactivation)	0.03 (Parameter deactivation)
	0.03 (Parameter activation)	0.03 (Parameter activation)	0.01 (Parameter activation)
Initial population diversity	Densely activated	Densely activated	Densely activated

Figures 4.15 a, b and c illustrate the comparison of the mean of M_1, M_2 and M_3 of test cases B_1, B_2 and B_3 over 300 generations. It is clear that the different mutation rates have led to different convergence results. Referring to Figures 4.15 a and b, test case B_2 with higher mutation rates for activating a gene performed the poorest in terms of M_1 and M_2. The solutions' overall mean rule-base size does not converge to less than 50 rules. It is observed that despite having higher chances of antecedent parts activation (due to mutation), there is no increase in the total number of rules (M_1) and rule length (M_2) over the generations. With greater chance of activating new antecedent part of a rule, a more detailed subspace (i.e. finer grid partitions) is used to map the input and output space (Refer to Section 4.2.2 (2)). However, the constant generation of solutions with more antecedent parts in existing rules also prevents the population from exploring solutions of small rule-bases.

Solutions in test case B_1, with 0.03 mutation rates to activate and deactivate genes, have failed to reduce their rule-bases size to less than 36 rules over the generations. Comparing test cases A_1 (Figures 4.13 a) and B_1 (Figure 4.15 a), the higher mutation rates of 0.03 do not produce solutions of smaller rule-bases over the generations. Similar to test case B_2, the failure of the population to converge to a small rule-base in test case B_1 has showed that greater variability in both rule activation and deactivation

(through mutations) may introduce long "takeover time" [159]. This means that new but not fitter offspring are generated. Furthermore, the higher chance of mutations in a rule-base creates an offspring that is dissimilar from its parents, where key arrangements of a rule-base (i.e. the rules and their antecedent parts) are re-configured. Comparing test cases B_1 and B_2 in Figure 4.15 c, despite the solutions of smaller rule-bases in test case B_1, its mean model accuracy (M_3) of the population remained poor. This phenomenon further highlights that the offspring are often unfit. To minimise drastic changes in model accuracy, the generation of offspring should have subtle rule-base changes.

Test case B_3 with mutation rates of 0.01 and 0.03 for activating and deactivating of genes respectively performed the best among the test cases in all objectives. The higher mutation rate for gene deactivation forces the population to explore the region of smaller rule-bases with shorter rules as shown in Figures 4.15 a and b. At the same time, in Figures 4.15 c, the mean models' accuracies are observed to improve steadily over the generation to approximately 87%. The population in test case B_3 showed greater momentum in producing and selecting solutions of smaller rule-bases while not compromising the model accuracy. Contrarily, the inability to converge towards a smaller rule-bases in test cases B_1 and B_2 can be seen as incapability to produce accurate solutions with small rule-bases. Hence, this has showed that achieving shorter innovation time (i.e. time to generate new best solution) with increasing mutation rate for gene activation is unsuitable.
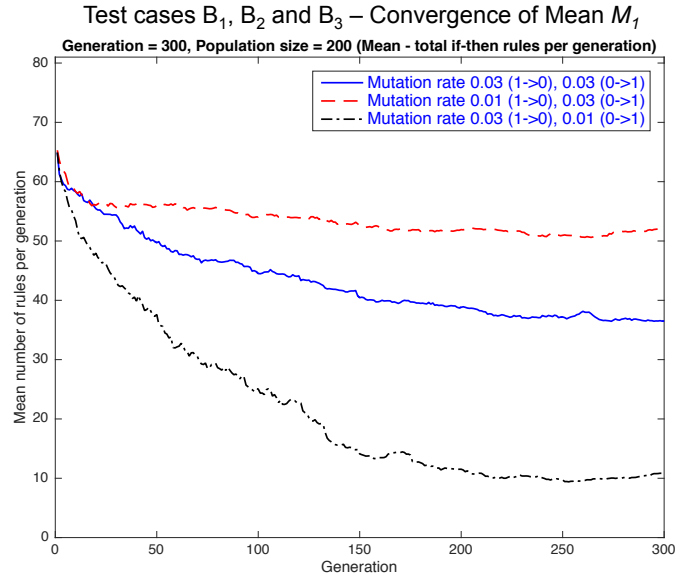
Figure 4.15 a. A comparison of the mean total number of IF-THEN rules, M_1, between (B_1) mutation rate = {0.03, 0.03} (B_2) mutation rate = {0.01, 0.03} (B_3) mutation rate = {0.03, 0.01} (initial population - densely activated, population size = 200, generations = 300).
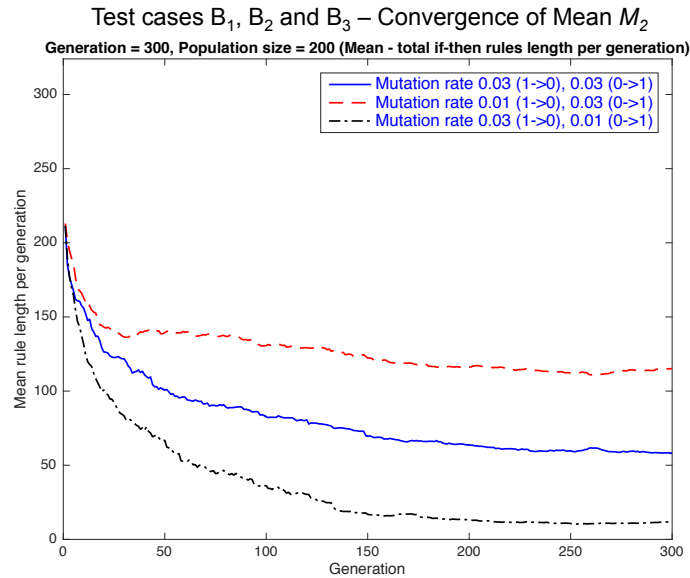
Figure 4.15 b. A comparison of the mean total rule length, M_2, between (B_1) mutation rate = {0.03, 0.03} (B_2) mutation rate = {0.01, 0.03} (B_3) mutation rate = {0.03, 0.01} (initial population - densely activated, population size = 200, generations = 300).
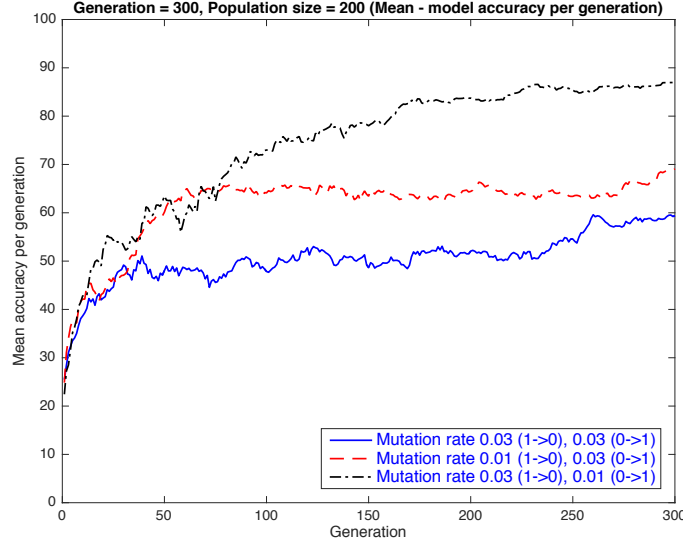
Figure 4.15 c. A comparison of the mean model accuracy, M_3, between (B_1) mutation rate = {0.03, 0.03} (B_1) mutation rate = {0.01, 0.03} (B_3) mutation rate = {0.03, 0.01} (initial population - densely activated, population size = 200, generations = 300).

The standard deviations of M_1 and M_3 among the populations for test cases B_1, B_2 and B_3 are illustrated in Figures 4.16 a and b respectively. From Figure 4.16 a, it is clear that the rule-base size diversity of test case B_3 grew significantly higher in the initial generations (from about 20th to 130th generation) as compared to test cases B_1 and B_2. The increase in M_1 diversity in test case B_3 can be explained with the higher mutation rate for deactivation of antecedent parts of a rule. For example, the offspring are forced to mutate towards a smaller rule-base, while the parent solutions with potentially more accurate yet larger rule-bases remained dominant. The ability to generate offspring with smaller rule-base in a subtle manner acts as an attractor for the population to explore similar regions of input and output space (i.e. small rule-bases). This also prevents the population from exploring in the wrong direction or away from small rule-bases. More importantly, a solution with small rule-base must also be accurate in order to be non-dominated. A non-dominated solution is superior in all objectives. The increase in population diversity in test case B_3 (Figure 4.16 a) signifies selection pressure where an offspring with smaller rule-base (refer to improving M_1 and M_3 in Figures 4.15 a and c) must also be more accurate in order to be dominant.

On the other hand, in test cases B_1 and B_2, the inability to explore the regions of smaller rule-bases has led to lower diversity of rule-base size throughout the generations (Figure 4.16 a). The generated offspring are expected to have similar or higher rule-base size as compare to their parent, due to higher chance of gene activations. As a result, tournament selection is performed between solutions of similar rule-base size; this is also observed from the model accuracy diversities of test cases B_1 and B_2, which remained in the range of 12 to 22% throughout the generations without converging to a smaller rule-base.

It should be noted that a generated offspring is likely to have poor model accuracy. This is observed in all test cases (Figures 4.13 b and 4.15 c) where the populations in the 1st generation have a mean M_3 of less than 30%. The inability of test cases B_1 and B_2 to generate a population with overall good model accuracy in the later generations highlights the importance of both population diversity and exploration of search space in the right direction. However, this must be performed in a subtle manner to prevent premature converge. For instance, in test cases A_1 and A_2, solutions with very small rule-bases in the early generation remained non-dominated by solutions with large rule-base of poor accuracy. This has led to a prematurely converged population with mean accuracy of more than 80% at only the 30th generation.
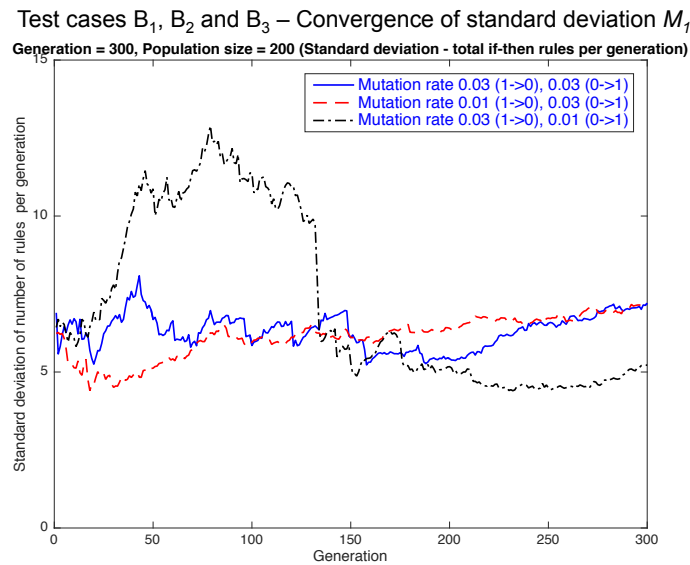
Figure 4.16 a. A comparison of the standard deviation of total number of IF-THEN rules, M_1, between (B_1) mutation rate = {0.01, 0.01}, (B_2) mutation rate = {0.03, 0.01} and (B_3) mutation rate = {0.05, 0.01} (initial population - densely activated,

population size = 200, generations = 300).
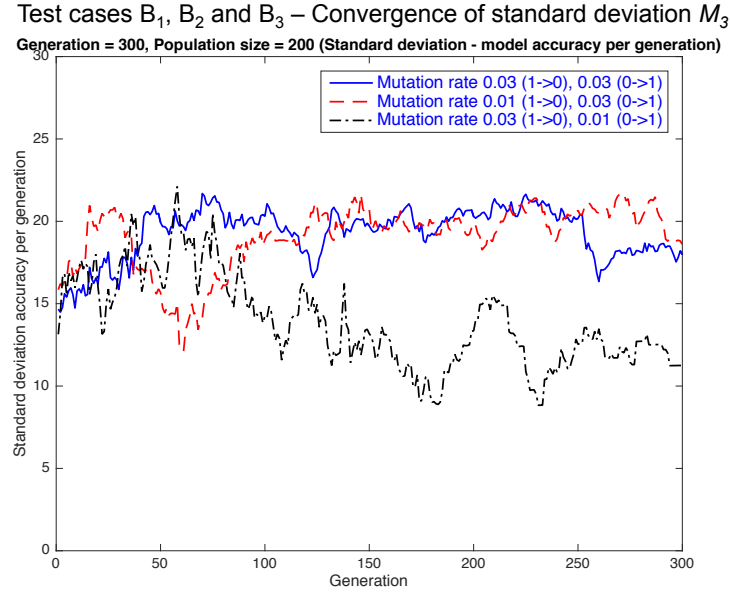
Figure 4.16 b. A comparison of the standard deviation of model accuracy, M_3, between (B_1) mutation rate = {0.01, 0.01}, (B_2) mutation rate = {0.03, 0.01} and (B_3) mutation rate = {0.05, 0.01} (initial population - densely activated, population size = 200, generations = 300).

Figure 4.17 illustrates the manner in which populations in test case B_3 converged over 300 generations in terms of objectives M_1 and M_3. Clearly, a higher mutation rate for deactivation of parameters has resulted in a population with smaller Fuzzy rule-bases [160] without compromising the exploration of search space. Figure 4.17 also provides another perspective of the gradual improvement of objectives M_1 and M_3 over the generations. Regions of solutions with small and inaccurate rule-bases in the search space are probed. Nonetheless, they remained non-dominated without taking over the population and create another local optima as observed in test case A_2 in Figure 4.11 d.
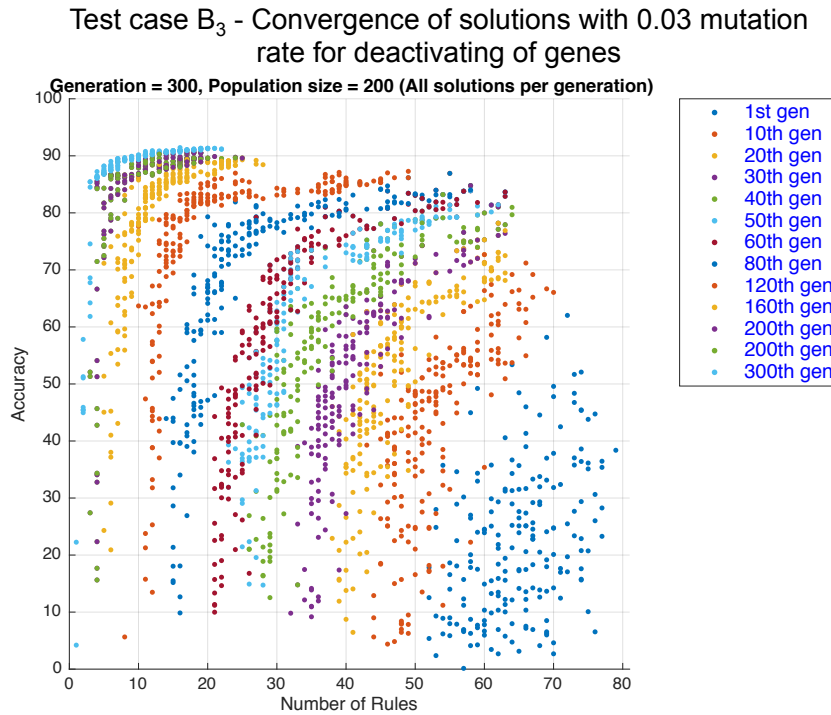
Figure 4.17. The impact of 0.03 mutation rate for deactivation of parameters over 300 generations (initial population - densely activated, population size = 200, generations = 300, mutation rate = {0.03, 0.01}).

4.4 Chapter Summary

Chapter 4 introduces the use of NSGA-II to optimise the complexity and interpretability of an ANFIS model, and evaluates the impact of different NSGA-II design heuristics during optimisation. NSGA-II technique is known for its ability to preserve non-dominated and diverse set of solutions. We have showed that thorough exploration of search space can be achieved through maintaining population diversity and selection pressure during optimisation. Maintaining population diversity should be performed at the start of GA search, which can be done with the use of an initial population of densely activated rule-base. The search for non-dominated solutions beginning from a densely activated rule-base allows fair competitions among solutions of similar rule-base sizes. For example, two solutions of 70 rules will compete for better model accuracy. In this thesis, the recommended densely activated rule-base ranges from 50 to 81 rules. Conversely, an evenly distributed initial population ranging from 1 to 81 rules starts off the GA search with a population

diversity that is relatively high. In this case, solutions with smaller rule-base, regardless of model accuracy performance, have the tendency to dominate the population. We have showed that this has led to premature convergence, as well as the possibility of convergence toward multiple local optima.

In addition, higher mutation rate for genes deactivation acts as an attractor to guide the population towards smaller rule-bases. This has shown to create diversity among the population and a greater selection pressure to explore new non-dominated solutions, particularly at early generations. In this thesis, mutation rates of 0.01 and 0.03 to activate and deactivate a gene are used. This configuration, including densely activated initial population, allows subtle mutation in the rule-base towards small rule-bases. The population, regardless of rule-base size, has shown to evolve towards similar model accuracy, which highlights that for the solutions to remain non-dominated, they must have small and accurate rule-bases. Lastly, a total of 300 generations is recommended to ensure that the GA search have sufficient time to explores the solution space thoroughly. Given that subtle changes to the solution's rule-base are recommended, 300 generations would allow non-dominated solutions to be searched over multimodal search space without premature convergence.

5 Investigation of Spatial Challenges in Real-World Indoor Environments

Chapter 5 investigates the spatial challenges found in real-world environments. Two WSN test beds, deployed in administrative offices, are described and compared in Section 5.1. A decision tool is introduced in Section 5.2, to select an optimal Fuzzy model among Pareto front for model interpretation. The decision is based on the importance of Fuzzy model generality on unseen data and the link failure prediction accuracy to minimise energy wastage. Subsequently, the chosen solutions are analysed in Section 5.3 using Fuzzy rule removal sensitivity approach, where individual rule is removed and the change in respective predictive conditions are monitored. It is observed that the removal of rules of the same parameters does not have the same contributions to the respective model's prediction performance. Instead, the contributions of parameters to the Fuzzy models' predictive performances are dependent on factors such as long-distance or short-distance communication, controlled experiments and real-world test beds. Lastly, Section 5.4 concludes the chapter.

5.1 Descriptions of WSN Test Beds in Real-World Environments

This section describes two WSN test beds deployed in administrative offices in the Solaris building (WSN@Solaris) and in the Vaucanson building (WSN@Vaucanson). Link quality parameters collected from these test beds are used as training inputs to developed ANFIS models for spatial-related link failure predictions.

5.1.1 Solaris Building (Single Storey Administrative Office)

WSN@Solaris is located in a single level administrative office of approximately 900

m^2. Figure 5.1 illustrates the floor plan of WSN@Solaris with the deployment locations of 21 routers and one coordinator. The office can be broken down into two areas. First is the centralised open-concept administrative area consisting of workstations and 1.2 m high desk partitions. Approximately 24 employees occupied this area. Second, the south and west sections of WSN@Solaris are made up of partitioned rooms consisting of meeting rooms, laboratories, and a pantry. The entire office is furnished with carpet flooring and false ceilings.

The routers in WSN@Solaris are deployed in a scattered manner as denoted as red circles in Figure 5.1. Figure 5.2 shows the photos of the actual routers' placements in WSN@Solaris. They are deployed among the workstations, in meeting rooms and on the walls along the corridors at approximately 0.5 m in height. The coordinator, denoted as a yellow triangle in Figure 5.1, is deployed in a location where nodes located further away are subjected to signal attenuation from partitioned rooms, while nodes deployed closer are subjected to human movements.

Figure 5.1. The deployment locations of 21 routers and one coordinator in WSN@Solaris.

Figure 5.2. The routers' deployment in WSN@Solaris. These routers are deployed in a meeting room, on a workstation, and on a wall along a corridor at 0.5 m in height.

5.1.2 Vaucanson Building (Two Storey Administrative Building)

WSN@Vaucanson is set up in a two storey administrative office of 3750 m^2. Figure 5.3 illustrates the combined two storey floor plans of WSN@Vaucanson with the deployment locations of 18 routers and a coordinator. Approximately 60 employees occupy the office during working hours. WSN@Vaucanson has a dense room layout, made up of administration offices, meeting rooms, conference hall, and a small data centre. The 18 routers are strategically deployed from the ceilings along the corridors, forming a grid layout such that data from sensor nodes (not shown in Figure 5.3) can be relayed to the coordinator deployed at the second storey. 14 routers are deployed on the first level and four others are deployed on the second level. The building is fitted with a heating system, however all nodes are deployed away from the drafts of ventilation units, cooling panels, fan-coils and any radiation elements.
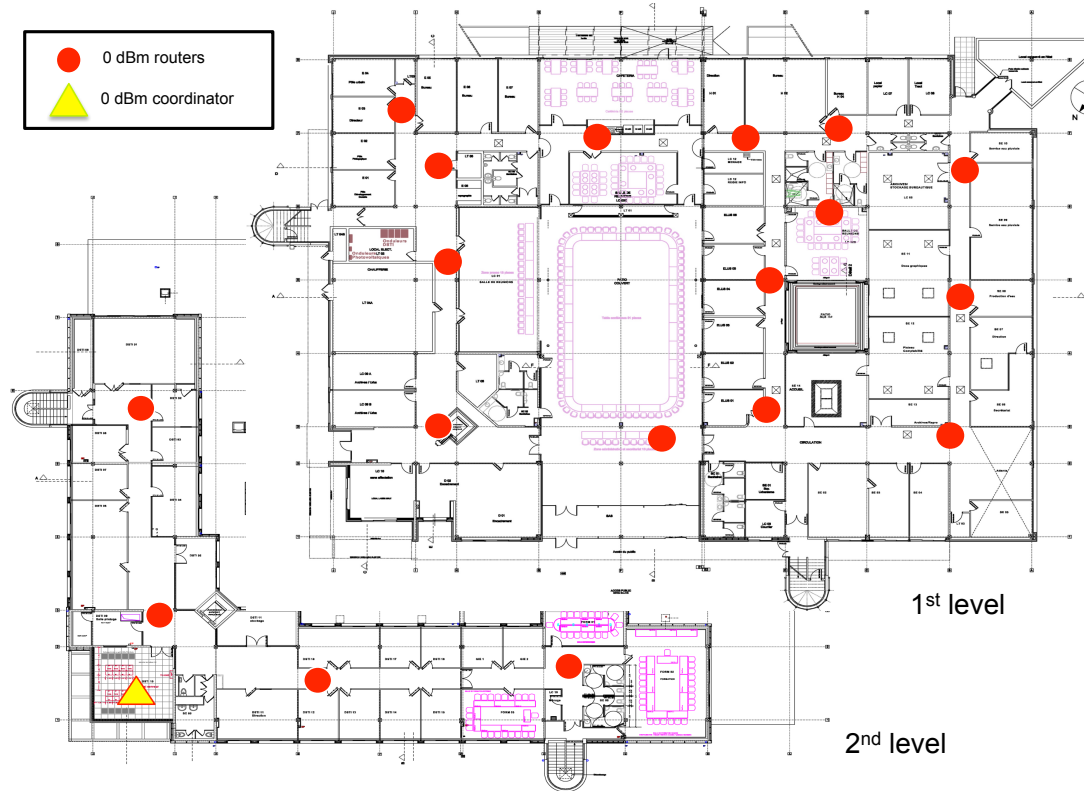
Figure 5.3. The deployment locations of 18 routers and one coordinator in WSN@Vaucanson.

5.1.3 Differences between Real-World Test Beds (WSN@Solaris and WSN@Vaucanson)

The following are two key differences between WSN@Solaris and WSN@Vaucanson.

1. Communication quality – WSN@Vaucanson is approximately four times the size of WSN@Solaris and there are fewer routers implemented. The routers in WSN@Vaucanson are deployed further apart from each other to achieve sufficient routing coverage. The communications between routers in WSN@Vaucanson are therefore subjected to greater signal path loss and increasing number of spatial challenges. In contrast to the denser router layouts in WSN@Solaris, communications between neighbouring nodes have longer range and are likely to have lower link budget.

2. Routing quality – The routers in WSN@Vaucanson provide relay options for nodes deployed deeper in the network. For example, nodes on the ground level

require intermittent routers to relay their packets to the coordinator deployed on the second level. Unlike the shorter communication range and shorter routing paths in WSN@Solaris, the longer routing paths in WSN@Vaucanson provide a realistic evaluation platform in terms of end-to-end routing quality.

The implementation of test beds with the contrast in WSN communication and routing performance provides a diverse platform for investigation into WSN link quality.

5.1.4 Key Differences between Controlled Experiments and Real-Test Beds

The key differences between the WSN test beds deployed in a real-world environments and controlled experiments are described as follows.

1. Environmental dynamics – Increased number of NLOS communications are expected in WSN@Solaris and WSN@Vaucanson due to the vast number of physical obstructions such as room partitions and multi-floors communication. In addition, real-world test beds are occupied during working hours, where the communications between nodes are subjected to physical obstructions such as human bodies. All dynamics in the real-world test beds are non-simulated. They are for instance, closing and opening of doors, placements of chairs, and moving human bodies. It is important to note that Wi-Fi interference (if any) is minimal. This is because all WSN nodes are deployed away from Wi-Fi access points and also operate at least 12 MHz away from Wi-Fi operating channels.

2. Number of nodes and flexibility of deployment – Real-world environments have larger deployment grounds and utilise more nodes for greater routing coverage. At the same time, the deployment locations of these nodes are not constrained. For example, the distances between nodes are not fixed. With more nodes available as well as the flexibility of deployment, link quality information of greater variability can be expected as compared to a controlled experiment.

3. Availability of routing paths – WSN@Solaris and WSN@Vaucanson are deployed with more routers and therefore have a denser network topology. This translates to an increase in the number of end-to-end routing paths and

more routing options between any two nodes. Unlike in controlled experiments, the communications between nodes are fixed.

5.1.5 Classification of Link Failures from Real-World Test Beds

In this section, WSN link failures from real-world test beds are classified according to their respective causes. In order to provide representative training inputs to model spatial-related link failures, only data of dedicated periods are used. These periods are from 12 am to 5 am and 12 pm to 5 pm representing non-working hours and peak working hours respectively.
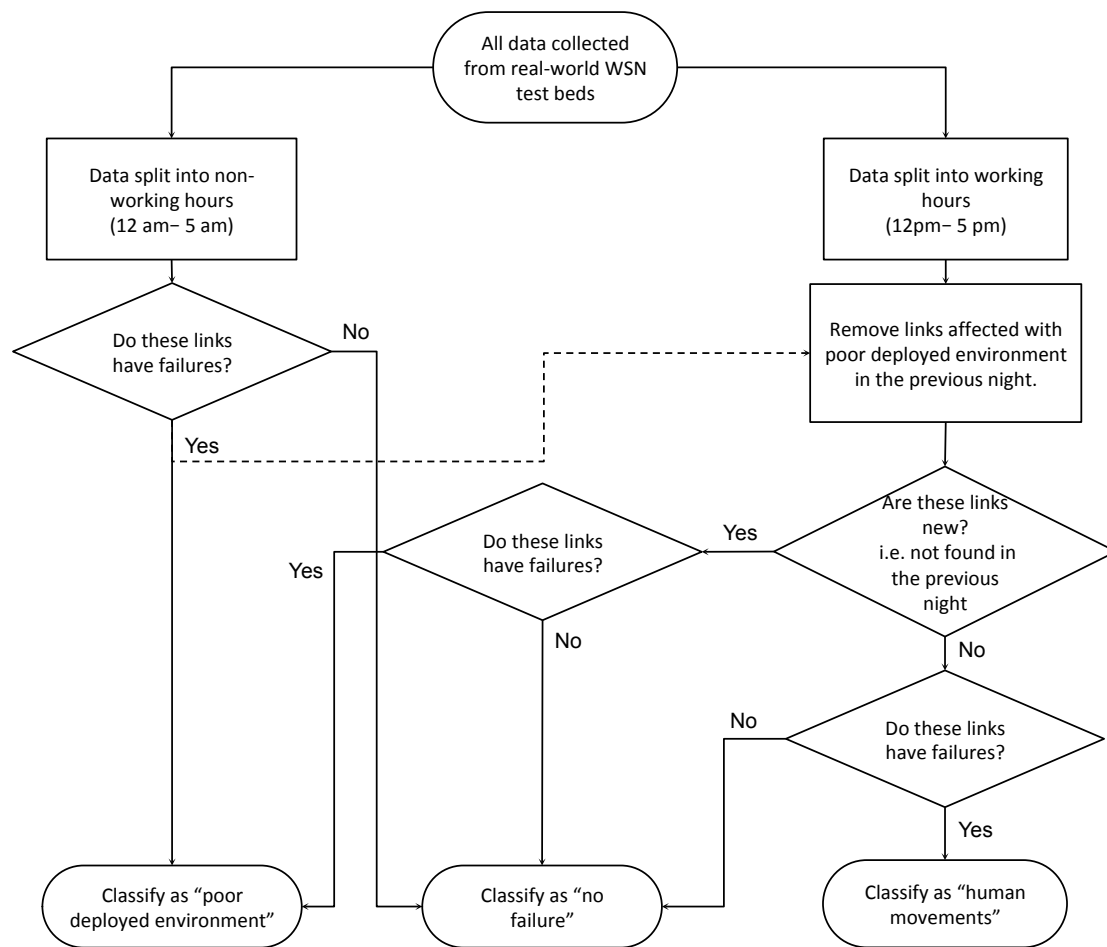
Figure 5.4. Flow diagram – Classification of spatial-related link failures from real-world test beds.

Figure 5.4 illustrates the flow diagram to classify link failures in WSN@Vaucanson and WSN@Solaris into poorly deployed environment and human movements. Any link failures that are captured during non-working hours are classified as caused by

poorly deployed environment. It is assumed that in this period, WSN is under no influence of human activities, where link failures are subjected to poor reception between communicating nodes. It is noted that these links affected by poorly deployed environment are filtered from the data of the next day. By doing so, the links that are already affected with poorly deployed environment are not confused with human movements. Newly discovered link failures during the working hours on the following day and are not found during non-working hours are also classified as poorly deployed environment. These new links with failure are not available during previous day's non-working hours, suggest that they had persistently failed due to poorly deployed environment. Lastly, further link failures found during working hours are classified as human movements. These links have not failed during non-working hours but have failed during working hours. This suggests that the introduction of human movements has led to link failures.

5.2 Selection of Fuzzy Solution From the Pareto Front

5.2.1 Model Accuracy and Interpretability Trade-Offs

In the absence of user preference, neither of the solution from the Pareto front is superior. Therefore, a decision tool is used to select a solution from the Pareto front for interpretation based on two factors. These factors are the importance of accurate spatial-related link failure prediction and model generality on unseen data.

1. Failing to predict the cause of link failure and energy wastage

In this section, a power consumption profile of a wireless sensor node's data transmission from a wake cycle is described. It is noted that a typical wireless sensor node is equipped with environmental sensing capabilities to measure its surrounding temperature, humidity, illumination and atmospheric pressure periodically.

Figure 5.5. Current ouputs of a wireless sensor node's data measurements and data transmission from a wake cycle.

Figure 5.5 illustrates the current outputs, which represent the energy consumptions of a wireless sensor node during its active duty cycle. Every active period lasts for approximately 160 ms and consists of the following events as denoted with current consumption peaks in Figure 5.5.

1. Initialisation of sensor elements – Start temperature and light measurements, read battery voltage, and reset pressure sensor.
2. Pressure sensor reset completed.
3. Pressure sensor calibrated.
4. Start pressure sensor's temperature measurement.
5. Pressure sensor's temperature measurement completed. Start pressure measurement.
6. Pressure measurement completed.
7. Temperature and luminance measurement completed. Start humidity measurement.
8. Humidity measurement completed. Switch off all sensors.
9. Clear-channel assessment, packet transmission and wait for acknowledgement.

The microcontroller [39] enters a deep sleep state in between the current peaks while

114

waiting for the next timer event. The current consumption is higher during the active period due to the activation of clock generator for sensor readings. The average power consumption of the node depends on the duration of each duty cycle and can be characterised as shown in Equation 5.1 below.

$$P_{avg} = (P_{sleep} * T_{sleep} + E_{active})/(T_{sleep} + T_{active}) \tag{5.1}$$

where,

T_{sleep} Duration of the sleep period

T_{active}: Duration of the active period

P_{sleep}: Power consumption during the sleep period

E_{active}: Energy consumption of a single active period

P_{avg}: Average power consumption the sensor node

This formula can be simplified as duty cycles scale longer (i.e. $T_{sleep} \gg T_{active}$).

$$P_{avg} = (P_{sleep} * T_{sleep} + E_{active})/T_{sleep} \tag{5.2}$$

$$P_{avg} = P_{sleep} + E_{active}/T_{sleep} \tag{5.3}$$

Given the power characterisation of T_{active}, P_{sleep}, and E_{active} as 160 ms, 15 μW and 651 μJ respectively, the average power consumption per duty cycle for four representative duty cycles is computed in Table 5.1.

Table 5.1. Average power consumption as a function of duty cycle.

Duty cycle length (T_{sleep})	Average power consumption (P_{avg})
5 minutes	17 μW
1 minute	26 μW
10 seconds	80 μW
1 second	663 μW

Sleep power is observed to be dominant for longer duty cycles (1 - 5 minutes) whereas active power is dominant for shorter duty cycles (1 - 10 seconds). It is apparent that the prolonging of active duty period increases the overall power consumption exponentially [77, 78, 79]. As such, further retransmission after a failed data transmission would prolong the active period of a node and escalates the total energy consumed. Therefore, detecting a link of poor quality and avoiding data transmission over it should be prioritised.

2. Model generality on unseen data for an interpretable solution

The number of Fuzzy rules and the total rule length are useful measures against the over-fitting of Fuzzy rule-based classifiers [155]. This is to say that the increase in the number of Fuzzy rules degrades the model's ability to generalise a system. Over-fitting happens when a modelled system corresponds too closely to the residual variation from a particular set of data such as noise in link quality information. Therefore, the Fuzzy model that fails to perform on unseen data is not a good representation of the network.

The Pareto fronts of the optimised Fuzzy models of WSN@Solaris and WSN@Vaucanson are shown in Figure 5.6 and Figure 5.7. These solutions are the fittest individuals among the population in the final 300th generation. Solutions in the Pareto front are ranked 1 using the fast non-dominated sorting method described in Section 4.2.1 where they are not dominated by any other solutions in the same generation. Pareto front consists of solutions with marginal rates of return, where an

improvement in one objective degrades another. Both Pareto fronts form knee shape curves, demonstrating the trade offs between model accuracy and size of Fuzzy rule-base. In both examples, degradations of models' accuracy are observed when the number of rules reduces to less than seven Fuzzy rules. This signifies the limitation of small Fuzzy rule-bases to provide accurate prediction. At the upper bound of this degradation, further increase in Fuzzy rule-base size has minor improvements in models' accuracy.
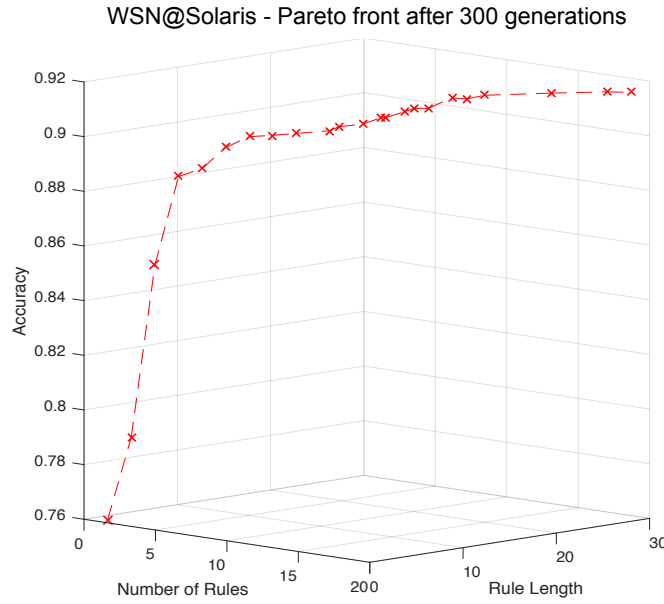
Figure 5.6. WSN@Solaris - Pareto front (initial population - densely activated, population size = 200, generations = 300, mutation rate = {0.03, 0.01}).
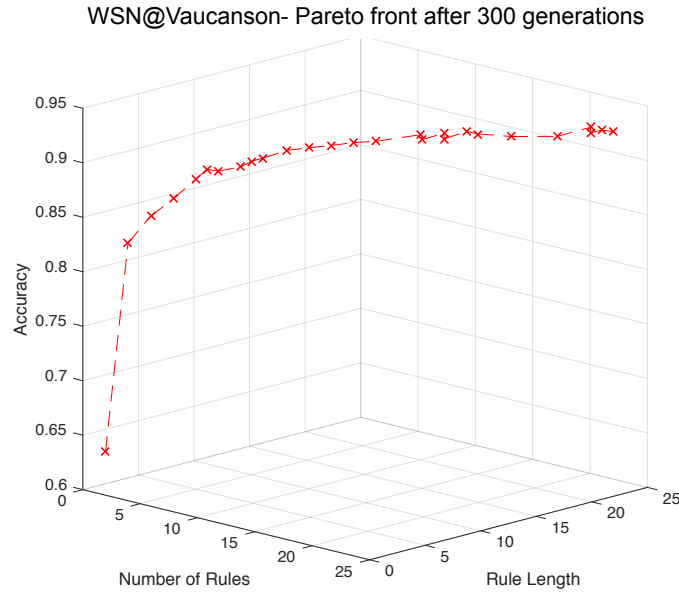
Figure 5.7. WSN@Vaucanson - Pareto front (initial population - densely activated, population size = 200, generations = 300, mutation rate = {0.03, 0.01}).

Fuzzy solutions of the Pareto fronts are evaluated with unseen validation set from 10% of the training data in Tables 5.2 and 5.3. In both examples, the differences between model accuracy of test and validation data set do not exceed 3.22%. The chosen solution should have the highest model accuracy at the point where any further reduction of rule-base size will greatly reduce the model accuracy.

Table 5.2. WSN@ Solaris – Comparison of the training and test accuracy. Solution indicated with (*) is selected for Fuzzy model interpretation.

No	Total number of Fuzzy rules	Total Fuzzy rules length	Model accuracy (Training data)	Model accuracy (Test data)	Rate of accuracy increment
1	1	1	0.787	0.7548	0.0782
2	2	2	0.8474	0.833	0.0253
3	3	3	0.8825	0.8583	0.0117
4	4	4	0.8974	0.87	0.0046
5	4	5	0.8998	0.8746	0.0056
6	5	5	0.9034	0.8802	0.0101
7	5	6	0.9043	0.8903	0.0026
8	6	6	0.9039	0.8929	0.002
9*	**6**	**7**	**0.9106**	**0.8949**	**0.0005**
10	7	7	0.9101	0.8954	0.006
11	7	8	0.9168	0.9014	0.0015
12	8	8	0.9219	0.9029	0.0015
13	8	9	0.9226	0.9044	0.0053
14	8	10	0.9216	0.9097	0.0013
15	9	11	0.927	0.911	-

Table 5.3. WSN@Vaucanson - Comparison of training and test accuracy. Solution indicated with (*) is selected for Fuzzy model interpretation.

No	Total number of Fuzzy rules	Total Fuzzy rules length	Model accuracy (Training data)	Model accuracy (Test data)	Rate of accuracy increment
1	1	1	0.6595	0.6545	0.1846
2	2	2	0.8713	0.8391	0.0101
3	3	3	0.8787	0.8491	0.0035
4	5	5	0.8846	0.8561	0.0166
5	6	6	0.8959	0.8726	0.0125
6*	**7**	**8**	**0.9037**	**0.8851**	**0.0092**
7	8	8	0.9117	0.8943	0.004
8	9	9	0.9148	0.8983	0.0015
9	10	10	0.9145	0.8998	0.0014
10	11	11	0.9165	0.9012	-
11	11	12	0.9179	0.9023	0.0023
12	12	12	0.9189	0.9046	-
13	12	13	0.9203	0.9048	0.0003
14	13	13	0.9193	0.9051	0.0004
15	14	14	0.9188	0.9055	-

5.3 Investigation of Individual Fuzzy rules in Optimised Fuzzy Model

In this section, a sensitivity analysis is used to determine the impact of individual Fuzzy rule on the model predictive accuracy. Individual rule is removed from the optimised Fuzzy model and the changes in prediction accuracy of the respective conditions – No Failure (NF), Human Movements (HM), and Poorly Deployed Environment (PDE) – are monitored. Table 5.4 and Table 5.5 illustrate the sensitivity analysis results of WSN@Solaris and WSN@Vaucanson respectively. The results for the different test beds are discussed in Sections 5.3.1 and 5.3.2 respectively, and are summarised in Section 5.3.3.

Removed rule leading to significant accuracy change indicates its relevancy to the overall model prediction performance, while a less important rule will have less contribution [140]. The training inputs are collected from real world test beds. Henceforth the Fuzzy models are expected to incorporate environmental noise. It is noted that the removals of individual rules may have drastic impact to the model accuracy, which are observed as outliers in Section 4.3. Therefore, to provide representative interpretation of the optimised models, only the removed rules with accuracy change of approximately 30% are discussed in Sections 5.3.1 and 5.3.2.

Figure 5.8 shows the final MFs for Mean RSSI, ACV RSSI, NTC and BNTC after 150 epochs of data training. The ranges and values of these MFs are referred during interpretation in the following sections.
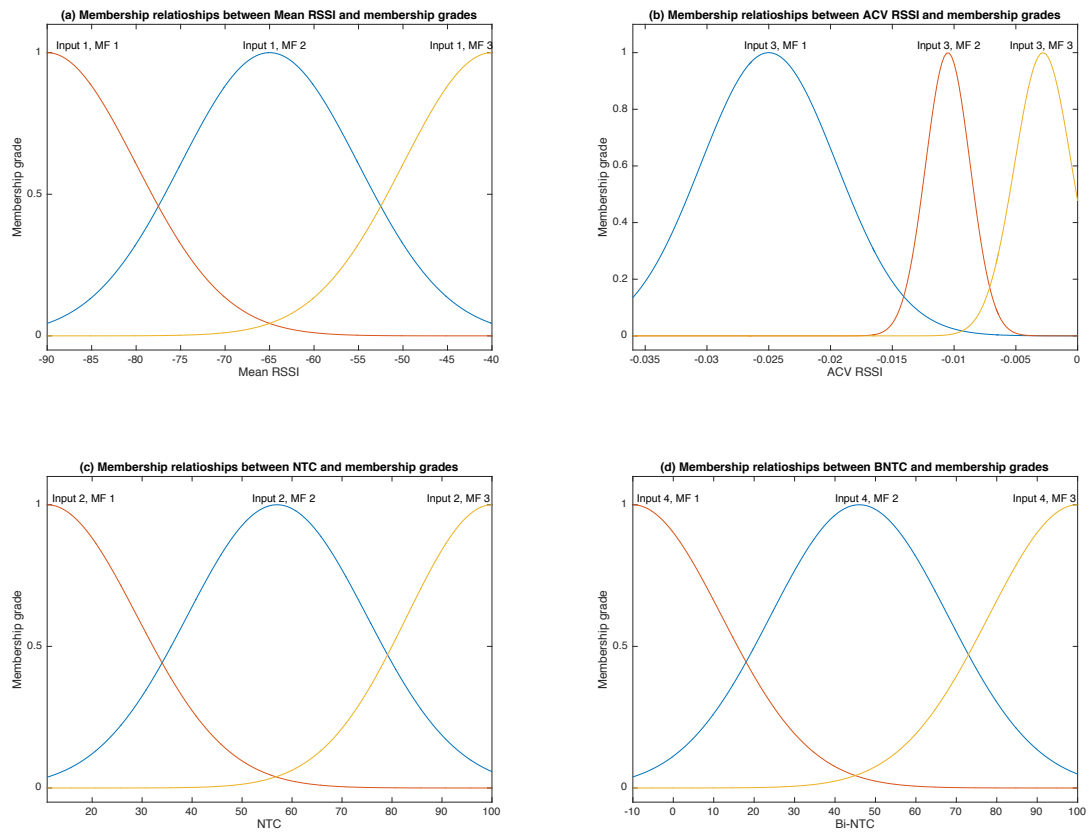
Figure 5.8. Final membership functions after 150 epochs of (a) Mean RSSI, (b) ACV RSSI, (c) NTC, and (d) BNTC.

5.3.1 WSN@Vaucanson
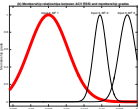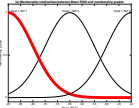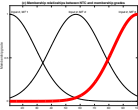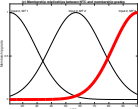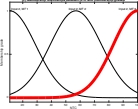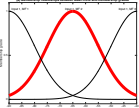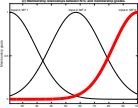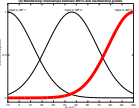
Rule index 2 – The removal of rule 2 (refer to Table 5.4) is found to degrade the prediction of HM by more than 50%, but has no substantial influence to NF and PDE. Rule 2 consists of the parameter "Poor" mean RSSI, representing a range of approximately -77 dBm to -89 dBm (refer to Figure 5.8). In other words, the "Poor" mean RSSI is capable of differentiating links that are affected by HM. Nodes in WSN@Vaucanson are deployed further apart and long-distance reception between nodes are expected. As such, communication at the sensitivity edge may be lost when human activities are introduced. Links with "Poor" mean RSSI are therefore subjected to failure due to HM.

Rule indices 3 and 4 – The removal of rules 3 and 4 has degraded the prediction of NF by 94% and 36% respectively. Rules 3 and 4 are represented by the parameter "High" NTC and can be considered as an optimal communication success rate, ranging from 78% to 100%. Removing the model's ability to characterise optimal communication success rate has clearly affected the model's ability to differentiate spatial-related link failures (i.e. HM or PDE) from NF. This can be understood since links with failure do not have optimal communication success rates. It is also observed that the prediction of HM and PDE are not affected. Therefore, it can be said that NTC is useful at detecting link failures but may be insufficient to differentiate the cause of link failures.

Rule index 6 – The removal of rule 6 has degraded the prediction of NF and HM by approximately 95% and 30% respectively. "*Intermediate*" *mean RSSI* represents a range of -53 dBm to -77 dBm. Rule 6 with "*Intermediate*" *mean RSSI* can identify links with no failure. Coupling rule 6 with the findings of rules 3 and 4, we can infer that majority of the links with no failures in WSN@Vaucanson operate with "*Intermediate*" *mean RSSI* and *"High" NTC*. Coupling rule 6 with the findings of rule 2 signifies that links with "*Intermediate*" *mean RSSI* are also easily subjected to failure due to HM.

Table 5.4. Sensitivity analysis of optimised link failure prediction Fuzzy model (WSN@Vaucanson) with rule removal.

Rule Index	Parameters				Degradation or improvement of conditions when rule is removed
	Mean RSSI	*ACV RSSI*	*NTC*	*BNTC*	A. No failure B. Human movements C. Poorly deployed environment
1	-		-	-	-13.99% -15.76% -18.11%
2		-	-	-	+2.57% **-57.64%** -7.87%
3	-	-		-	**-94.37%** -7.32% -10.08%
4	-	-		-	**-36.66%** -6.05% +3.31%
5	-	-		-	-3.05% -9.39% +4.41%
6		-	-	-	**-95.34%** **-30.57%** +5.2%
7	-	-			-1.13% -6.21% +3.62%

5.3.2 WSN@Solaris
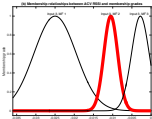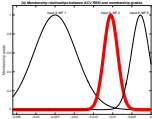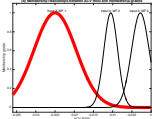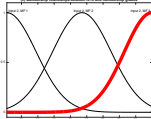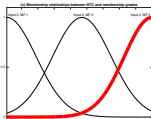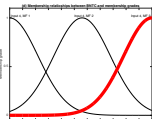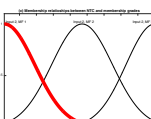
Rule index 3 – Rule 3 consists of *"Low" ACV RSSI* with a variation about -0.024 value. The removal of rule 3 (refer to Table 5.5) degrades the prediction of HM at approximately 51%. This rate is higher than what is observed in rules 1 and 2, where the *"Intermediate" ACV RSSI* only affects the predictability of HM by only 12%. *"Intermediate" ACV RSSI* value varies from -0.001 to -0.0105. We can infer that HM-related link failures in WSN@Solaris experienced varying received signal strength, and can be better distinguished with *"Low" ACV RSSI* rather than *"Intermediate" ACV RSSI*.

Rule index 4 – Rule 4 consists of *"High" NTC* ranging from approximately 78% to 100%. Similar to WSN@Vaucanson, *"High" NTC* is observed to degrade the predictability of NF significantly by approximately 85%. This is explained with links with no failure generally have consistently high communication success rates.

Rule index 5 – Rule 5 consists of two parameters. They are *"High" NTC* and *"High" BNTC* ranging from 78% to 100% and 72% to 100% respectively. *"High" NTC* and *"High" BNTC* represents the good quality incoming and outgoing links and can be associated with link symmetry between two nodes. The removal of rule 5 has degraded the prediction HM by 29.6%, which can be interpreted as the link symmetry characteristic is able to differentiate HM-related links failures.

Table 5.5. Sensitivity analysis of optimised link failure prediction Fuzzy model (WSN@Solaris) with rule removal.

| Rule Index | Parameters | | | | Degradation or improvement of conditions when rule is removed |
	Mean RSSI	ACV RSSI	NTC	BNTC	A. No failure B. Human movements C. Poorly deployed Environment
1	-		-	-	+1.61% -11.66% +4.6%
2	-		-	-	+1.61% -12.11% +5.13%
3	-		-	-	-27.71% **-51.12%** +2.14%
4	-	-		-	**-85.14%** -6.73% -27.35%
5	-	-			-16.47% **-29.6%** 8.55%
6	-	-		-	0% 1.59% -8.55%

125

5.3.3 Discussions

1. **Network layer parameters are poor differentiators of link failures caused by human movements or poorly deployed environment**

Similar to the findings from controlled experiments in Chapter 3, network layer parameters are observed to be capable of identifying links with no failures from link failures. However, both *NTC* and *BNTC* do not play a significant role in differentiating the different causes of spatial-related link failures (i.e. poorly deployed environment to human movements). The relation between *"High" NTC* and links with no failure suggests that failures on these links, if any, are not persistent.

2. **Parameter *mean RSSI* is not as dominant in real-world test beds**

The parameter *mean RSSI* is not as dominant in the real-world test beds as compared to in controlled test beds in Chapter 3. This can be attributed to the differences in test bed setups between real-world environments and controlled experiments. The variations in measured RSSI in a controlled experiment are limited. In an experiment with 23 WSN nodes that are deployed in offices [43], RSSI is found not to correlate well with distance in indoor environments and during daytime, where human movements are common. Given that there is more link information available in real-world test beds and no two links are the same, consistency in measured RSSI cannot be expected. As such, *mean RSSI* has limited contribution to the model prediction performance in WSN@Solaris and WSN@Vaucanson.

Figure 5.9 shows the RSSI readings between two nodes in WSN@Solaris. The fluctuations of RSSI during working hours were observed to be greater than non-working hours. Despite the static environment during non-working hours, the measured RSSI are found to be likely stronger during working hours. This can be contributed to the constructive and destructive multipath fading effects [12]. For instance, environmental changes during working hours may have provided a constructive effect on measured RSSI (i.e. opening of a door leading to an improved direct path communication) and had subsided during non-working hours (i.e. closing of a door). As such, a poorer *mean RSSI* does not always translate to the presence of human movements in the environment.

**Measured RSSI between two nodes during working hours and
non-working hours**
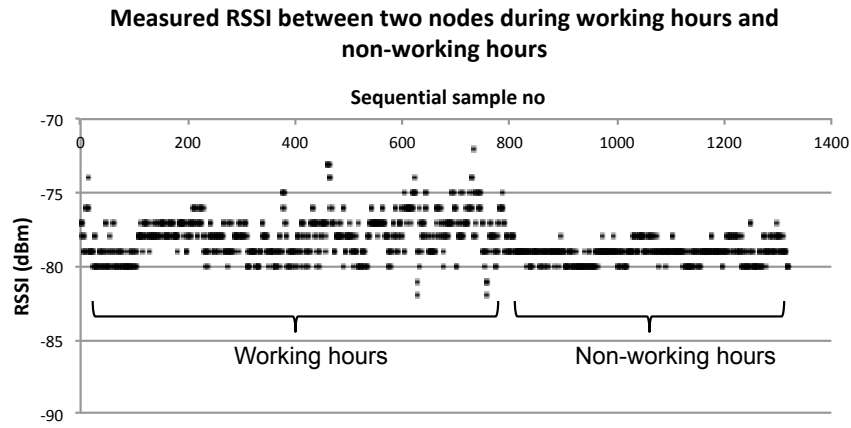
Figure 5.9. RSSI readings btween two nodes deployed in Solaris office during working hours and non-working hours. Constructive and destructive effects on RSSI readings can be expected despite the environmental settings.

3. The importance of *ACV RSSI* in real-world environment

The severity of multipath fading is said to exhibit a linear dependence with increasing human density, while long-term fading is a direct consequence of human presence [41]. WSN nodes are deployed among the presence of human occupants and long term fading can be expected as shown in Figure 5.9. Given that the human movement in the controlled experiments is simulated with a single human walking profile, its influence on WSN communication is minimal relative to real-world test beds. As such, *ACV RSSI* has performed better in real-world test beds than in controlled experiments.

Furthermore, the fading levels under NLOS conditions are expected to be higher than in LOS conditions [44]. With the vast number of physical obstructions in real-world test beds, the fading levels introduced by human movements under NLOS communication may have further contributed to the ability of *ACV RSSI* to detected HM.

4. Impact of short-range and long-range communication on link reliability

Nodes in WSN@Solaris have shorter distance communications relative to WSN@Vaucanson. The short distance communications can be equated with a wide range of RSSI [51], where a small variation in measured RSSI causes a large bias in

127

distance estimation. This is to say that the measured signal strength on a shorter distance communication is sensitive with the changes in the environment. As such, nodes in WSN@Solaris are more sensitive to the presence of human movements, which is reflected on *ACV RSSI*'s ability to detect HM.

On the other hand, nodes in WSN@Vaucanson are deployed far apart from each other. These links that are communicating at the sensitivity edge are likely to fail with increasing changes in the environment. For instance, nodes that are already communicating with *"Poor" mean RSSI* are likely to fail when the presence of human movements are introduced. Environments with frequent human mobility such as a clinic [161], office hallway [162], and research laboratory [43] have shown that mobile attenuators are the root cause of signal strength variation. Furthermore, the presence of human activities leads to more environmental changes such as closing and opening of doors, and moving of chairs, which can further degrade the already poor communicating nodes. As such, HM detection under long-distance communication is better distinguished with *"Poor" mean RSSI* rather than *ACV RSSI*

5.4 Chapter Summary

This chapter discussed the selection and interpretation of optimised Fuzzy models based on two real-world test beds; namely WSN@Solaris and WSN@Vaucanson. A decision tool is designed to select a solution from the Pareto front for model interpretation with the considerations of model generality on unseen data and optimal model accuracy. Consequently, sensitivity analysis is performed on the chosen model where individual rule is removed and the model accuracies of the respective predictive conditions are monitored.

The removal of rules with the same parameters does not have same effect on the prediction performance of models for the respective test beds. For instance, *mean RSSI* is observed to play a more important role in WSN@Vaucanson than in WSN@Solaris, whereas *ACV RSSI* is more critical in WSN@Solaris. Four conclusions are drawn from the Fuzzy model interpretation. First, the network layer parameters (*NTC* and *BNTC*) are useful for detecting link failures but are poor at differentiating the causes of spatial-related link failures. Second, due to the vast number of links in the large test beds coupled with the complexity of real-world

dynamics, *mean RSSI* is found not as significant in real-world test beds as compared to controlled experiments. Third, *ACV RSSI* has better contribution in detecting non-simulated human movements in real-world environments than in controlled experiment. Fourth, the impact of spatial-related link failures on physical layer parameters is dependent on the communication distance between nodes. For instance, *ACV RSSI* and *mean RSSI* performed better under short-distance and long-distance communications respectively.

Model interpretation in this chapter not only identifies influential features of a model, but also provides insights to the modelled system's behaviour. For instance, human activities are found to affect a pair of long distance communicating nodes (WSN@Vaucanson) more than short distance communicating ones (WSN@Solaris). Such examples signify the need to avoid long distance communication for packet routing at certain periods of the day, which is detectable with poor *mean RSSI*. With this knowledge, an increase in the communication link budget (i.e. transmission power control) could be potentially useful to minimise the impact of human activities during peak hours.

6 Long-Term WSN Routing Stability in Real-World Environment

WSN reliability is often assessed based on node-to-node communication performance through link characterisation. On comparison to short-term link assessments, long-term routing stability is an aspect of WSN that receives relatively less attention because the former focuses in routing protocol implementations [163]. Therefore, this chapter aims to investigate the long-term routing stability of ZigBee PRO implemented wireless sensor nodes deployed in real-world environments. In Section 6.1, related work on routing stability in a wireless network context is discussed. Section 6.2 presents the process of collating the actual routing paths of wireless sensor nodes taken from WSN@Solaris and WSN@Vaucanson test beds. The routing path stability is then evaluated in Section 6.3, where parameters such as relative routing path usage counts, usage rate of unique next hops and switching frequency counts are introduced. In Section 6.4, the characteristics of network bottlenecks are discussed and solutions to overcome these challenges are proposed. Lastly, Section 6.5 concludes with a summary of the key findings presented in this chapter.

6.1 Related Work on Monitoring Routing Stability

Chapter 2 reviewed that the existing WSN test beds are often designed to assess the performance of node-to-node communication through link characterisation. For example, the quality of node-to-node communication is measured using packet delivery and environmental noise factors [13, 66], spatial and temporal characteristics of packet loss [27, 64], and temporal consecutive link failures [25]. To our best knowledge, there is limited work conducted to investigate the long-term WSN routing stability in a real-world indoor environment.

A network topology is made up of interconnected routing paths across the network, while a routing path is made up of intermediate routers forming node-to-node connections. The lossy and unstable nature of wireless links can introduce routing

instability in WSN [164]. Routing instability refers to the phenomenon of frequent changes along routing paths between a source and destination node. The implemented routing protocol has to respond to node-to-node link failures, and makes changes along the routing path to improve its end-to-end reliability. Similar to link stability, the stability of generated routing path depends on its adaptability and robustness to overcome the dynamics within the deployed environment.

Authors in [164] evaluated the routing stability of 802.11 a/b/g mesh technology networks in terms of routing path prevalence, persistence and oscillation. It is found that the Wireless Local Area Network (WLAN) connectivity between a source and destination pair is seldom static. The routing paths between nodes are used for more than 40% of the time. In addition, 57.7% of the nodes pairs have a dominant route usage of less than one minute and a routing path oscillation of approximately 5000 times over four days. The deployment of WLAN routers is fixed. Since there are a limited number of routers within the reception range, their routing options are also limited. Unlike in a WLAN, WSN is usually designed for a wide deployment of nodes that forms a dense interconnected mesh network.

A *Competence* metric is introduced in [165] to differentiate long-term stable links for routing, while eliminating the unstable ones. To characterise long-term link stability, *Competence* incorporates the history of link quality into exponential weighted moving average as the weight of the smoothing filter. Furthermore, *Competence* compensates the variability of wireless communication by specifying upper and lower Packet Delivery Rate (PDR) bounds. PDR bounds account for short-term variation in delivery performance. It is found that the end-to-end (E2E) PDR varies significantly during the daytime. E2E PDR is measured at approximately 55% between the hours of 8 AM and 8 PM, dropping from 90% in the evening hours. *Competence* indicates the links as "poor" during the day, highlighting that these links have long-term link instability. In addition, the reduction in the quality of links during the day introduces the number of counts in which parent nodes switch between node pairs. This phenomenon triggers further packet losses from network maintenance packets, leading to greater energy consumption and route changes. However, a stable route enforced by a *Competence*-implemented protocol may increase traffic loads on affected nodes. In this chapter, we have shown that the most dominant next hop may

also operate on links with failures and not all routers have "good" routing options. The choice of routing path is largely dependent on the resources available and the types of routing mechanisms used.

Long-range link characterisation of WSN operating at 868 MHz is conducted in [166]. A node constructs a list neighbouring nodes within reception range in its NT. It is observed from the variations within NT that the number of nodes within receptive range changes constantly and satiability is uncommon. A proactive approach (i.e. short-term link quality estimation) is said to be ineffective at choosing reliable nodes, since a "reliable" next hop may become redundant in the next moment. Although the list of connected nodes in NT changes frequently, a group of stable neighbours still exists. A long-term stable connection with these nodes is discovered to have either less than -75 dBm in RSSI value or within one-fifth of the radio range at about 70 m. This suggests that for a connection to overcome the dynamics in the deployed environment, sufficient link budget must be available.

Existing link quality estimation techniques (discussed in Section 2.2) often implement short-term link quality assessment [35, 58, 59, 60, 61, 62, 163]. The link quality between two nodes is evaluated through methods such as decoding of received packets, probing network with additional overheads and over-listening of transmission in the channels. Short-term link quality assessments are regarded as reliable as long as the evaluation of link quality is accurate as the moment of communication. However, because the stability characteristic of a link is often not persistent, short-term link evaluation may not be representative [164, 165, 166].

Distributed wireless network system involves many uncertainties [165]. It is impractical to expect a stable network, yet expect WSN nodes to operate on a single reference value. Changes along routing paths are to be expected. The routing path selection is largely subjected to the implemented routing protocol. However, persistent changes in routing paths are undesirable. Re-routing requires the use of a network broadcast mechanism, which has shown to trigger further changes in the next hop due to increasing packet collisions [63, 165]. An unstable routing path suggests frequent link failures, thus necessitating additional network maintenance overheads such as retransmission and re-routing.

Routing stability impacts network protocols that require synchronisation between nodes. For instance, a duty cycling protocol that allocates transmission periods, and a multi-radio network that re-assigns radio channels between nodes. Given a routing mechanism that re-routes upon failure, the most commonly implemented routing path, though not optimal, may be seen as most robust. The ability to measure routing path stability therefore provides insights into the quality of links, as well as the adaptability and robustness of generated routing paths. Section 6.3 shows that the communication quality of a network can be captured from its long-term routing stability performance.

6.2 Capturing Routing Stability (ZigBee PRO)

6.2.1 ZigBee PRO Routing

ZigBee is designed primarily for mesh topology networks where nodes can communicate directly, indirectly and non-hierarchically. A ZigBee mesh network is illustrated in Figure 6.1. Nodes (Routers, coordinator and end devices) are interconnected, forming alternative routing paths for one another, and minimising the reliance on a particular node. It comprises a coordinator and routers and/or end devices. An end device and router can be associated with a router or the coordinator. Either the router or coordinator through which the new node joins the network will be its 'parent'. Vice versa, the new node will act as the 'child'. An end device is designed to communicate directly with its own parent, while a router and the coordinator can communicate directly with any other router or coordinator within the radio range.
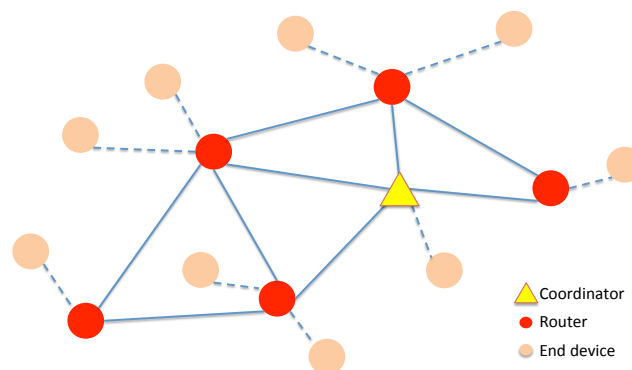
Figure 6.1. An illustration of mesh network topology in ZigBee network.

In ZigBee PRO, a node with the highest probability of successful communication with

the child is considered a potential parent. This probability metric is referred to as the link cost. Poor link cost suggests a lower probability of a successful packet delivery. Link cost in wireless microcontroller JN5168 [39] is measured using the Link Quality Indicator (LQI). LQI indicates the signal strength of a received packet, measured on every received packet as an integer ranging from 0x00 to 0xff. For example, LQI values 0x00 and 0xff are associated with the lowest and highest quality IEEE 802.15.4 signals in received signal strength respectively, where the LQI value is uniformly distributed between these two limits.

Path cost is used to assess the quality of end-to-end routing path. Path cost is a summation of the link cost of nodes that forms the routing path. A routing path with a higher path cost is assumed to have better quality. Equation 6.1 shows how path cost is calculated.

$$Cost\{P\} = \sum_{i=i}^{L} LQI_{D_i D_{i+1}} \qquad (6.1)$$

where P is the routing path between two nodes, L is the number of hops along the routing path, and LQI is the link cost between device i (D_i) and its next hop towards destination node (D_{i+1}).

ZigBee PRO utilises Ad Hoc On-Demand Distance Vector (AODV) protocol where routes between source and destination nodes are formed only upon request. The coordinator and router discover and maintain the routes within the network. Discovering a new routing path requires the source node to broadcast a Routing Request (RREQ) message that addresses the destination node. Intermediate nodes receiving the RREQ broadcast will incorporate its link cost and rebroadcast it. This process is repeated until RREQ reaches the destination node. Eventually, the destination node may receive multiple RREQ messages (broadcasted by multiple intermediate nodes) and the route with the least path cost (accumulated link cost) will be selected by returning a Route Response (RREP) message via the reverse path.

6.2.2 Computing Routing Paths Using Information from Neighbouring Table and Routing Table

NT and RT information are collected from routers in the WSN@Solaris and WSN@Vaucanson at an interval of approximately 25 minutes continuously for 6 days. This information is used to compute the actual routing paths taken from all routers towards the coordinator. The pseudo-code presented in Table 6.1 (Algorithm 1) traces and collates nodes that form the links along the routing paths.

In Algorithm 1, the source node first checks for the destination node in its RT (the destination node is always the coordinator). If the coordinator is found, the source node will forward the message to the next hop assuming it has direct/indirect connection with the coordinator. This process is repeated until the coordinator is not found in the next hop's RT. Subsequently the latest next hop will check its NT for the coordinator. If the coordinator is found, the routing path between the original source node and coordinator is collated. Otherwise, the collation of routing path is considered to have failed, meaning no routing path is available between the source router and the coordinator at the point of data query.

In ZigBee, keep-alive pings are broadcasted by routers every 15 seconds to inform the network that it is alive. An existing link between two routers is considered to be absent if four consecutive pings were not received. If so, all information associated with the neighbour is erased from NT and RT. For instance, communication between router A and router B is subjected to high failure and if no keep-alive pings from router A were received for a minute, router B then proceeds to delete all of router A's information from its NT and RT. This removal is reflected as changes in the computed routing paths.

Table 6.1. Algorithm 1 – Pseudo code used to trace and collate node-to-node routing paths from the sampled NT and RT information.

Algorithm 1: Pseudo-code to trace and collate the routing path from individual routers towards the coordinator.

Output: Return a sequential node-to-node routing path from a source node (router) to the destination node (coordinator)

Input Variables:

S: Source node

C: Destination node (coordinator)

H: Next hop

R: Relay node

RT: Routing Table

NT: Neighbour Table

P: Routing Path

Method:

(1) $P = \{S\}$ % Initiating the routing path with source node address

(2) Given a list of *NT* and *RT* of 10 minutes window period

(3) $R = S$ % Replace source node as relay node

(4) **While** *C* is found in *RT* of *R*

(5) $P = \{P, H\}$ % Insert next hop address into the routing path

(6) $R = H$ % Replace next hop as relay node

(7)   % Repeat while loop until *C* is not found in *RT* of *R*

(8) **If** *C* is found in *NT* of *R*

(9) $P = \{P, C\}$ % Routing path towards *C* is found

(10) **Else** % *C* is not found in both *NT* and *RT* of *R*

(11) $P = \{P, \text{"failed"}\}$ % Routing path is not found

(12) **End**

(13) **End**

6.3 Long-Term Routing Stability in Real-World Environments

6.3.1 Routers' Routing Path Usage Counts

To understand a WSN's routing behaviour in a real-world environment, the number of times the routers are used as part of the routing paths (usage count) in WSN@Solaris are monitored. Actual routing paths are computed over six days using Algorithm 1. Figure 6.2 illustrates five routing paths taken from router 6BD4 in WSN@Solaris. Each of these rioting paths shows an example of a routing path initiated by a different unique next hop; they are the coordinator 6209, routers 6BC9, 6BE0, 6C61 and 6BDC. Router 6BD4 is deployed at a height of 0.5 m in the west of WSN@Solaris. Referring to Figure 6.2 a, a direct connection to the coordinator 6209 is possible. However, doing so requires transmitted signals to propagate across a dense environment that includes partitioned walls, meeting rooms and multiple partitions of workstations. As shown in Figure 6.2 b to 6.2 e, intermediate relay routers are also used. Router 6BD4 is observed to be in close proximity to all its relay next hops, contrary to the final hop of the routing path, where signals have to propagate for a longer distance towards coordinator 6209. This difference can be explained by the surrounding dense environment, which leads to a limited link budget where only nearby routers can provide good link-to-link connections.

The number of times a router is used as part of routing paths is marked in orange in Figure 6.3. 190 unique routes were expected from an individual router over six days (values may vary depending on the query latency). However, a router may be utilised more often, up to a total of 733 times, if it also acts as a relay node. For illustration purposes, the pink circle in Figure 6.3 denotes the approximate reception range of the coordinator (based on the routers' ability to connect). It is observed that nodes closer to the reception edge of the coordinator were utilised more often than those deployed nearer to the coordinator. This is because these routers were used more often as a relay for others deployed further away. A routing path may reflect the least number of hops [40]. This is because the route with the lowest depth (least hop) from the coordinator will be selected if the path costs of all possible routing options are the same. As long as the destination node is within reception range, the source node will

opt for direct communication. In addition, nodes that are out of the coordinator's reception range will connect to routers that are at the edge of its reception range to minimise the total hop count.

(a)

(b)

(c)

(d)

(e)

Figure 6.2. Five routing paths generated from source router 6BD4 to coordinator 6209. These routing paths illustrate the use of five different unique next hops of router 6BC6, which include (a) coordinator 6209, (b) router 6BC9, (c) router 6BE0, (d) router 6C61 and (e) router 6BDC.
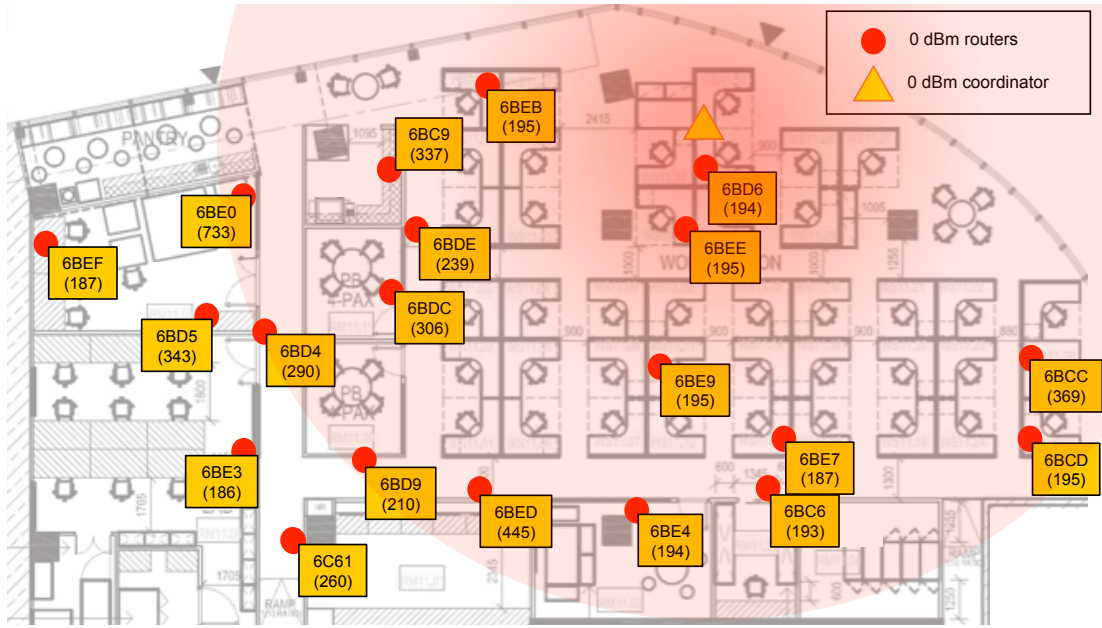
Figure 6.3. Routers' routing path usage count computed from actual routing paths in WSN@Solaris. The pink circle denotes the approximate reception range of coordinator *6209*, based on the routers' connection ability.

6.3.2 Next Hops' Usage Rate and Routing Path Stability

Referring to Figure 6.3, an abnormally high routing path usage can be observed on certain routers as compared to other routers in similar regions. For example, routers 6BCC, 6BE0 and 6BED have 369, 733 and 445 routing path usage counts respectively. To understand this phenomenon, we take a closer look at the unique next hops of individual source routers that form the routing paths towards the coordinator. The usage counts and rates of unique next hops in WSN@Solaris over the span of six days are shown in Table 6.2. Evidently, the unique next hops of a source node are interchangable. Their usage rates range from 0.5% to 100% depending on the source router. A unique next hop with a 100% usage rate signifies that the respective source router (i.e. source node 6BD6, 6BE4, 6BE7, 6BE9 and 6BEE) has only one direct connection to the coordinator.

Table 6.2. The usage counts and rates of unique next hops that link respective source routers to the coordinator in WSN@Solaris.

Source node	Unique next hop towards coordinator	Usage counts of unique next hop (%)	Counts of unique next hop with predicted failure
Router 6BC6	Coordinator 6209	190 (~98.9%)	5
	Router 6BCC	1 (~0.5%)	1
	Router 6BE7	1 (~0.5%)	0
Router 6BD4	Coordinator 6209	21 (12%)	5
	Router 6BC9	1 (~0.6%)	1
	Router 6BDC	63 (~36%)	18
	Router 6BE0	46 (~26.2%)	5
	Router 6C61	44 (~25.1%)	15
Router 6BC9	Coordinator 6209	187 (~99.5%)	26
	Router 6BEB	1 (~0.5%)	0
Router 6BCC	Coordinator 6209	192 (~99.5%)	13
	Router 6BC6	1 (~0.5%)	0
Router 6BCD	Coordinator 6209	18 (~9.23%)	11
	Router 6BCC	175 (~89.7%)	7
	Router 6BE7	2 (~1%)	1
Router 6C61	Router 6BD4	20 (~10.2%)	1
	Router 6BD9	4 (~2.1%)	0
	Router 6BED	171 (~87.7%)	1
Router 6BD5	Router 6BD4	13 (~7%)	2
	Router 6BDC	1 (~0.5%)	0
	Router 6BE0	170 (~91.4%)	1
	Router 6BE3	2 (~1.1%)	2
Router 6BD6	Coordinator 6209	194 (100%)	0
Router 6BD9	Coordinator 6209	167 (~85.6%)	30
	Router 6BDC	5 (~2.6%)	0
	Router 6BED	17 (~8.7%)	0
	Router 6BEE	6 (~3.1%)	0
Router 6BDC	Coordinator 6209	155 (~81.1%)	12
	Router 6BC9	1 (~0.5%)	0
	Router 6BD4	10 (~5.2%)	3
	Router 6BD9	6 (~3.1%)	3
	Router 6BED	1 (~0.5%)	1

	Router 6BEE	18 (~9.4%)	3
Router 6BDE	Coordinator 6209	194 (~99.5%)	0
	Router 6BC9	1 (~0.5%)	0
Router 6BE0	Coordinator 6209	135 (~70.7%)	8
	Router 6BD4	56 (~29.3%)	0
	Router 6BDC	1 (~0.5%)	1
Router 6BE3	Router 6BD5	156 (~85.2%)	0
	Router 6BD9	3 (~1.6%)	1
	Router 6BDC	21 (~11.5%)	4
	Router 6BED	3 (~1.6%)	2
Router 6BE4	Coordinator 6209	194 (100%)	9
Router 6BE7	Coordinator 6209	174 (100%)	7
Router 6BE9	Coordinator 6209	195 (100%)	0
Router 6BEB	Coordinator 6209	5 (~2.6%)	2
	Router 6BC9	145 (~74.7%)	14
	Router 6BDE	44 (~22.7%)	4
Router 6BED	Coordinator 6209	189 (~99%)	13
	Router 6BD9	2 (~1%)	1
Router 6BEE	Coordinator 6209	194 (100%)	21
Router 6BEF	Router 6BDC	3 (~1.6%)	3
	Router 6BE0	184 (~98.4%)	1

Routers 6BD4 and 6BCD from Table 6.2 are used as examples to illustrate the differences in dominating next hops. Router 6BD4 has five unique next hops over the six-day period, as compared to three unique next hops in router 6BCD. The usage rates of router 6BD4's unique next hops – coordinator 6209, and routers 6C61, 6BE0, 6BDC, 6BC9 – range between 0.6% and 36%. While the usage rates of router 6BCD's unique next hops – routers 6BCC, 6BE7, and coordinator 6209 – ranges from 1% to 89.7%. It is observed that router 6BCD was connected directly to the router 6BCC with a usage rate of 89.7%. In contrast, the most connected next hop of router 6BD4 accounts for only 36%. The consistency in dominant next hop explains why certain routers have greater routing path usage counts. For instance, router 6BCC has an abnormally high routing path usage count of 369 (refer to Figure 6.3) since it acts as the dominant next hop for router 6BCD.
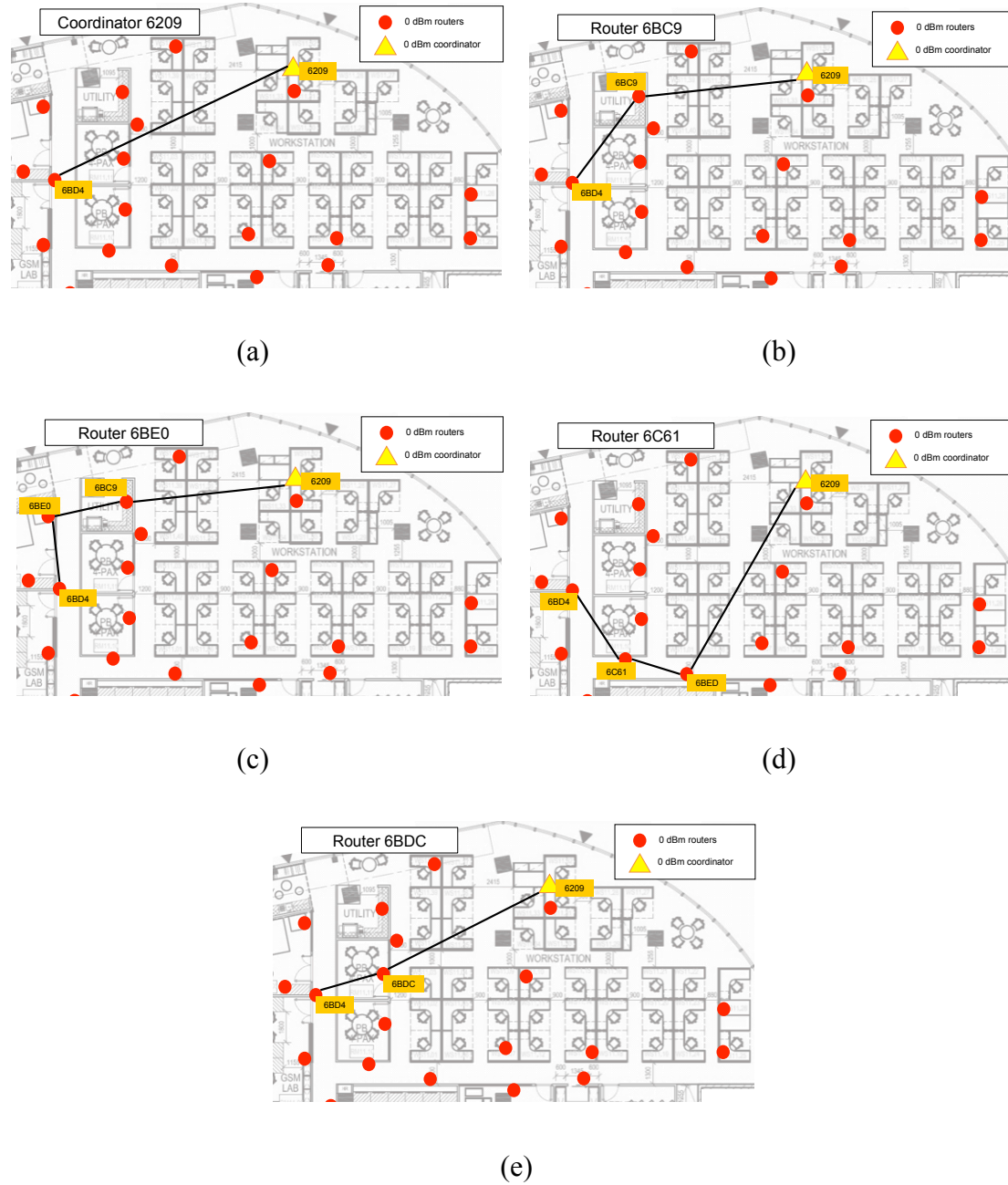
(a)

(b)

(c)
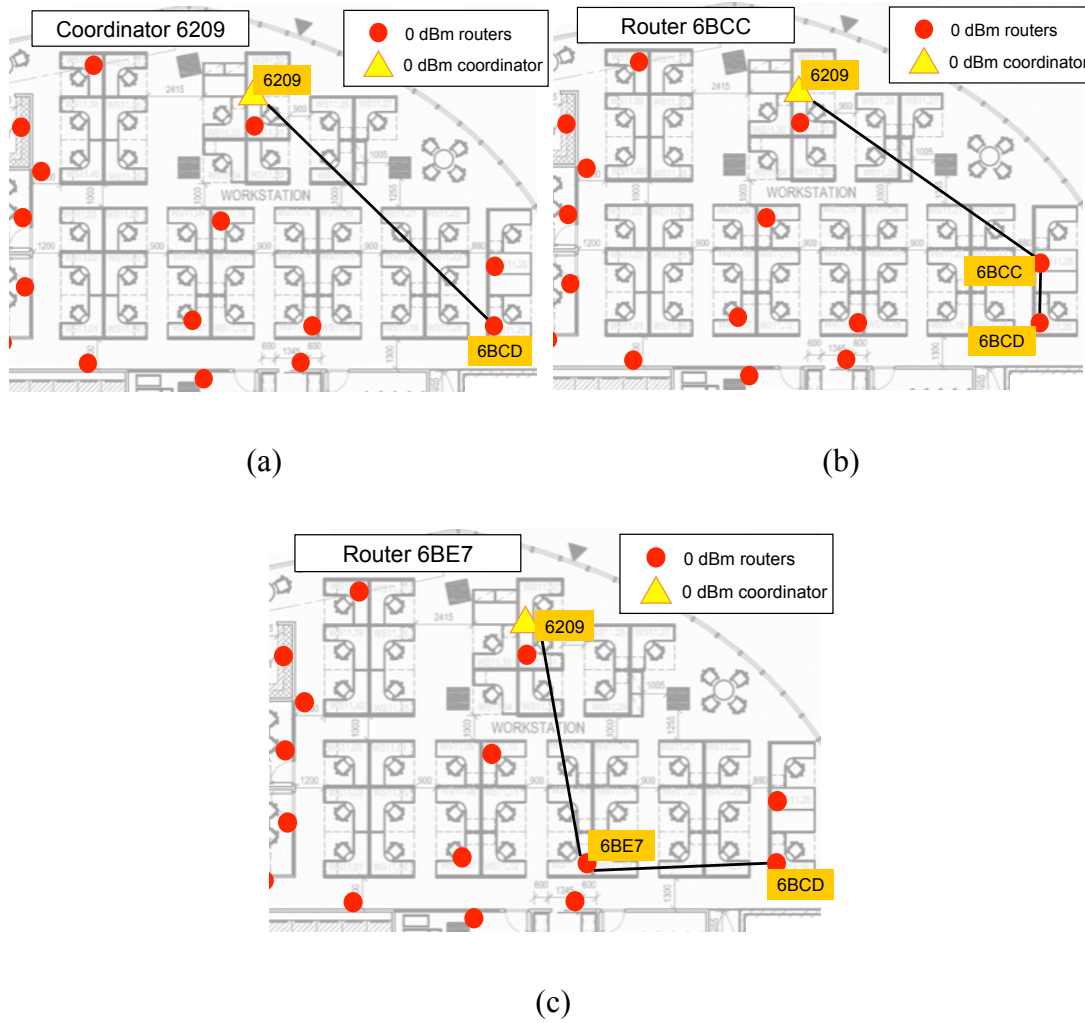
Figure 6.4. Three routing paths generated from source router 6BCD to coordinator 6209. These routing paths illustrate the use of three different next hops of router 6BCD. They are (a) coordinator 6209, (b) router 6BCC and (c) router 6BE7.

Figure 6.4 illustrates three routing paths taken from router 6BCD to the coordinator 6209. These routing paths were initiated by the different unique next hops. Router 6BCD is deployed at the eastern region of the open office space in WSN@Solaris, which comprises of preliminary workstations, chest-height partitions and a building pillar. A direct communication between router 6BCD and the coordinator is possible as shown in Figure 6.4 a, thus minimising routing hop count. Nevertheless, router 6BCC is still used as a relay next hop 89.7% of the time. Routing paths are re-constructed when they experience link failures and better routes are available. A stable network topology can be seen as a network of individual stable routing paths that are also made up of individual stable links. Routing paths are observed to be

consistently adapting to the dynamics of the real-world environment and more than one unique next hop can be expected. As such, router 6BCD's consistency in having router 6BCC as the dominant next hop (89.7%) can be inferred as being more stable than having a direct connection to the coordinator. Furthermore, the more frequent switching between next hops on router 6BD4 than on router 6BCD signifies the instability of routing paths generated by the former.

6.3.3 Chances of Link Failure based on Unique Next Hops' Usage Rate

As link failures are common in WSN, it is important for WSN protocols to find the optimal routing paths between communicating devices so as to avoid operating on links with potential failures. In this section, link failures found along actual routing paths are analysed.
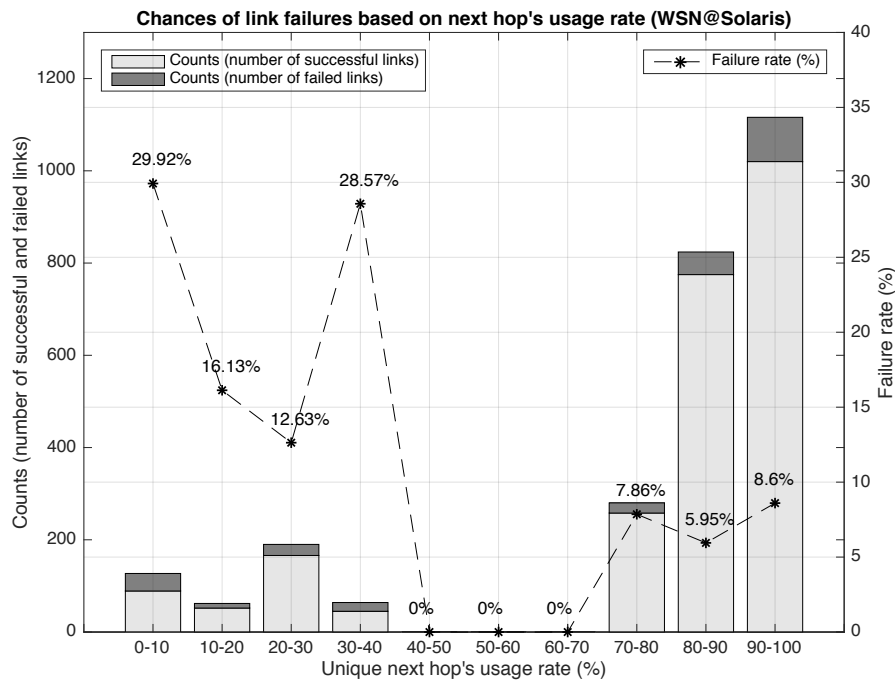
Figure 6.5. Probability of link failures based on unique next hops' usage counts in WSN@Solaris.
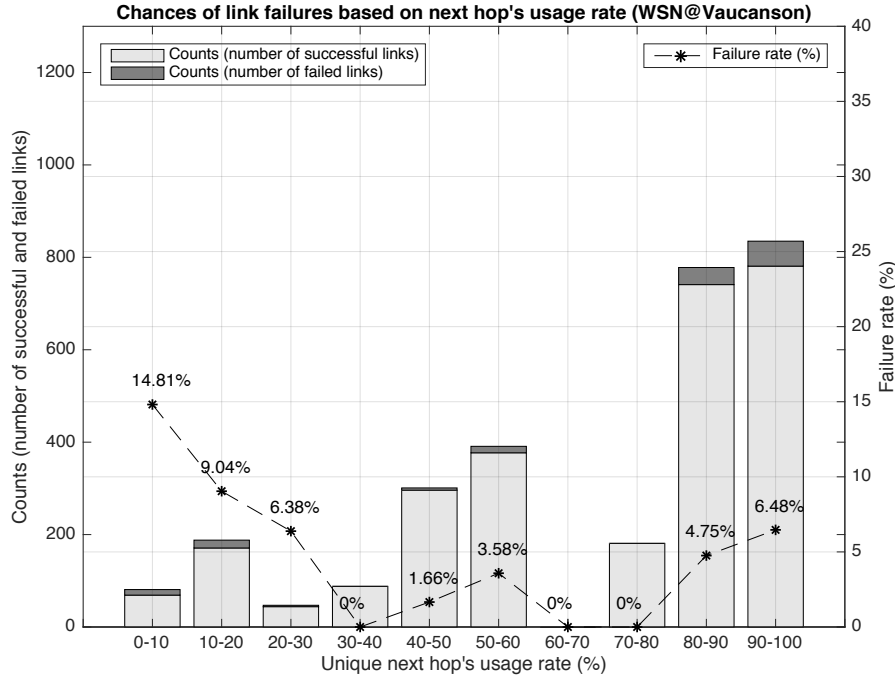
Figure 6.6. Probability of link failures based on unique next hops' usage counts in WSN@Vaucanson.

The number of link failures found in the unique next hops of individual routers in WSN@Solaris is shown in Table 6.2. It shows that link failures on actual routing paths in real-world WSN test bed should be expected. Depending on the usage count of unique next hops, the number of detected link failures varies. Figures 6.5 and 6.6 illustrate the link failure rate based on the usage rate of the unique next hop in WSN@Solaris and WSN@Vaucanson. This signifies that majority of the routing paths in the network are consistent and used as long-term solutions. It is also observed that as the unique next hop's usage rate decreases, the causes of link failure increased. For example, unique next hops in WSN@Solaris with more than 90% usage rate were utilised a total of 1116 times. 96 of them have experienced link failures (i.e. nodes not found in source router's NT) and this accounts for 8.6% of the link failure rate. On the other hand, the failure rate increased to 29.92% when the usage rate of unique next hop is less than 10%. Figures 6.5 and 6.6 also show that dominant next hops do not operate on links with zero failures. This is because the routers opted for long-distance communication to minimise hop counts even if the link quality is not optimal. The increased likelihood of finding link failures in non-dominant next hops suggests that

144

these routes operate on poorer quality links that were short-lived, hence the lower usage rate. Since a router may be used as a relay for nodes deployed further in the network, a less dominant next hop (referred to as minority next hop) could pose as potential network bottlenecks. Therefore, it is critical to monitor the usage rate of next hops so that appropriate solutions can be devised to minimise the use of minority next hop.

6.3.4 Unsustainable Route despite Dominant Next Hops

In this section, Switching Frequency Count (SFC) is introduced to evaluate the routing path stability via the number of counts in which a next hop changes. SFC is the sum of counts of every change in the next hop of a source node towards the coordinator. A source node with a greater SFC has a higher chance of changing its current next hop. Given that a next hop changes when there is a link failure, an increase in SFC signifies frequent link failures and route discoveries between affected source nodes and the connected next hop(s).

Figures 6.7 to 6.11 show the SFC of five source routers in WSN@Solaris and the periods in which the most dominant next hops are not used. These figures illustrate the connection periods of the respective source routers between the dominant and minority next hops. The peaks in Figures 6.7 to 6.11, if any, indicate the periods when minority next hops were used and a dominant router was not. Each of these periods last for approximately 20 minutes, where the higher the peaks, the longer it takes for the source router to revert to its dominant next hop.

In Figure 6.7, source router 6BE9 with 0 SFC has the same next hop (coordinator 6209) throughout its deployment cycle. In Figure 6.8, source router 6BED with 2 SFC, had momentarily switched to a minority source next hop before switching back to the dominant one. In this example, source routers with a low SFC have stable connections with their dominant next hops. When the source routers fail, the minority next hops act as routing redundancies, albeit they were utilised for a brief period since they have a greater chance of experiencing link failures as shown in Section 6.3.3.

In Figure 6.9, router 6BEB is observed to switch between its dominant next hop router 6BC9 and minority ones for 35 times in six days. Similarly, router 6BD4, in Figure 6.10, also has a high SFC of 42. Referring to Table 6.2, the dominant next hop usage

rates of routers 6BEB and 6BD4 are 74.7% and 36% respectively. The contrast in usage rates while having similar SFC highlights the differences in reception quality across dominant next hops. Router 6BEB's usage of dominant next hop is divided into multiple periods, signifying failures along dominant paths. It takes a longer period for the minority next hop to fail and to revert to the dominant next hop. On the other hand, router 6BD4 experiences an undesirable constant switching of next hops. Authors in [167] highlighted that in a WLAN test bed (IEEE 802.11 a/b/g), routing paths with a higher dominance rate are found to have a greater routing stability with less oscillation. This work has shown that such observations are not appropriate for low-power WSN applications. Despite having a dominant route, frequent switching of next hops can be expected for a low-power WSN.
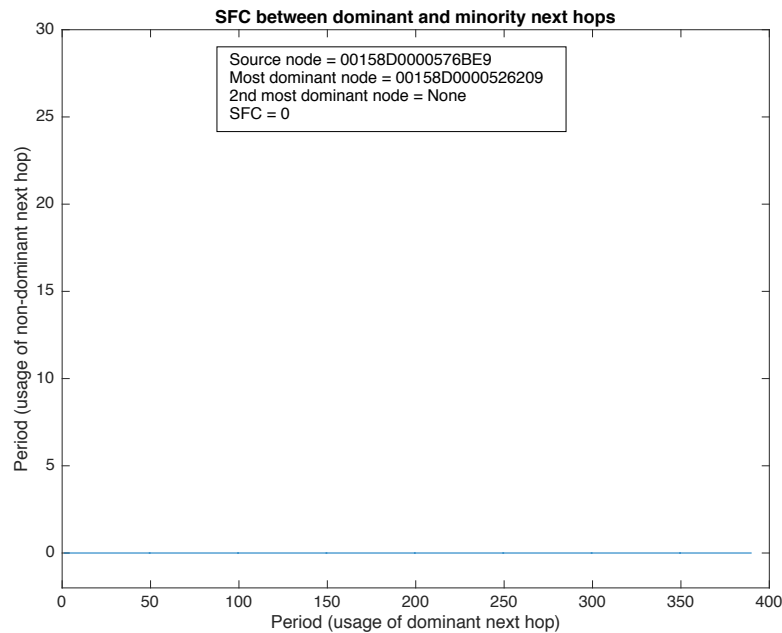
Figure 6.7. SFC between source router 6BE9 and its most dominant next hop coordinator 6209.
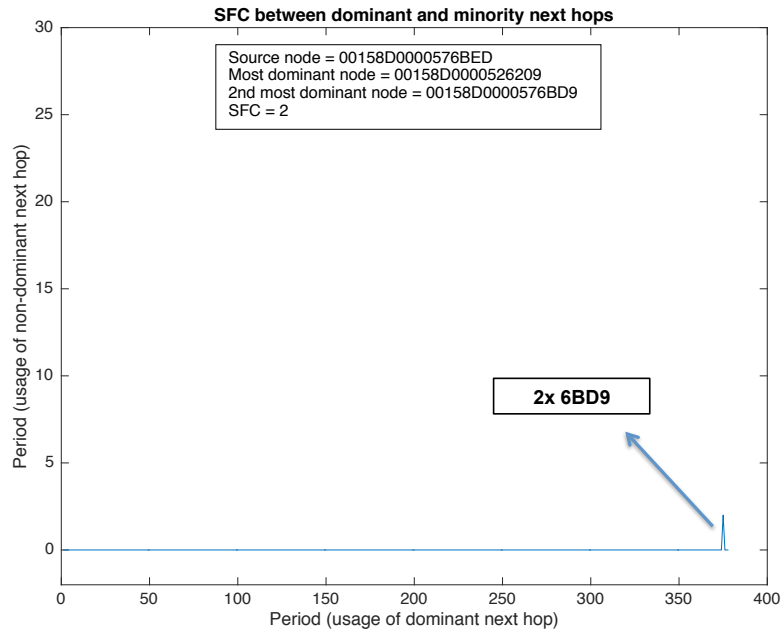
Figure 6.8. SFC between source router 6BED and its dominant next hop coordinator 6209.
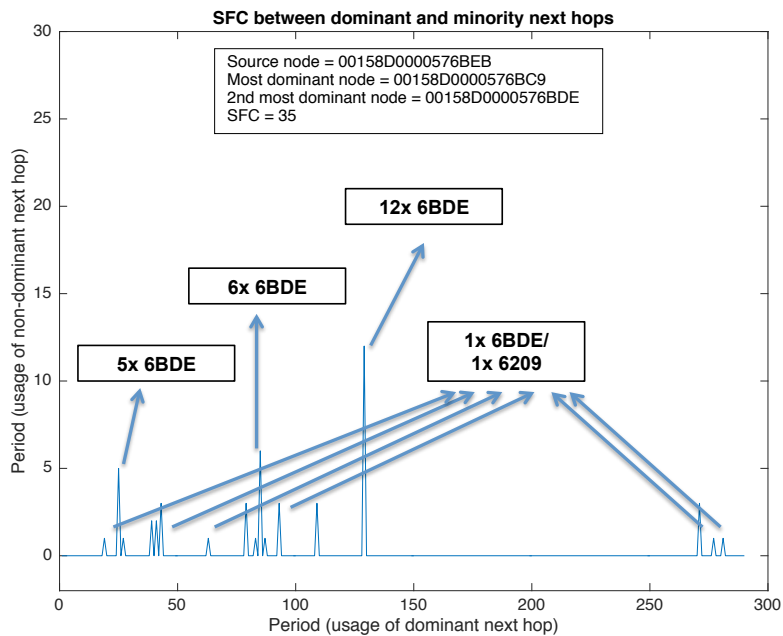
Figure 6.9. SFC between source router 6BEB and its dominant next hop router 6BC9.
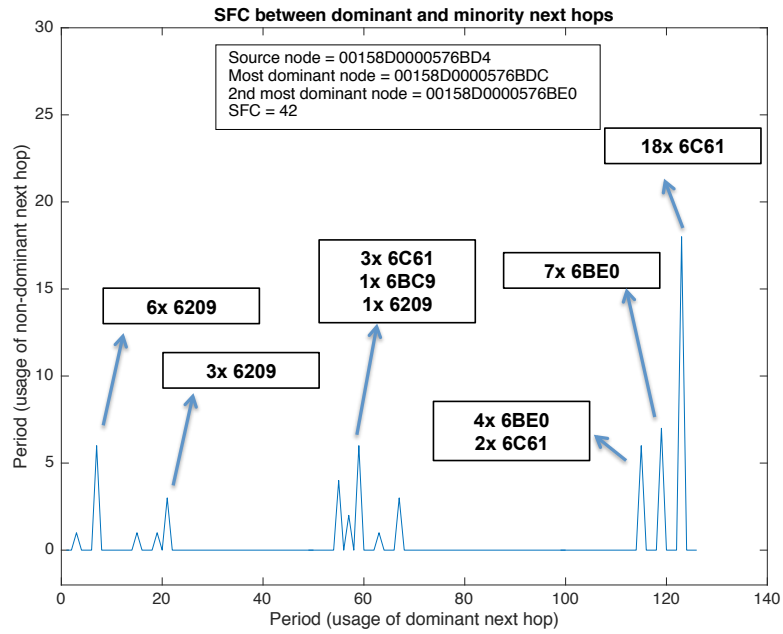
Figure 6.10. SFC between source router 6BD4 and its dominant next hop router 6BDC.
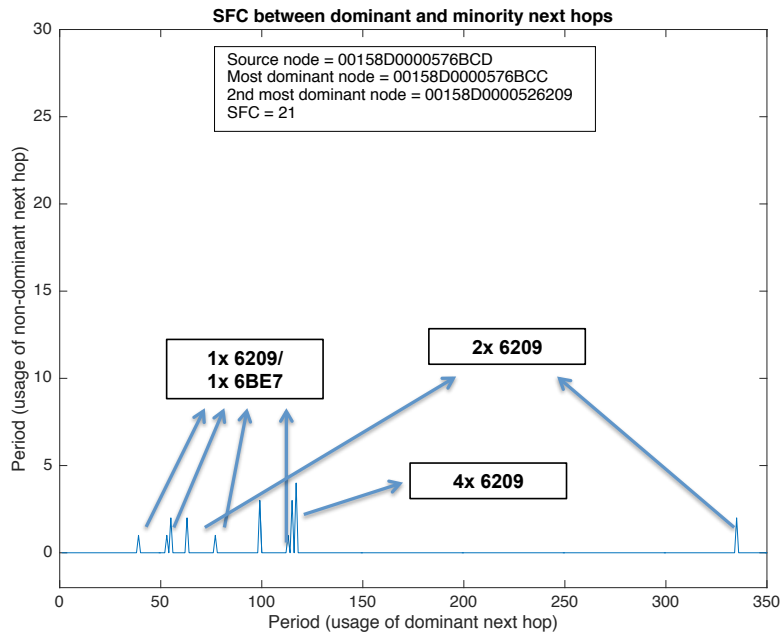
Figure 6.11. SFC between source router 6BCD and its dominant next hop router 6BDC.

6.4 Identifying Network Bottlenecks Using Routing Stability Measures

Persistent link failures on bottleneck nodes may cause reliability issues for the rest of the network since they are utilised more often than others. The communication performance of bottleneck nodes affects dependant nodes that are deployed away from the coordinator. The following are three characteristics of bottleneck nodes and suggested solutions.

1.   Relatively high routing path usage count

As mentioned in Section 6.3.1, a router with a relatively high routing path usage count suggests that it is utilised as a dominant next hop for nodes deployed deeper in the network. Relative high routing path usage counts are influenced by the routing protocols implemented, and the routing options available. In this work, a routing path reflects the least number of hops [40]. A router may be selected as a dominant next hop as long as it can provide the shortest route towards the coordinator. Doing so creates a reliance on certain nodes in the network.

Such potential bottlenecks can be detected when there are abnormally high routing path usage counts. A possible solution to avoid over-reliance on specific nodes is to divert the existing traffic to an alternate routing path by deploying an additional router in the region. By doing so, routing redundancy can be improved.

2.   Unsustainable minority next hops

The routing paths within WSN@Solaris and WSN@Vaucanson vary throughout their deployment cycles. The usage rate of next hops relative to a source router can distinguish a dominant next hop from a minority one. In Section 6.3.3, minority next hops are explained to be more likely to operate on links with failures than dominant ones. In Figure 6.9, the high SFC of router 6BEB can be attributed to the temporary usage of the minority next hop that lasts for only one period. Similar observation can be made for router 6BCD in Figure 6.11. The use of minority next hops is found to be short-lived as it causes an increase in switching between nodes. For a source router to revert to its dominant next hop, the existing minority next hop has to fail before

activating the re-routing process. The need for the minority next hop to fail before switching to a better routing option is an indication of poor energy utilisation.

Since routing discovery is the primary energy consumption activity, there is a need to avoid unnecessary re-routing and the consistent use of unsustainable minority next hops. To do so, a routing protocol may perform immediate retransmission to the 2nd most dominant next hop (based on the usage rate) when the initial retransmission fails. By doing so, the need for re-routing is delayed, since the dominant next hop is likely to be available in the next transmission period. Unless both dominant next hops fail persistently, the re-routing process may resume.

3. Limited routing options

Every source router has a fixed number of neighbouring node(s) that can provide a route towards the coordinator. Having limited routing options, a source router would toggle between neighbours if any of them fails. Therefore, a source node with a relatively high SFC, coupled with the lack of dominant next hop suggests the unavailability of stable routing options where none of the neighbouring nodes can provide a long-term routing solution.

To resolve this issue, it is proposed that the routing protocol should notify the user application when nodes have limited routing options. An additional router must be deployed in the region to improve the overall routing redundancy.

6.5 Chapter Summary

Chapter 6 demonstrates the importance of link failure prediction models and the need for monitoring long-term routing stability. Monitoring and analysing of long-term routing stability on real-world test beds (WSN@Solaris and WSN@Vaucanson) provides useful insights to network behaviour that existing instantaneous link quality assessment techniques could not i.e. SFC, and identification of the most dominant and minority next hops.

It is discovered that routing paths between individual routers and the coordinator are rarely static. These routing paths are found to switch among next hops and can be categorised based on their usage rate, into the most dominant or minority next hops.

The application of the developed link failure prediction model (from Chapter 5) found that minority next hops operate on links with up to 29.9% failure rate. In addition, through the use of a SFC parameter, minority next hops are observed to be temporary solutions when a dominant next hop is not available. Lastly, three characteristics of network bottlenecks are described and suggested solutions are provided to avoid the use of nodes with an abnormally high routing path usage counts and unsustainable minority next hops.

7 Conclusion

7.1 Concluding Remarks

WSN being prime examples of high performance mixed signal technologies are very attractive to the businesses and are expected to grow both in the number of deployments and in the nodes per deployment. This thesis investigated the practicalities of this complex technology given that evidence from field trials have showed frequent network instability in real-world deployments and the limitations of WSN optimisation protocols to provide precise solutions to the cause of link failures.

This thesis brings to light the WSN performance evaluation strategies to improve WSN communication reliability. Of particular significance are the unique data extraction platform of WSN devices and their deployments in real-world large-scale indoor environments. The realistic setups of WSN tests beds provided representative platforms to evaluate the impact of persistent Wi-Fi traffic and spatial network challenges on WSN communication reliability, and long-term WSN routing stability in real-world environment. The data collected from both uncontrolled experiments and real-world test beds were used to develop ANFIS prediction models for link failures caused by spatial challenges. In order to further evaluate the training input parameters on their ability to identify spatial challenges, NSGA-II is used to reduce the complexity of the Fuzzy rule-bases while maintaining the overall model accuracy. To understand the dominance of Fuzzy rules used, sensitivity analysis was performed on the chosen model where individual rule was removed and the model accuracies of the respective predictive conditions were monitored. Through long-term routing stability measures, it is discovered that the routing paths between routers and the coordinator in real-world WSN test beds are rarely static. More importantly, the minority next hops are found to operate on links with up to 29.9% failure rate. This phenomenon highlights the importance of NI and developed spatial-related link failure prediction models to monitor long-term routing stability and identification of network bottlenecks respectively.

This chapter discusses the main contributions of this thesis and highlights the novelties, limitations as well as recommendations for future work.

7.2 Contribution to Knowledge

1. The development of real-world WSN test beds and the extraction of ZigBee PRO performance indicators

Existing research on WSNs is largely simulation based [37, 38] or are conducted on small-scale experiments, which may not be applicable in real-world environments. The nature of low-power radio propagation in occupied indoor environments introduces lower dependability of WSN's wireless communication. Due to the complex nature of the transmission medium in the indoor environments, a small imperfection in the network can be manifested in ways not tested in the simulation [15]. Most existing simulators and path loss models are incomplete [37, 38, 100]. Every simulator has specific features that work well in the respective domain since they inherit the different approach and theoretical models to investigate different problem. However, this has led to accuracy and authenticity issues when limited and different simulation settings are used. For instance, simulations and theoretical models may not take into account the different protocol stacks and type of application. Due to these, simulation can only be used for performance estimations, but not to be relied for accurate results due to the complexity of radio propagation.

Similar observation is made by Kurt and Tavli, who demonstrated that analytical models cannot determine path losses between communicating nodes accurately [100]. Assessing WSN performance based on probability path loss errors is ineffective. For instance, overestimating the path loss would lead to overestimated number of sensor nodes required. Vice versa, underestimated path loss leads to under-established network connectivity. This further leads to performance assessment errors in terms of required number of hops, total neighbouring nodes, and network coverage. It is identified that the usability of simulation (with theoretical models) can be improved if the following areas are taken into consideration during modelling; they are not limited to background noise, clock drift, characteristics of wireless module used, antenna height, antenna polarisation, and ground reflectivity. All of which varies across

different test beds [40, 100].

In this thesis, actual ZigBee PRO wireless sensor nodes were deployed in real-world environments. These nodes were implemented with NI with minimal infrastructure changes to extract NT and RT information from the ZigBee PRO stack. The extracted information was processed into four link quality parameters – *Mean RSSI*, *ACV RSSI*, *NTC* and *BNTC* – which are relevant and relatable to the existing link quality parameters found in the literature and mirror the properties of communicating node's signal strength, signal deviation, communication success probability and link asymmetry. The development of these WSN test beds under the influence of environmental dynamics had provided representative platforms to evaluate WSN communication reliability.

2. **A novel investigation to understand the impact of IEEE 802.15.4 and IEEE 802.11 bgn standards on each another**

The controlled experiments with dynamic setups between IEEE 802.15.4 and IEEE 802.11 bgn devices have demonstrated that their abilities to co-exist in the same frequency spectrum were dependent on two factors. First, there must be sufficient operating distance between the IEEE 802.15.4 nodes, and between the IEEE 802.15.4 nodes and the Wi-Fi interference source. Second, the different communication standards must operate on a transmission frequency separation of at least 12 MHz. These experiments have also demonstrated that transmission failures of IEEE 802.15.4 nodes under persistent flooding of Wi-Fi UDP packets were largely due to channel access failure rather than corrupted data packets. Therefore, in order to minimise the impact of Wi-Fi interference, careful configurations and deployments of WSN devices must be put in place.

3. **Understanding the impact of spatial challenges and Wi-Fi interference on WSN communication reliability through controlled experiments**

Controlled experiments were conducted for detailed evaluations of WSN link quality parameters under the influence of persistent Wi-Fi traffic, poorly deployed environment and human movements. Results from these experiments highlighted that the individual link quality parameter behaved differently under different network

challenges. As such, the model's training inputs must be carefully selected to produce a best-possible prediction model. For example, the physical layer parameters were better at distinguishing spatial challenges than network layer parameters, and the count of CCA failures was better at detecting persistent Wi-Fi traffic than PRR. It is concluded from these findings that WSN link failures must not be generalised and considered as a single entity. Detection mechanism for the cause of link failures and precise solution must be in place to improve WSN communication reliability.

4. Reduction of Fuzzy rule-base for interpretation

NSGA-II was used to reduce the complexity of ANFIS models without sacrificing model accuracy. The reduction of Fuzzy-rule-base had provided an alternative approach to analyse the optimised Fuzzy rules and their inputs. It was found that the dominance of Fuzzy rules was dependent on factors such as the WSN node's communication range and environmental settings (controlled or uncontrolled).

Due to the unique formulation of Fuzzy rule-base optimisation, specific NSGA-II settings must be put in place to achieve adequate exploration of search space and avoiding premature convergence. In particular, maintaining population diversity and selection pressure throughout the GA search were found to be key factors. Sufficient population diversity was achieved at the beginning of GA search with the use of initial population of densely activated rule-bases. The initial population of densely activated rule-bases forces solutions of similar rule-base size to compete among each other. Thus, the selection pressure for non-dominated solutions was emphasised on models with higher accuracy. In addition, a higher mutation rate for deactivation of parameters (Fuzzy antecedent parts) was implemented. By doing so, greater diversity among the population in terms of Fuzzy rule-base sizes was created. This had led to a greater selection pressure for the exploration of new non-dominated solutions of smaller rule-base sizes.

5. Monitoring of long-term WSN routing stability in real-world environments

Instantaneous assessment of WSN link quality is often preferred in the existing research. However, since WSN communication is highly temporal and the assessments of link quality were performed using limited information, instantaneous

assessments of link quality are not always accurate. In this thesis, the measure of long-term of WSN routing stability provided an alternative means to monitor WSN communication reliability. For instance, the rate of routing paths changes over time was studied instead of the typical link-to-link performance measure.

Network parameters to identify potential network bottlenecks were introduced. These parameters are namely, relative routing path usage count, usage rate of unique next hops and switching frequency counts. The use of these parameters and the spatial-related link failure prediction models had discovered that up to 29.9% of the less dominant routing paths in real-world test beds were connected to link with failures. Such links were found to be short-lived and had contributed to the phenomenon of network instability. The need to avoid the use of less dominant links and to identify network bottlenecks in the network highlighted the importance of monitoring long-term WSN routing stability.

6. Network management system to investigate WSN network challenges

Overall, this research brings together a building block for a sustainable resource-constrained WSN architecture to investigate network challenges pertaining to WSN communication reliability. This building block validated on real-world test beds and developed with minimal infrastructure change, is suitable for a Network Management System (NMS) [168] to detect, diagnose and remedy network reliability issues in a deployed WSN. "In-network" extraction of information such as the node operating states (i.e. number of neighbouring nodes and E2E routing paths) and link quality between communicating nodes permits NMS to perform management control tasks to improve the reliability of WSN communication. These tasks are, for example, configuration of a node's retransmission limit, transmission power, and duty cycling interval. We have also showed that through the development and interpretation of optimised ANFIS-based prediction models that are trained using data collected from controlled and uncontrolled test beds, the influence of link quality parameters under specific network challenge can be studied. In addition, NI has shown to be effective at extracting meaningful mesh-network (i.e. ZigBee PRO) performance information, which allows us to investigate bottlenecks in a large-scale network.

7.3 Limitation and Recommendations for Future Work

The outcomes of this research can be used to inform future work in the area of WSN. However, the results from this thesis require further evaluation with a broader approach, including the use of more real test beds, implementing on different applications, different hardware systems, as well as different protocols.

1. Optimisation subjected to individual test beds

The results and interpretations of optimised models are dependent on the knowledge and experience of user making the evaluation, as well as the type of deployed environment, configurations and deployments of WSN nodes, and even the implemented optimisation protocol. The interpretation of optimised Fuzzy model is subjective in nature. The use of "universal" interpretation metric may be controversial since designing of indexes takes into account designers' interpretation preferences. In addition, such metric may not be applicable for different systems or applications. Therefore, instead of an interpretation metric, the use of more training inputs that represent different characteristics of a wireless communication is recommended. These characteristics are for example, noise level, severity of deep fading, short-term *bursty* link and transmission latency. Since cross-layer parameters are valued, providing more information about a wireless link during modelling can produce a more accurate model with specific Fuzzy sets.

In addition, results from this work may be used to improve the evaluation approach of WSN communication within a simulator. For instance, instead of regarding a link with poor *mean RSSI* as bad, the simulator can classify this link as highly susceptive to failure due to human activity, since poor *mean RSSI* do not always translate to failure. This inclusion of addition information allows a WSN simulator to represent the dynamicity of a real-world test bed more realistically.

2. Remote and uncontrolled WSN test beds

WSN test beds in uncontrolled environments produced realistic information about the communication performance of deployed devices and also serve as a validation platform for prediction models implemented. However, given that the environments

are remote such as 3rd party building, it is difficult to account for packet losses in all conditions. For example, IP network faults leading to IP packet loss and delay, and unexpected power outages shutting down of WSN operations or specific nodes. Accounting for packet losses in such situations require a dedicated fault detection system where the loss of information can be differentiated with packet losses due to wireless communication failures. This can be done with periodic monitoring of existing network maintenance packets such as "keep alive" messages, sequence number of transmitted packets, and network re-join status from nodes that are alive. Any periodic gaps in collected data can be counterchecked with network maintenance packets to verify if nodes were alive or where disconnected from the network.

3. **Suggestions to improve WSN communication reliability under spatial related network challenges**

It is concluded in Chapter 2 that a unique solution is required to mitigate the different network challenges. Similarly, Chapter 5 showed that spatial related network challenges can have different impacts on different WSN test beds (i.e. controlled experiments, WSN@Solaris and WSN@Vaucanson). In the future work, solutions designed to mitigate these network challenges are recommended to be customised depending on their impacts on the WSN communication reliability. For instance, temporal human movements are likely to affect a pair of long distance communicating nodes (in WSN@Vaucanson) than short distance communicating ones (in WSN@Solaris). In other words, a long distance communication, detectable with poor *mean RSSI*, is more likely to fail under the presence of human activities, as there is limited link budget. In this situation, an increase in the communication link budget to minimise the impact of human activities is suggested. This can be achieved through increasing the transmission power of affected nodes with poor *mean RSSI*.

On the other hand, nodes with shorter-range communication in WSN@Solaris may not require an increase in link budget since human activities may not introduce persistent link failures. In this situation, delaying retransmission [10, 11] could be sufficient. In addition, nodes communicating under poorly deployed environment may not be a persistent network issue if the affected node is not a dominant next hop. In this situation, because the link is not utilised for data routing, no immediate solution is

necessary. Otherwise if the affected node is used as a dominant next hop, diverting of network traffic with a network re-routing mechanism could be useful to reduce the reliance on affected nodes.

Overall, this work shows the importance of understanding the behaviour of link quality parameters under different network challenges. It should be noted that the solution should be WSN application-dependent, where minimal impact to the existing application in terms of energy consumption and operation must be considered.

References

[1] "Put your buildings to work: A smart approach to better business outcomes (White paper)," Honeywell and IHS, Inc., 2015.

[2] "Improving performance with integrated smart buildings (White paper)," Siemens Industry Inc., 2013.

[3] S. Khandavilli, "Intel creates smart building using IoT," Intel Corporation., 2017.

[4] B. Bangerter, S. Talwar, R. Arefi, and K. Stewart, "Networks and devices for the 5G era," *IEEE Comm. Mag,* vol. 52, no. 2, pp. 90-96, 2014.

[5] C. Wang, F. Haider, X. Gao, X. You, X, Y. Yang, D. Yuan, H. Aggoune, H. Haas, S. Fletcher, and E. Hepsaydir, "Cellular architecture and key technologies for 5G wireless communication networks," *IEEE Comm. Mag.,* vol. 52. no. 2, pp. 122–130, 2014.

[6] "Internet of Things: Wireless sensor network (White paper)," *Int. Electro-Tech. Comm.,* 2014.

[7] U. B. Desai, B. N. Jain, and S. N. Mechant, "Wireless sensor networks: Technology roadmap," Ministry of Inf. and Comm. Tech. India, 2007.

[8] Q. Dong, L. Yu, H. Lu, Z. Hong, and Y. Chen, "Design of building monitoring systems based on wireless sensor networks," *Wireless Sens. Netw.,* vol. 2. no. 9, pp. 703-709, 2010.

[9] H. Grindvoll, O. Vermesan, T. Croshbie, R. Bahr, N. Dawood, and G. M. Revel, "A wireless sensor network for intelligent building energy management based on multi communication standard – A case study," *Journal of ITcon,* vol. 17, pp. 43-62, 2010.

[10] M.H. Alizai, O. Landsidel, J.A. Bitsch, S. Gotz, and K. Wehrle, "Bursty traffic over bursty links," *in SenSys '09*, pp. 71-84, New York, USA, 2009.

[11] M.H. Alizai, O. Landsidel, K. Wehrle, and A. Becher, "Challenges in short-term wireless link quality estimation," *in FGSN '08,* 2008.

[12] L. Mottola, G. P. Picco, M. Ceriotti, S. Guna, and A. L. Murphy, "Not all wireless sensor networks are created equal: A comparative study on tunnels," *ACM Trans of Sens Netw,* vol. 7, no. 2, 2010.

[13] E. Aguirre, P. L. Iturri, L. Azpilicueta, J. J. Astrain, J. Villadangos, and F. Falcone, "Analysis of wireless sensor network topology and estimation of optimal

network deployment by deterministic radio channel characterization," *in Proc. of Sensors and Applications,* vol. 15, no. 2, pp. 3766-3788, 2015.

[14] Z. Farid, R. Nordin, and M. Ismail "Recent advance in wireless indoor localisation techniques and systems," *Journal of Comp. Netw. and Comm*, vol. 2013, 2013.

[15] D.Ganesan, D. Estrin, A. Woo, and D. Culler, "Complex behaviour at scale: An experimental study of low-power wireless sensor network," UCLA CS Tech. report, 2002.

[16] N. Baccour, M. B. Jamaa, A. Koubaa, and D. Rosario, "RadiaLE: A framework for designing and assessing link quality estimators in wireless sensor networks", *Ad Hoc Netw. 9*, pp. 1165-1185, 2011.

[17] L. M. Kamarudin, A. Zakaria, A. Y. M .Shakaff, D. L. Ndzi, C. M. Nor, N. Hassan, and S. Mamduh, "The study of human movement effect on signal strength for indoor wireless sensor network deployment," *IEEE Conf. on Wireless Sens.,* pp 30-35, Kuching, Malaysia, 2013.

[18] S. Ahmed, S. Bouk, N. Javaid, and I.S asase, "Combined human, antenna orientation in elevation direction and ground effect on RSSI in wireless sensor network," *10th IEEE Int. Conf. on Frontiers of Info. Tech.,* pp. 46-49, Islamabad, India, 2012.

[19] J. Nazabal, P. Iturri, L. Azpilicueta, F. Falcone, and C. Valdivielso, "Performance analysis of IEEE 802.15.4 compliant wireless devices for heterogeneous indoor home automation environment," *Journal of Antennas and Propagation,* vol. 2012, 2012.

[20] I. Chatzigiannakis, G. Mylonas, and S. Nikoletseas, "Modelling and evaluation of the effect of obstacles on the performance of wireless sensor network," *39th Annual IEEE Simulation Symp.*, AL, USA, Huntsville, USA, 2006.

[21] M. Takai, J. Martin, and R. Bagrodia, "Effects of wireless physical layer modelling in mobile ad hoc networks," *in Proc. MobiHoc '01*, pp. 87-94, Long Beach, CA, USA, 2001.

[22] H. Ayadi, A. Zouinkhi, T. Val, A. Bassche, M. N. Abdelkrim, "Network lifetime management in wireless sensor networks," *IEEE Sensors Journal,* vol. 18, no. 15, pp. 6438-6445, 2018.

[23] A. Ayadi, O. Ghorbel, A. M. Obied, M. Abid, "Outlier detection approaches for wireless sensor networks: A survey," *Computer Networks,* vol. 129, no. 1, pp. 319-

333, 2017.

[24] Z. Zhang, A. Mehmood, L. Shu, Z. Huo, Y. Zhang, M. Mukherjee, "A survey on fault diagnosis in wireless sensor networks," *IEEE Access*, vol. 6, pp. 11349-11364, 2018.

[25] K. Srinivasan, M. A. Kazandjieva, S. Agarwal, and P. Levis, "The β-factor: Measuring wireless link burstiness," *in Proc. of SenSys '08*, New York, USA, 2008.

[26] C. U. Bas, and S. C. Ergen, "Spatio-temporal characteristics of link quality in wireless sensor networks," *IEEE WCNC,* Shanghai, China, 2012.

[27] J. Zhao, and R. Govindan, "Understanding packet delivery performance in dense wireless sensor networks," *in SenSys'03,* pp. 1-13, California, USA, 2003.

[28] L. Doherty, J. Simon, and T. Watteyne, "Wireless sensor network challenges and solutions (White paper)," Linear Technology Cooperation, 2012.

[29] H. Maaskant, S. Duquennoy, V, Handziski, P. Zand, and G. Exarchakos, "Improved reliability experimentation and validation report," EIT ICT Lab, 2015.

[30] D. Puccinelli, and M. Haenggi, "Multipath fading in wireless sensor networks: Measurements and interpretation," *in Proc. of IWCMC*, pp. 1039–1044, Vancouver, Cananda, 2006.

[31] S. Aslam, F. Farooq, and Shahzad Sarwar, "Power consumption in wireless sensor networks", *in Proc. FIT '09,* no. 14, Abbottabad, Pakistan, 2009.

[32] W. Su, and T. L. Lim, "Cross-layer design and optimisation for wireless sensor networks*", Int. Journal of Sens. Netw.,* vol. 6, no.1, pp. 3-12, 2006.

[33] B. Pavkovic, M. Batic, and N. Tomasevic, "The importance of cross-layer considerations in a standardized WSN protocol stack aiming for IoT," *Ubiquity Symp.* vol. 15, no. 2, 2015.

[34] "Wireless sensor networks: signal processing and communications perspectives," John Wiley & Sons, pp. 69-344, 2007.

[35] N. Baccour, A. Koubaa, M. B. Jamma, D. Rasario, H. Youssef, M. Alves, and L. B. Becker, "F- LQE: A Fuzzy link quality estimator for wireless sensor network," *EWSN 2010*, pp. 240-255, 2010.

[36] C. L. Lim, M. Bolt, A. Syed, P. Ng, C. Goh, and Y. Li, "Dynamic performance of IEEE 802.15.4 devices under persistent Wi-Fi traffic," *Int. Conf. of RIOT*, pp. 1-6, Singapore, 2015.

[37] A. Abuarqoub, M. Hammoudeh, F. Al-Fayez, O. Aldabbas, "A survey on wireless sensor networks simulation tools and testbeds," *In Sensors, Transducers, Signal Conditioning and Wireless Sensors Networks Advances in Sensors: Reviews,* vol. 3, Chap 14, 2017.

[38] J. Moritz, "Investigation of deployment-specific simulation for the optimization of wireless sensor network", Ph.D Thesis, Technical University of Braunschweig, 2018.

[39] "JN5168-001-Myy Datasheet", NXP Laboratories UK, 2013.

[40] "ZigBee PRO Stack User Guide", NXP Laboratories UK, 2014.

[41] R. Akl, D. Tummala, and X. Li, "Indoor propagation modelling at 2.4 GHz, for IEEE 802.11 networks," *In the sixth IASTED Int. Multi-Conf. on Wireless and Optical Comm,* Banff, Canada, 2006.

[42] J. S. Turner, M. F. Ramli, L. M. Kamarudin, A. Zakaria, A. Y. M. Shakaff, D. L. Ndzi, C. M. Nor, N. Hassan, and S. M. Mamduh, "The study of human movement effect on signal strength for indoor WSN deployment," *ICWISE 2013*, pp. 30-35, Kuching, Malaysia, 2013.

[43] E. B. Hamida, and G. Chelius, "Investigating the impact of human activity on the performance of wireless networks—An experimental approach," *IEEE Int. Symp. on WoWMoM,* pp. 1-8, Montreal, QC, Canada, 2010.

[44] G. Horvat, S. Rimac-Drlje, and D. Zagar, "Fade depth prediction using human presence for real life WSN deployment," *Radioengineering*, vol. 22, no. 3, 2013.

[45] W. Yuan, X. Wang, J. P. Linnartz, and L. G. Niemegeers, "Coexistence performance of IEEE 802.15.4 wireless sensor networks under IEEE 802.11 b/g interference," *Wireless Personal Comm.*, vol. 68, no. 2, pp. 281-302, 2013.

[46] Y. Tang, Z. Wang, T. Du, D. Makrakis, and H. Moutftah, "Study of clear channel assessment mechanism for Zigbee packet transmission under Wi-Fi interference," *IEEE 10th CCNC*, Las Vegas, NV, USA, 2013.

[47] N. LaSorte, S. Rajab, and H. Refai, "Experimental assessment of wireless coexistence for 802.15.4 in the presence of 802.11 g/n", *IEEE EMC Symposium*, Pittsburgh, PA, USA, 2012.

[48] L. Angrisani, M. Bertocco, D. Fortin, and A.Sona, "Experimental study of coexistence issues between IEEE 802.11 b and IEEE 802.15.4 wireless sensor networks," *IEEE Trans. on Instr. and Measurement*, vol. 57 (8), pp. 1514-1523, 2008.

[49] W. Guo, W. M. Healy, and M. C. Zhou, "Impacts of 2.4-GHz ISM band interference on IEEE 802.15.4 wireless sensor network reliability in buildings," *IEEE Transactions on Instrumentation and Measurement,* vol. 61 no. 9, pp. 2533-2544, 2012.

[50] G. Jesus, A. Casimiro, and A. Oliveira, "A survey on data quality for dependable monitoring in wireless sensor networks," *Sensors,* vol. 17 (9), 2017.

[51] Q. Dong, and W. Dargie, "Evaluation of the reliability of RSSI for indoor localization," in ICWCUCA 2012, pp. 1-6, Clermont Ferrand, France, 2012.

[52] L. Zhang, and G. Wang, "Design and implementation of automatic fire alarm system based on wireless sensor networks," *in Proc. of the ISIP'09*, vol. 2, no. 9, pp. 410-413, 2009.

[53] S. Bertoldo, O. Rorato, C. Lucianaz, and M. Allgretti, "A wireless sensor network ad-hoc designed as anti-theft alarm system for photovoltaic panels," *WSN,* vol. 4, no. 9, pp. 107-112, 2012.

[54] V. Raghunathan, C. Schurgers, S. Park and MB. Srivastava, "Energy-aware wireless microsensor network," *IEEE Signal Proc. Mag.* vol. 19, no. 2, pp. 41-50, 2002.

[55] K. Z. Panatik, K. Kamardin, S. A. Shariff, S. Yuhaniz, N.A. Ahmad, O. M. Yusop, and S. A. Ismail, "Energy Saving in wireless sensor networks," *IEEE 3rd International Symposium on Telecommunication Technologies,* Kuala Lumpur, Malaysia, 2016.

[56] J. A. Khan, H. K. Qureshi, and A. Iqbal, "Energy management in wireless sensor networks: A survey," *Computers & Electrical Engineering,* vol. 41, pp. 159-176, 2015.

[57] N. Baccour, A. Koubaa, L. Mottola, M. A. Zunga, H. Youssef, C. A. Boano, and M. Alves, "Radio link quality estimation in wireless sensor networks: A survey," *ACM Transaction Sensor Network,* vol. 8 (4), pp. 34, 2012.

[58] Y. Xu, and W. C. Lee, "Exploring spatial correlation for link quality estimation in wireless sensor networks," *Fourth annual IEEE Int. Conf. PERCOM'06*, Pisa, Italy, 2006.

[59] G. Zhou, T. He, S. Krishnamurthy, and J. Stankovic. "Impact of radio irregularity on wireless sensor networks," *In Proc. of the 2nd MobiSys'04*, Boston, Massachusetts, USA, 2004.

[60] M. Doddavenkatappa, M. C. Chan, and B. Leong, "Improving link quality by

exploiting channel diversity in wireless sensor networks," *2011 IEEE 32nd Real-Time Systems Symposium,* pp. 159-169, Vienna, Austria, 2011.

[61] A. Cerpa, J. L. Wong, M. Potkonjack, and D. Estrin, "Temporal properties of low power wireless links: Modelling and implications on multi-hop routing," *in Proc. of the 6th ACM Int. Symp. on MobiHoc'05,* pp 414-425, Urbana-Champaign, IL, USA, 2005.

[62] R. Fonseca, O. Gnawali, K. Jamieson, and P. Levis, "Four-bit wireless link estimation," *in Proc. of the 6th International Workshop on HotNets*, Atlanta, USA, 2007.

[63] A. Woo, T. Tong, and D. Culler, "Taming the underlying challenges of reliable multi-hop routing in sensor networks", *in Proc. of the 1st Int. Conf. on SenSys '03,* pp. 14–27, Los Angeles, California, USA, 2003

[64] A .E. Cerpa, N. Busek, and D. Estrin, "SCALE: A tool for simple connectivity assessment in lossy environments," CENS technical report, 2003.

[65] T. Watteyne, S. Lanzisera, A. Mehta, and K. S. J. Pister, "Mitigating multipath dading through channel hopping in wireless sensor networks," *in Proc. of IEEE ICC 2010,* pp. 1–5, Cape Town, South Africa, 2010.

[66] K. Srinivasan, P. Dutta, A. Tavakoli, and P. Levis, "Understanding the causes of packet delivery success and failure in dense wireless sensor networks," *in Proc. of the 4th Int. Conf. on SenSys '06* pp. 419–420, Boulder, Colorado, USA, 2006.

[67] M. Zuniga, and B. Krishnamachari, "Analysing the transitional region in low power wireless links," *First Annual IEEE Comm. Society Conf. on Sensor and Ad Hoc Comm. and Netw.,* Santa Clara, CA, USA, 2004

[68] G. Zhou, T. He, S. Krishnamurthy, and J. A. Stankovic, "Models and solutions for radio irregularity in wireless sensor networks," *Journal ACM Transactions on Sensor Network*, vol. 2 (2), pp. 221-261, 2006.

[69] S. Duan, and X. Yuan, "Exploring hierarchy architecture for wireless sensor network management", *IEEE International Conference on Wireless and Optical Communication Networks,* Bangalore, India, 2006.

[70] J. Hill, R. Szewczyk, A. Woo, S. Hollar, D. Culler, and K. Pister, "System architecture directions for networked sensors," *in Proc. of the ninth International Conference on Architectural support for programming languages and operating systems,* vol. 28, no. 5, pp. 93-104, Cambridge, Massachusetts, USA, 2000.

[71] Q. Fang, J. Gao, and L. J. Guibus, "Locating and bypassing holes in sensor

networks", *in Proc. of the 23th Annual Joint Conference of the IEEE Computer and Communications Societies*, pp. 2458–2468, Hong Kong, China, 2005.

[72] N. Ahmed, S. S. Kanhere, and S. Jha, "The holes problem in wireless sensor networks: A survey," *Mobile Computing and Communications Review*, vol. 1 (2), 2005.

[73] R. Jurdak, X. R. Wang, O. Obst, and P. Valencia, "Wireless sensor network anomalies: Diagnosis and detection strategies," *Intelligence Based Systems Engineering*, vol. 10, pp. 309–325, 2011.

[74] W. R. Heinzelman, A. Chandrakasan, and H. Balakrishnan, "Energy-efficient communication protocol for wireless microsensor networks," *in Proc. of the 33rd Hawaii International Conference on System Sciences,* Maui, USA, 2000.

[75] N. Majadi, "U-LEACH: A routing protocol for prolonging lifetime of wireless sensor network," *International Journal of Engineering Research and Applications*, vol. 2 (4), pp. 1649-1652, 2012.

[76] Y. Jaradat, M. Masoud, I. Jannoud, T. A. Sharar, and A. Zerek, "Performance analysis of homogeneous LEACH protocol in realistic noisy WSN", *19th International Conference on Sciences and Techniques of Automatic Control and Computer Engineering (STA),* Sousse, Tunisia, Tunisia, 2019.

[77] F. Alfayeza, M. Hammoudeha, and A. Abuarqoub, "A survey on MAC protocols for duty-cycled wireless sensor networks," *Procedia Computer Science*, vol. 73, pp. 482-489, 2015.

[78] J. Saraswat, and P. P. Bhattacharya, "Effect of duty cycle on energy consumption in wireless sensor network," *International Journal of Computer Networks & Communications (IJCNC),* vol. 5 (1), 2013.

[79] Z. Li, M. Li, and Y. Liu, "Towards energy-fairness in asynchronous duty-cycling sensor networks," *Journal ACM Transactions on Sensor Networks (TOSN),* vol. 10 (3), 2014.

[80] S. Gowrishankar, T. G. Basavaraju, D. H, Manjaiah, and S. K. Sarkar, "Issues in wireless sensor networks," *in Proc. of the World Congress on Engineering,* vol. 1, 2008.

[81] G. Horvat, S. Rimac-Drlje, and D. Zagar, "Fade depth prediction using human presence for real life WSN deployment," *Radioengineering*, vol. 22, no. 33, pp. 758-768, 2013.

[82] K. Srinivasan, P. Dutta, A. Tavakoli, and P. Levis, "An empirical study of low-

power wireless," *ACM Transactions on Sensor Networks,* vol. 6 (2), 2010.

[83] K. Srinivasan, and P. Levis, "RSSI is under appreciated," *in Proc. of the third workshop on embedded networked sensors, EmNets*, 2006.

[84] M. Zuniga, and B. Krishnamachari, "Analysing the transitional region in low power wireless links," *First Annual IEEE Communications Society Conference on Sensor and Ad Hoc Communications and Networks*, Santa Clara, CA, USA, 2004.

[85] R. D. Gomes, D. V. Querioz, I. E. Fonseca, M. Alencar, "A simulation model for industrial multi-channel wireless sensor network," *Journal of Communication and Information Systems*, vol. 32, no. 1, 2017.

[86] V. Baljak, and K. Tei, "Classification of faults in sensor readings with statistical pattern recognition," *The Sixth International Conference on Sensor Technologies and Applications*, pp. 270-276, 2012.

[87] C. A. Boano, N. Tsiftes, T. Voigt, J. Brown, and U. Roedig, "The impact of temperature on outdoor industrial sensornet applications," *IEEE Transactions on Industrial Informatics*, vol. 6 (3), pp. 451-459, 2010.

[88] J. Luomala, and I. Hakala, "Effects of temperature and humidity on radio signal strength in outdoor wireless sensor networks," *Federated Conference on Computer Science and Information Systems,* Lodz, Poland, 2015.

[89] K. Bannister, G. Giorgetti, and S. K. S. Gupta, "Wireless sensor networking for hot applications: Effects of temperature on signal strength, data collection and localization," *in Proc. of the 5th HotEmNets workshop*, Virginia, USA, 2008.

[90] T. Schmid, Z. Charbiwala, R. Shea, and M. B. Srivastava, "Temperature compensated time synchronization," *Journal IEEE Embedded Systems Letter*, vol. 1 (2), pp. 37-41, 2009.

[91] C. Alberto, M. Zungia, J. Brown, and U. Roedig, "TempLab: A test bed infrastructure to study the impact of temperature on wireless sensor networks," *in Proc. of the 13th international symposium of Information processing in sensor networks*, Berlin, Germany, 2014.

[92] Z. Rong, and T. S. Rappaport, "Wireless communications: Principles and practice, solutions manual," Prentice Hall PTR, Upper Saddle River, NJ, 2001.

[93] J. Miranda, R. Abrishambaf, T. Gomes, P. Goncalves, J. Cabral, A. Tavares, and J. Monteiro, "Path loss exponent analysis in wireless sensor networks: Experimental evaluation," *11th IEEE International Conference of Industrial Informatics*, Bochum, Germany, 2013.

[94] M. Cheffena, "Propagation channel characteristics of industrial wireless sensor networks," *IEEE Antennas and Propagation Magazine*, vol. 58, no. 1, pp. 66-73, 2016.

[95] R. He, Z. Zhong, L. Xiong, and J. Ding, "The effect of reference distance on path loss prediction based on the measurements in high-speed railway viaduct scenarios," *6th International ICST Conference on Communications and Networking in China,* Harbin, China, 2011.

[96] G. Mao, B. D. O. Anderson, and B. Fidan, "Path loss exponent estimation for wireless sensor network localization," *Computer Networks*, vol. 51, no. 10, pp. 2467-2483, 2007.

[97] D. Wang, L. Song, X. Kong, and Z. Zhang, "Near-ground path loss measurements and modelling for wireless sensor networks at 2.4 GHz," *International Journal of Distributed Sensor Networks*, vol. 8, no. 8, 2012.

[98] N. A. M. Razali, M. H. Habaebi, N. F. Zulkurnain, M. R. Islam, and A. Zyoud, "The distribution of path loss exponent in 3D indoor environment," *International Journal of Applied Engineering Research*, vol. 12, no. 18, pp. 7154-7161, 2017.

[99] Z. Gao, W. Li, Y. Tian, F. Pang, W. Cao, and J. Ni, "Wireless channel propagation characteristics and modelling research in rice field sensor networks," *Sensors*, vol. 18, no. 9, 2018.

[100] S. Kurt, B. Tavli, "Path loss modeling for wireless sensor networks: Review of models and comparative evaluations," I*EEE Antennas and Propagation Magazine,* vol. 59, no. 1, 2017.

[101] Y. R. Tsai, T. Y. Lin, K. J. Yang, "Sensing coverage for randomly distributed wireless sensor networks in shadowed environments," *IEEE International Conference on Sensor Networks, Ubiquitous, and Trustworthy Computing (SUTC'06),* Taichung, Taiwan, 2008.

[102] A. Bildea, "Link quality in wireless sensor networks," Ph.D Thesis, Université de Grenoble, 2013.

[103] L. Nassef, "On the effects of fading and mobility in on-demand routing protocols," *Egyptian Informatics Journal*, vol. 11 (2), pp. 67074, 2010.

[104] S. Y. Han, and N. B. Abu-Ghazaleh, "On the effect of fading on ad-hoc networks,"   [Online],   Available   at: http://wwwlib.umi.com/cr/binghamton/fullcit?.p.1422359, Accessed on: Aug. 8, 2019.

[105] P. Pettinato, N. Wirstrom, J. Eriksson, and T. Voigt, "Multi-channel two way time of flight sensor network ranging scheme for wireless sensor network," *European Conference on Wireless Sensor Networks,* pp. 163-178, 2012.

[106] L. Nassef, R. Elhebshi, and L. Jose, "Evaluating performance of Wireless Sensor Network in realistic smart grid environment," *International Journal of Wireless & Mobile Networks (IJWMN)*, vol. 10, no. 3, 2018.

[107] K. Whitehouse, A. Woo, F. Jiang, J. Polastre, and D. Culler, "Exploiting the capture effect for collision detection and recovery," *The Second IEEE Workshop of Embedded Networked Sensors*, pp. 45-52, Queensland, Australia, 2005.

[108] A. Woo, and D. Culler, "A transmission control scheme for media access in sensor networks," *in Proc. of the 7th annual international conference on MobiCom '01,* pp. 221-235, Rome, Italy, 2001.

[109] J. Polastre, J. Hill, and D. Culler, "Versatile low power media access for wireless sensor networks," *in Proc. of the 2nd International Conference on Embedded Networked Sensor Systems*, pp. 95–107, Maryland, USA, 2004.

[110] D. Barthel, M. Heusse, and A. Duda, " Hidden nodes avoidance in wireless sensor networks," *IEEE International Conference on Wireless Networks, Communications and Mobile Computing*, Maui, USA, 2005.

[111] B. Hull, K. Jamieson, and H. Balakrishnan, "Mitigating congestion in wireless sensor networks," *in Proc. 2nd International Conference on Embedded networked sensor systems, SenSys,* pp. 134–147, Baltimore, USA, 2004.

[112] M. A. Kafi, D. Djenouri, J. Ben Othman, and N. Badache, "Congestion control protocols in wireless sensor networks: A survey," *IEEE Communications Survey & Tutorials*, vol. 16 (3), pp. 1369-1390, 2014.

[113] S. Brahma, M. Chatterjee, K. Kwiat, and P. K. Varshney, "Traffic management in wireless sensor networks: decoupling congestion control and fairness," *Journal Computer Communication,* vol. 35 (6), pp. 670–681, 2012.

[114] G. Wu, F. Xia, L. Yao, Y. Zhang, and Y. Zhu, "A hop-by-hop cross-layer congestion control scheme for wireless sensor networks," *Journal of Software,* vol. 6, pp. 2434-2440, 2011.

[115] S. A. Shah, B. Nazir, and I. A. Khan, "Congestion control algorithms in wireless sensor networks: Trends and opportunities," *Journal of King Saud University - Computer and Information Sciences,* vol. 29 (3), pp. 236-245, 2017.

[116] J. Kang, Y. Zhang, and B. Nath, "TARA - Topology-aware resource adaptation

to alleviate congestion in sensor networks," *IEEE Transactions on Parallel and Distributed Systems,* vol. 18 (7), pp. 919-931, 2007.

[117] Y. Xiao, X. Zhao, H. Wang, and C. H. Hsu, "Energy-aware multipath routing for data aggregation in wireless sensor networks," *20th IEEE International Conference on Parallel and Distributed Systems (ICPADS)*, Hsinchu, Taiwan, 2014.

[118] G. Dhand, and S. S. Tyagi, "Data aggregation techniques in WSN: Survey", *Procedia Computer Science*, vol. 92, pp. 378-384, 2016.

[119] J. Yun, B. Lee, J. Li and k. Han, "A channel switching scheme for avoiding interference of between IEEE 802.15.4 and other networks," *International Multi-symposiums on Computer and Computational Sciences,* Shanghai, China, 2008.

[120] S. U. Yoon, R. Murawski, E. Ekici, S. Park, and Z. H. Mir, "Adaptive channel hopping for interference robust wireless sensor networks," *IEEE International Conference on Communication,* Cape Town, South Africa, 2010.

[121] P. L. Iturri, E. Aguirre, L. Azpillicueta, and J. J. Astrain, "Implementation and analysis of ISM 2.4 GHz wireless sensor network systems in Judo training venues," *in Sensors*, vol. 16 (8), 2016.

[122] J. N. AI-Karaki, R. UI-Mustafa, and A. E. Kamal, "Data aggregation in wireless sensor networks - exact and approximate algorithm," *Workshop on High Performance Switching and Routing*, pp. 241-245, Phoenix, USA, 2004.

[123] "WRT160NL Datasheet", Linksys by Cisco, 2009.

[124] "IPerf - The TCP/UDP Bandwidth Measurement Tool" Ipref, Accessed on Dec 2014,

[125] "Keysight N6705 DC Power Analyzer - User guide", Keysight Technologies, Edition 11, Jan 2015.

[126] A. Basheer, and M. Hakmeer, "Artificial neural networks: Fundamentals, computing, design, and application," *Journal of microbiological methods*, vol. 43, no.1, pp. 3-31, 2000.

[127] A. Badri, Z. Ameli, and A. M. Birjandi, "Application of artificial neural networks and Fuzzy logic methods for short term load forecasting," *Energy Procedia*, vol. 14, pp. 1883-1888, 2012.

[128] N. Kumari, Sunita, and Smita, "Comparison of ANNs, Fuzzy logic and Neuro-Fuzzy integrated approach for diagnosis of coronary heart disease: A survey," *International Journal of Computer Science and Mobile Computing*, vol. 2 (6), pp.

216-224, 2013.

[129] Z. J. Viharos, and K. B. Kis, "Survey on Neuro-Fuzzy systems and their applications in technical diagnostics and measurement," *Measurement,* vol. 67, pp. 126-136, 2015.

[130] E. H. Mamdani, and S. Assilian, "An experiment in linguistic synthesis with a fuzzy logic controller," *International Journal of Man-Machine Studies,* vol 7 (1), pp. 1-13, 1975.

[131] J. S. S. Jang, "ANFIS: Adaptive network-based Fuzzy inference system", *IEEE Transactions on Systems, Man and Cybernetics*, pp. 665-685, 1993.

[132] T. Takagi, and M. Sugeno, "Fuzzy identification of systems and its applications to modelling and control," *IEEE Transactions on Systems, Man, and Cybernetics*, vol. 15 (1), 1985.

[133] M.J. Gacto, R. Alcalá, and F. Herrera, "Interpretability of linguistic fuzzy rule-based systems: An overview of interpretability measures," *Information Sciences,* vol. 181, pp. 4340-4360, 2011.

[134] S. Guillaume, "Designing Fuzzy inference systems from data: An interpretability-oriented review," *IEEE Transactions on Fuzzy Systems*, vol. 9 (3), pp. 426-443, 2001.

[135] J. M. Alonso, L. Magdalena, and G. G. Rodriguez, "Looking for a good Fuzzy system interpretability index: An experimental approach," *International Journal of Approximate Reasoning*, vol. 51 (1), pp. 115-134, 2009.

[136] M. Fazzolari, R. Alcala, Y. Nojima, H. Ishibuchi, and F. Herrera, "A review of the application of multiobjective evolutionary Fuzzy systems: Current status and further directions*," IEEE Transactions on Fuzzy Systems*, vol. 21 (1), pp. 45-65, 2013

[137] H. Ishibuchi, Y. kaisho and Y. Nojima, "Design of linguistically interpretable Fuzzy rule-based classifiers: A short review and open questions," *Journal of Multiple-Vlaued Logic & Soft Computing,* vol. 17(2), pp. 101, 2011.

[138] E. P. Klement, L. T. Koczy, and B. Moser, "Are Fuzzy systems universal approximators?," *International Journal of General Systems*, vol. 28 (2-3), pp. 259-282, 1999.

[139] H. Ishibuchi, and Y. Nojima, "Tradeoff between accuracy and rule length in Fuzzy rule-based classification systems for high-dimensional problems," *in Proc. Eleventh International Conference. Inf. Processing Manage, Uncertainty in Knowledge-Based System*, pp. 1936–1943. 2006,

[140] M. Dong, N. Wang, "Adaptive network-based fuzzy inference system with leave-one-out-cross-validation approach for prediction of surface roughness," *Applied Mathematical Modelling*, vol. 35, no, 3, pp. 1024-1035, 2011.

[141] M. Setnes, R. Babuska, U. Kaymak, and H. R. N. Lemke, "Similarity measures in Fuzzy rule base simplification," *IEEE Transaction on Systems, Man, and Cybernetics*, vol. 28 (3), 1998.

[142] J. Casillas, O, Cordon, H. Triguero, and L. Magdelena, "Interpretability issues in fuzzy modelling," *Studies in Fuzziness and Soft Computing*, vol. 128, 2003.

[143] D. Dubois, and H. Prade, "Gradual rules in approximate reasoning," *Information Science*, vol. 61, pp. 103-122, 1992.

[144] Discussions on Interpretability of Fuzzy systems using simple examples," in *Conf. IFSA-EUSFLAT*, Lisbon, Portugal, 2009

[145] P. K. Shukla, and S. P. Tripathi, "A review on the interpretability-accuracy trade-off in evolutionary multi-objective fuzzy systems (EMOFS)," *Information 2012*, vol. 3, pp. 256-277, 2012.

[146] Adaptation and application of multi-objective evolutionary algorithms for rule reduction and parameter tuning of fuzzy rule-based systems," *Soft Computing*, vol. 13, no. 5, pp 419–436, 2009.

[147] H. Ishibuchi, Y. Kaisho, and Y. Nojima, "Complexity, interpretability and explanation capability of Fuzzy rule-based classifiers," *IEEE International Conference on Fuzzy Systems, Jeju* Island, South Korea, 2009.

[148] G. Rigatos, and Q. Zhang, "Fuzzy model validation using the local statistical approach," *Fuzzy Sets and Systems*, vol. 160, pp. 882-904, 2009.

[149] A. Riid, K. Saastamoinen, and E. Rustern, "Redundancy detection and removal tool for transparent mamdani systems," *Intelligent Systems: From Theory to Practice,* pp. 397–415, 2010.

[150] K. Deb, A. Pratap, S. Agarwal, and T. Meyarivan, "A fast and elitist multiobjective genetic algorithm: NSGA-II," *IEEE Transactions on Evolutionary Computation*, vol. 6 (2), 2002.

[151] D. Kunkle, "A Summary and Comparison of MOEA Algorithms," Internal Report, College of Computer and Information Science Northeastern University, 2005.

[152] L. Bui, H. Abbass, D. Essam, and D. Green, "Performance analysis of evolutionary multi-objective optimization methods in noisy environments,"

Proceedings of the 8th Asia Pacific Symposium on Intelligent and Evolutionary Systems, 29-39, 2004.

[153] H. Ishibuchi, "A Fuzzy reasoning method for handling Fuzzy rules with different specificity levels," *18th IEEE International Conference of the North American Fuzzy Information Processing Society*, New York, USA, 1999.

[154] E. Lughofer, "On improving performance and increasing usability of EFS," *Evolving Fuzzy Systems – Methodologies, Advanced Concepts and Applications*, pp 213-259, 2011.

[155] H. Ishibuchi, and Y. Nojima, "Analysis of interpretability-accuracy tradeoff of fuzzy systems by multiobjective fuzzy genetics-based machine learning," *International Journal of Approximate Reasoning*, pp. 4-31, 2007.

[156] M. Cococcioni, B. Lazzerini, and F. Marcelloni, "Towards efficient multi-objective genetic Takagi-Sugeno fuzzy systems for high dimensional problems," *Computational Intelligence in Expensive Optimization Problems*, pp. 397-422, 2010.

[157] H. M. Pandeya, A. Chaudharyb, and D. Mehrotra, "A comparative review of approaches to prevent premature convergence in GA," *Journal Applied Soft Computing*, vol. 24, 2014.

[158] P. A. D. Gomez, and D. F. Hougen, "Initial population for genetic algorithms: A metric approach," *in Proc. of the 2007 International Conference on Genetic and Evolutionary Methods*, Las Vegas, Nevada, USA, 2007.

[159] D. E. Goldberg, "The design of innovation: Lessons from and for competent genetic algorithms", *Genetic Algorithms and Evolutionary Computation*, pp. 44, 2002.

[160] H. Ishibuchi, and T. Yamamoto, "Fuzzy rule selection by multi-objective genetic local search algorithms and rule evaluation measures in data mining," *Fuzzy Set and Systems,* vol. 141 (1), pp. 59-88, 2002.

[161] J. Ko, T. Gao, R. Rothman, and A. Terzis, A, "Wireless sensing systems in clinical environments: Improving the efficiency of the patient monitoring process," *IEEE Engineering in Medicine and Biology Magazine,* vol. 29 (2), pp. 103-109, 2010.

[162] J. S. Turner, M. F. Ramli, L. M. Kamarudin, A. Zakaria, A. Y. M. Shakaff, D. L. Ndzi, C. M. Nor, N. Hassan, and S. M. Mamduh, "The study of human movement effect on signal strength for indoor WSN deployment," *IEEE Conference on Wireless Sensor Networks in Wireless Sensor (ICWISE),* pp. 30-35, Kuching, Malaysia, 2013.

[163] N. Shabbir and S. R. Hassan, "Routing protocols for wireless sensor networks

(WSNs)," *in Wireless Sensor Networks - Insights and Innovations*, 2017

[164] K. Ishibashi, and K. Yamaoka, "A study of network stability on wireless sensor networks," *IEEE 9th International Conference on Next Generation Mobile Applications, Services and Technologies*, Cambridge, UK, 2015.

[165] S. Lin. J. B. Zhang, G. Zhou, L. Gu, J. A. Stankovic, and T. He, "Towards stable network performance in wireless sensor network," *in Proc. of the 2009 30th IEEE Real-Time Systems Symposium,* pp. 227—237, Washington, USA, 2009.

[166] B. Pavkovic, F. Theoleyre, D. Barthel, and A. Duda, "Experimental analysis and characterization of a wireless sensor network environment," *in Proc. of the 7th ACM workshop of performance evaluation of Wireless Ad Hoc, Sensor, and Ubiquitous Networks*, pp. 25-32, Bodrum, Turkey, 2010.

[167] M. Bezahaf, L. Iannone, M. D. Amorim, and S. Fdida, "Insights into the routing stability of a multi-hop wireless test bed," *Ad Hoc Networks (ADHOCNETS),* pp. 82. 97, 2010.

[168] W. L. Lee, A. Datta, and R. Oliver, "Network Management in Wireless Sensor Networks," [online] Available: http://www.csse.uwa.edu.aurwinnielNetwork_Management_in_WSNs.pdf, Accessed on: Aug. 8, 2019